An atomic force microscopy study of the crystal growth interface of solution grown potassium hydrogen phthalate

Ester, Guy R.

Award date:
1999

Awarding institution:
University of Bath

AN ATOMIC FORCE MICROSCOPY STUDY OF THE CRYSTAL GROWTH INTERFACE OF SOLUTION GROWN POTASSIUM HYDROGEN PHTHALATE

Submitted by Guy R. Ester

for the degree of PhD at the University of Bath, 1999

ProQuest LLC
789 East Eisenhower Parkway
P.O. Box 1346
Ann Arbor, MI 48106-1346

ABSTRACT

Atomic force microscopy (AFM) has been used to study the (010) face of potassium hydrogen phthalate (KAP) crystals grown from aqueous solution. In order to achieve the necessary level of surface protection during removal from solution a novel protection method was developed. The surface was withdrawn from solution through a jet of compressed air.

In order to be able to make the link between the defect structure of the crystal and the growth interface a detailed X-ray topographical analysis was performed. This showed the crystals to be of very low defect density. Furthermore the only dislocation observed in the (010) sector able to produce a step on the surface was characterised as having the <110> Burgers vector.

Two growth mechanisms were observed to operate on the (010) face of KAP crystals studied using AFM. On most crystals, a spiral growth mechanism was observed. On a minority of crystals a two dimensional nucleation and growth mechanism occurred at the higher range of supersaturations (above 15%).

In the case of a spiral mechanism it was generally noted that growth hillocks were dominated by a small number of non co-operating spiral sources. The spirals were all observed to be anisotropic and polygonised. The degree of polygonisation was found to vary as a function of supersaturation.

The step spacing was found to have an inverse relation with the supersaturation, as predicted theoretically. From an inverse plot of step spacing against supersaturation it was possible to calculate the step edge free energies of both the fast and slower moving steps. These were 40 erg/cm^2 and 8 erg/cm^2 respectively.

ACKNOWLEDGEMENTS

I would like to thank Dr. P.J. Halfpenny for his guidance during the practical work, for stimulating discussions on crystal growth and his assistance whilst I was writing up. Thanks are also due to CLRC Daresbury Laboratory and the School of Materials Science, University of Bath for support of the CASE studentship. Assistance from the technical staff of the School of Materials Science and from the Centre for Electron Optical Studies, University of Bath is also acknowledged.

My thanks and admiration are also due to my wife Catriona who endured a prolonged period of strain whilst I wrote this thesis. A final word of thank you to my son Daniel, who was only present during the last three months of writing, but nonetheless contributed to me finishing it.

This thesis is dedicated to my mother and father.

LIST OF SYMBOLS

a distance between neighboring sites on the surface

A factor in the BCF equation given by: $\frac{2\pi\alpha V_m}{X_s kT}$

A_0 activation energy for nucleation

b Burgers vector

C_0 factor in the BCF equation given by: $\frac{\pi X_s}{X_0 \ln\left(\frac{2X_s}{\gamma a}\right)}$

C_B bulk solute concentration

C_E equilibrium solute concentration

d interplanar spacing

D deflection

D_s diffusion coefficient

E applied electric field

F force

F_a structure factor

g diffraction vector

G Gibbs free energy

H enthalpy

k boltzmans constant

k_s spring constant

l line direction of a dislocation

n	number of molecules
$\mathbf{n}$	growth normal
N_i	average surface impurity density
r	radius
r_e	equilibrium radius of the hollow core of a dislocation
R	normal growth rate of a surface
s	strain
S	entropy
t	thickness
T	temperature
$\mathbf{u}$	displacement vector
V	unit cell volume
V_0	velocity of an unhindered step
V_m	molecular volume
w	evaporation energy
w_k	energy required for kink formation
X_s	displacement of adsorbed molecules
X_0	inter-kink distance
y_o	distance between successive steps on the surface
α	step edge free energy
β	factor in the BCF equation given by: $\left(\frac{1+X_s\tau}{a\tau_s}\right)^{-1}$
γ	surface energy per unit area

γ_e Eulers constant

λ wavelength

μ chemical potential

μ_o linear absorption coefficient

μ_s shear modulus

ν frequency factor of the order of the atomic frequency of vibration

ν_∞ velocity of a straight step on a crystal surface

θ angle of incidence

θ_b Bragg angle

ρ_c critical two-dimensional nucleus radius

σ supersaturation

σ_r supersaturation ratio

τ relaxation time necessary to re-establish equilibrium near a kink site

τ_s mean life of an adsorbed species

ω angular velocity of a growth spiral

ξ_g extinction distance

TABLE OF CONTENTS

1. INTRODUCTION

1.1 BRIEF HISTORICAL OVERVIEW

The word '*crystal*' (resembling ice) was introduced to the world during the classical period, at a time when the first serious thoughts about the nature and structure of matter began. The study of the mechanism of the formation of crystals, which has evolved today into the science of crystal growth, began many thousands of years later during the seventeenth century. In 1669 Steno[1] noticed the constant angles maintained between different faces on quartz crystals, Häuy and Keppler[2] formulated the concept of a unit cell and finally in the nineteenth century the concepts of a crystal lattice and the 32 different crystal classes were introduced.

The thermodynamic criteria developed in 1878 by Gibbs[3] were not applied to the problem of crystal growth for a number of years, leading to a period of empirical work on crystal growth by people such as Tamman and de Coppet[4] who studied the metastable zone in particular. The earliest recorded empirical studies on the influence of impurities on crystal growth were by de Lisle in 1783[5].

By the twentieth century a molecular model of the crystal growth process had been introduced by Stranski[6] and Kossel[7] and growth kinetic equations were derived by Becker & Doring[8] and Volmer[9]. The addition of a continuous source of steps was provided by Frank in 1949[10] and a detailed formulation of the consequences of this coupled with the influence of surface diffusion were published in 1951 by Burton, Cabrera & Frank[11].

1.2 INDUSTRIAL APPLICATIONS

For the work presented here the subject of 'crystal growth' may be reduced to 'crystal growth from solution'. Crystal growth from solution differs from other types of crystal growth, such as melt and vapour growth, by the fact that the crystal grows in a mother phase which is markedly different in composition from the crystal itself.

Often crystal growth from solution is divided somewhat arbitrarily into two regimes - high temperature and low temperature growth. In the case of the work here, the crystals were grown at (near) ambient temperature, and hence fall into the low temperature regime.

Low temperature crystal growth from solution was first studied due to its relative abundance. Many salts readily crystallise from solution, and hence are easy to study from an experimental point of view. In the modern world, however, crystal growth from solution is also a very important industrial process. Huge volumes of commodities such as sodium chloride, ammonium chloride and sucrose are crystallised from low temperature solutions at some point during their production cycles. One of the largest industries in the world, the pharmaceutical industry, also produces large quantities of high cost materials involving a crystallisation step. Typical problems in these industries are the lack of ability to control crystal size and shape. For example the caking of hygroscopic substances may reduced by choosing a shape which minimises surface contact between grains. In many cases the problems encountered in industrial crystallisation are solved empirically. This observation reflects the fact that crystal growth theories are as yet incomplete in form.

1.3 OBJECTIVES

A major difficulty in the progress of crystal growth theories has largely been due to the difficulty associated with experimentally obtaining parameters relevant to the growth interface. This problem is mainly due to the very high resolutions required to observe a surface structure coupled with the desirability of in-situ observations. In an attempt to circumvent these problems many fundamental crystal growth studies have turned to computer simulations[12], most commonly using Monte Carlo or molecular dynamic methods. Although such simulations often provide useful information concerning the crystal growth interface, they are clearly not a flawless substitute for reliable experimental information.

In recent years a new class of microscope, known as scanning probe microscopes, has been developed. These microscopes offer the opportunity to significantly advance the understanding of the science of crystal growth since they overcome both of the disadvantages mentioned above - they may be used in-situ and provide high (potentially molecular) resolution. It was the major objective of the work here to make use of this new technique to gain further insights into the crystal growth process. In order to achieve this, two commercial scanning probe microscopes were used.

In a study with the objective of using and evaluating a new analytical technique it is invaluable to have a good model compound on which to work. Such a compound is potassium hydrogen phthalate, and it is on this material that all the work presented here is based. As will become evident from the theoretical section, a good knowledge of the defect structure of a crystal is of fundamental importance when carrying out a

comprehensive study of crystal growth. For this reason a thorough X-ray topography study on potassium hydrogen phthalate is also included in this work.

2. THEORY

2.1 CRYSTAL THEORY

2.1.1 CRYSTAL STRUCTURE

The properties of a solid are strongly dependent on the arrangement of the constituent atoms or molecules, in addition to the nature of the bonding between them. Generally speaking there may exist two types of arrangement - either there is long range order present in the packing of the atoms/ molecules or there is not. In the case of an ordered structure the term crystalline is used, whereas in the case of a disordered structure the solid is said to be amorphous. Most solids are composed of many, relatively small, crystalline regions which are oriented randomly with respect to one another. Such solids are termed polycrystalline. Note that even in case of polycrystalline material, individual grains typically exceed 0.1 mm in dimension, and are therefore orders of magnitude larger than the atomic spacing ($\approx$ 0.5 nm). Thus there is still the condition of long range order within each crystal grain. The work presented here is concerned exclusively with single crystals.

In order to define more rigorously what is meant by crystalline structure, it is possible to select a small group of atoms within a crystal, which are arranged in a cell defined by the directions *hkl*. The unit cell is defined as the smallest sized cell which may be used to create the entire crystal by repeated translations in the *hkl* directions. The situation is shown graphically in figure 2.1 below, using a body centred cubic lattice as an example.

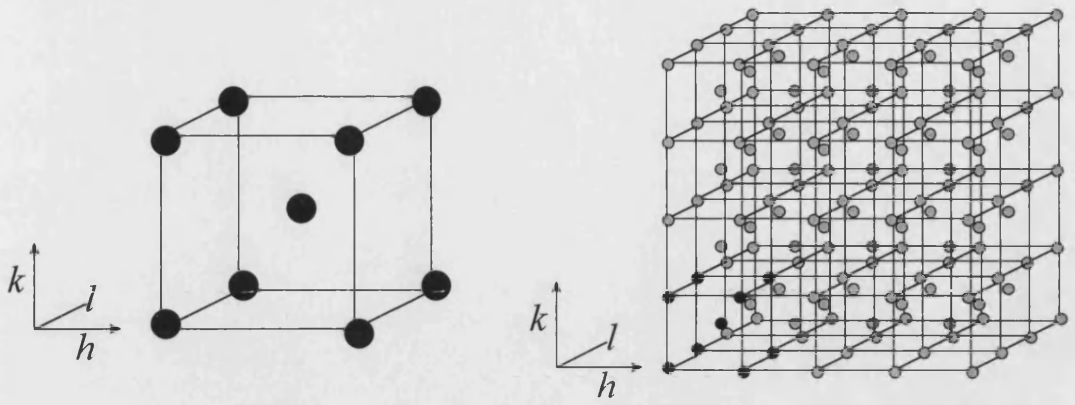

(a) (b)

Fig. 2.1 *In figure (a) the unit cell of the body centred cubic structure is shown schematically. Figure (b) illustrates how an entire single crystal of the structure may be produced by repeated translation of the unit cell.*

Using the formal geometrical theory of three dimensional structures it may be shown that only fourteen unique unit cells exist. However, since in each unit cell, every point may consist of a number of atoms or molecules the actual number of possible arrangements is restricted only by symmetry arguments. This increases the possible number of arrangements to 230.

Frequently when discussing crystal structure it is necessary to refer to planes and directions within the specific structure. In order to facilitate this, several conventions exist, and are discussed below.

Miller indices are the shorthand notation used to define planes. The Miller indices for a plane may be derived with reference to the unit cell. If the unit cell has dimensions *hkl* then the intercept of a plane with these three axes is characteristic for that plane. The Miller indices are simply the reciprocals of the intercepts, expressed as similar fractions. In figure 2.2 below the (111) plane is shown for the case of a cubic lattice.

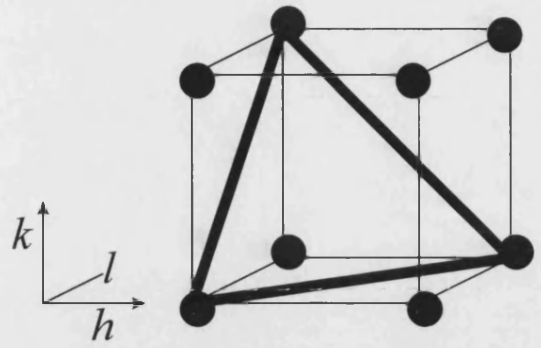

Fig. 2.2 *(111) plane in a cubic lattice*

Note that there exist families of planes with essentially the same character, but possessing different indices. For example (110),(101),(011) etc. To simplify the discussion of such families of planes the brackets { } are used, whilst the brackets ( ) are reserved for specific planes.

When discussing the directions existing within a crystal structure a standard vector notation is used, defined within *hkl* space. In order to be able to distinguish directions from planes a different set of bracket conventions is used. Particular directions are denoted by [ ], whilst families of directions are denoted < >.

2.1.2 Crystal Defects

Although it is possible to theoretically visualise a situation in which a crystal is perfect, i.e. every lattice point is filled with a corresponding atom or molecule, in practice this situation is not encountered. Every crystal existing at above 0 K must contain defects. Crystal defects may be grouped by geometric considerations and are thereby classified as either point defects, line defects or planar defects. These are discussed in turn below.

2.1.2.1 Point Defects

A number of different point defects exist. Here, however, only the so-called Schottky defect and Frenkel defect are considered. These are both shown schematically in figure 2.3 below.

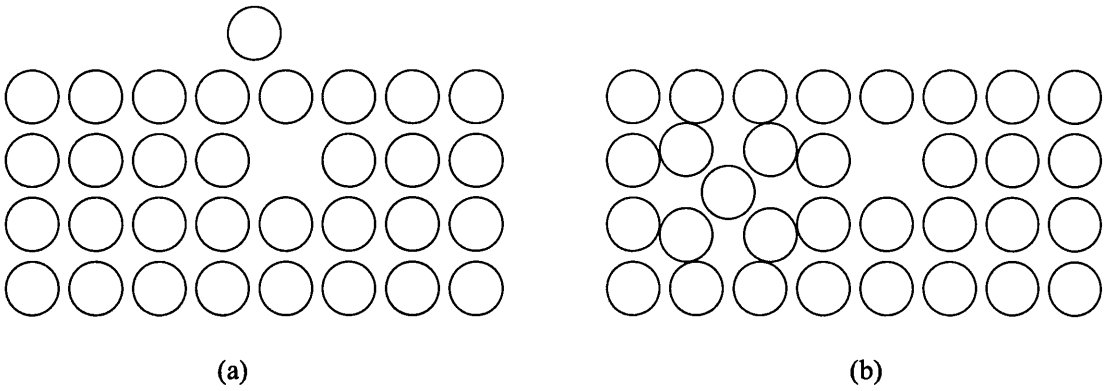

Fig. 2.3 *In figure (a) the formation of a Schottky defect is illustrated, whilst in figure (b) the Frenkel defect is shown.*

In the formation of a Schottky defect a vacancy is created, whilst the Frenkel defect contains a self interstitial. At temperatures above 0 K there is an equilibrium concentration of such defects, which follows from thermodynamic arguments. In the usual way the change in free energy may be written:

$$\Delta G = \Delta H - T\Delta S \qquad (2.1)$$

where: G = free energy

H = enthalpy

T = temperature

S = entropy

As the number of defects increases the associated increase in disorder will increase the entropy. Therefore it follows that for non-zero values of T a net decrease in G will result due to the defects. On the other hand the energy required to displace an atom is associated with H, which therefore increases the free energy. The equilibrium number of defects will correspond to a free energy minimum, which may be calculated for each value of T.

2.1.2.2 Line Defects

Line defects are more usually known as dislocations, and may exist in three basic forms, namely the edge dislocation, the screw dislocation and the mixed dislocation. As the name implies, mixed dislocations are considered to have both an edge and a screw component. Edge dislocations may be considered to consist of an additional 'half plane' of atoms which terminate within the crystal. The situation is illustrated in figure 2.4

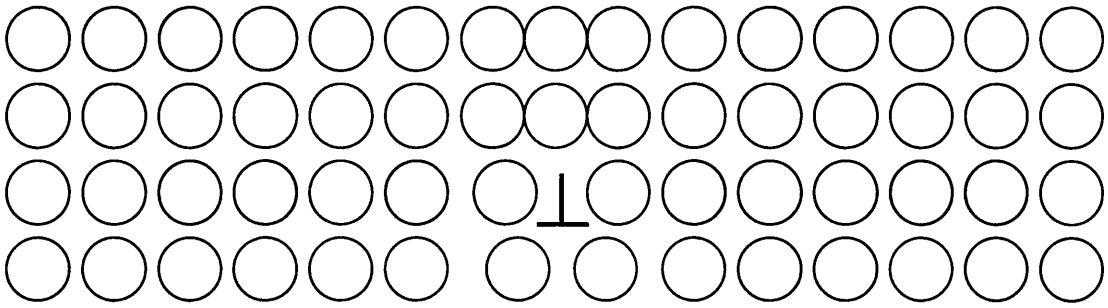

Fig. 2.4 *Schematic illustration of an edge dislocation (represented by an inverted T). An edge is created where the plane of atoms (represented by circles) terminates in the crystal centre. The surrounding atoms are shifted from their equilibrium position thus causing strain within the lattice.*

In order to characterise dislocations the concept of the Burgers vector is used. The Burgers vector of a dislocation is defined as the magnitude and direction of the slip resulting from the motion of a single dislocation. The Burgers vector of an edge dislocation is shown in a simplified manner in figure 2.5

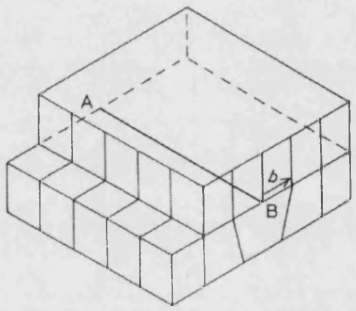

Fig. 2.5 *Edge dislocation showing Burgers vector* ***b****. Note that the vector is perpendicular to the line of the dislocation (modified from Kelly & Groves[13]).*

In figure 2.6 the essential difference between the edge and screw dislocation is shown schematically. The Burgers vector of the screw dislocation is parallel to the line direction.

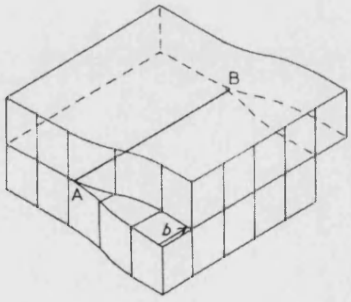

Fig. 2.6 *Screw dislocation showing Burgers vector* ***b****. Note that the vector is parallel to the line of the dislocation (modified from Kelly & Groves[13]).*

In the case of a mixed dislocation, a component of screw and edge are both present, and therefore the Burgers vector lies at an angle between 0 and 90 degrees to the line direction of the dislocation.

As already stated, the presence of dislocations in crystal lattices causes a strain due to the displacement of atoms from their minimum potential energy positions. The energy associated with this strain may be estimated for a screw dislocation, and can is approximately equal to:

$$E_s \approx \mu b^2 l + \frac{\mu b^2 l}{10} \qquad (2.2)$$

where: μ_s = shear modulus

b = Burgers vector

l = line direction of the dislocation

2.1.2.3 Planar Defects

Planar defects are of the atomic dimension in one direction and, but may extend over many atoms in the other directions. Planar defects may be classified as either internal, as in the case of grain boundaries or external as in the case of solid-gas or solid-liquid interfaces. In the work here single crystals are studied and therefore internal planar defects are not relevant. The solid-liquid interface on the other hand is of fundamental importance in crystal growth kinetics which is discussed next.

2.2 *CRYSTAL GROWTH KINETICS*

As a precursor to the discussion on crystal growth kinetics, a number of conventions concerning the calculation of the supersaturation are given here. Assuming activity coefficients of 1 then:

$$\Delta\mu = kT\ln\left(\frac{C_B}{C_E}\right) \qquad (2.3)$$

where: μ=chemical potential

C_E = equilibrium solute concentration

C_B = bulk solute concentration

The supersaturation ratio is defined as:

$$\sigma_r = \ln\left(\frac{C_B}{C_E}\right) \qquad (2.4)$$

and therefore:

$$\sigma_r = \frac{\Delta\mu}{kT} \qquad (2.5)$$

For small values of supersaturation the first term in the Taylor series expansion is approximately correct. This implies:

$$\frac{\Delta\mu}{kT} = \ln(1+\sigma) \approx \sigma \qquad (2.6)$$

where: $\sigma = (C_B - C_E)/C_E$

For some of the work considered here, the supersaturations are relatively high and for these cases the approximation given in equation 2.4 is not valid.

2.2.1 Crystal Growth Based on Nucleation and Growth Theories

In the original theories dealing with the growth of crystals from a supersaturated medium a common model system used was the perfect (i.e. defect free) Kossel[14] crystal. An example of such a crystal is shown in figure 2.7 below.

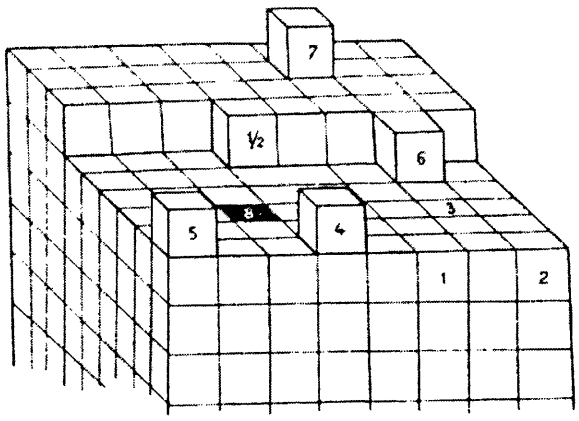

Fig. 2.7 *Kossels crystal model[14]*
1.) edge 2.) corner 3.) surface 4.) edge adsorbed molecule 5.) corner adsorbed molecule 6.) edge position 7.) surface adsorbed molecule 8.) surface hole ½.) kink or repeatable step.

On the surface of this crystal a large number of potential binding sites for new growth units exist. For a given growth unit to become permanently incorporated in the crystal it must undergo a number of steps: initial adsorption on the surface from the medium; (surface) diffusion of the unit to a growth site and orientation and dissipation of the heat of transition. In energetic terms the most favourable sites have the largest number of bonds with the new growth unit. Thus the potential sites illustrated in figure 2.7 may be ranked in order of preference:

- Optimal sites have more than three bonds - a growth unit arriving at these sites is readily incorporated into the crystal bulk (sites 1 and 3 in figure 2.7).
- The least favourable sites have less than three bonds - for these sites desorption of the molecule is likely to occur shortly after adsorption on the surface (sites 4-7 in figure 2.7)
- For the case of three bonds with the surface (labelled ½ in figure 2.7), the edge free energy before and after adsorption of the growth unit remains unchanged - in both cases three 'edges' of the growth unit are exposed. Growth at such sites may therefore readily occur. The name given to this type of site is a kink site. They are particularly important in crystal growth since they form a repeatable step.

From the above arguments it will be appreciated that all sites present on the surface which may form three or more bonds with arriving growth units will be rapidly filled. Once this has occurred no sites will remain. Thus even at low supersaturations, Kossel crystals will quickly be bounded by flat surfaces. For further growth of the crystal a nucleation step now needs to be overcome, due to the lack of suitable sites. This nucleation barrier is analogous to that encountered in bulk precipitation, however, in this case a two, rather than three dimensional nucleus is required. Many small nuclei will transiently form on the surface, but the condition for stability is an overall reduction in energy. This means that the extra energy generated by the production of a step at the edge of the nucleus needs to be more than offset by the reduction in energy due to the phase change. If the process is isobaric and isothermal then:

$$\Delta G = -nkT\ln\left(\frac{C_B}{C_0}\right) \qquad (2.7)$$

where: ΔG is the change in Gibbs free energy associated with the phase change

n is the number of transferred molecules

If a nucleus of monomolecular height is formed with a radius r and step free energy α then the increase in energy associated with the step is given by:

$$\Delta G = 2\pi r\alpha \qquad (2.8)$$

Using an energy balance approach gives:

$$\Delta G = -nkT\ln\left(\frac{C_B}{C_0}\right) + 2\pi r\alpha \qquad (2.9)$$

The number of molecules n in the nucleus is given by:

$$n = \left(\frac{\pi r^2}{V_m}\right) \qquad (2.10)$$

where V_m is the molecular volume.

combining (2.9) and (2.10):

$$\Delta G = 2\pi r\alpha - \left(\frac{\pi r^2}{V_m}\right)kT\ln\left(\frac{C_B}{C_0}\right) \qquad (2.11)$$

For some critical value of r (denoted r_c), there will exist a maximum in ΔG, above which the nucleus remains stable. This is given by differentiating with respect to r and setting the result equal to zero, from which:

$$r_c = \frac{\alpha V_m}{kT\ln\left(\frac{C_B}{C_0}\right)} \qquad (2.12)$$

Growth of a nucleus with a radius of at least r_c will therefore result in an overall reduction in energy. This will readily occur via kink sites until the surface is once again flat and the process repeats itself. From this basic framework it will be appreciated that three variations of growth kinetics result from this mechanism.

1. In comparison with nucleation the growth phase is very fast i.e. the growth rate is dominated by the nucleation step.
2. In comparison with nucleation the growth phase is slow i.e. growth is the rate controlling mechanism.
3. Some situation between these two extremes, where many nuclei (including nuclei on nuclei) may form and coalesce.

In theory, high supersaturations should give rise to the third case, whilst for low supersaturations the first case should occur. The second case is considered unlikely for most systems, since growth is nearly always faster than nucleation.

In practice it is rather difficult to compare theory with experimental results because reliable estimates of the step edge free energy are elusive. Nonetheless, using some reasonable assumptions certain general conclusions may be drawn. The most important of these is the fact that at low supersaturations the nucleation barrier becomes prohibitively high. This has been discussed at length by various authors[11,15]. Burton Cabrera & Frank[11], for example, apply the activation energy for nucleation as described by Volmer[9] to a typical growth supersaturation of 1%. Since the number of nuclei produced per second contains as a factor $e^{\left(\frac{-A_0}{kT}\right)}$, where A_0 is the activation energy for nucleation (half the total edge free energy of a critical nucleus), then by using some reasonable values for nearest neighbour interaction they arrive at

$A_0/kT \approx 3.6x10^3$ thereby excluding the possibility for a reasonable growth rate at low supersaturations. The conclusion from this is that whilst a two-dimensional nucleation and growth mechanism would be possible at high supersaturations, at low supersaturations it is highly unlikely.

2.2.2 Spiral Growth Mechanisms

The solution to the puzzle of crystal growth at low supersaturations was provided in 1949 by Frank[16], who, together with Burton and Cabrera, published the now famous BCF[11] paper. His genius was in recognising that real crystals are not in general defect free, but contain a (usually) large number of line defects known as dislocations. These may be divided into three classes namely edge, screw and mixed dislocations. For the case of screw dislocations (or mixed dislocations with a component of the Burgers vector normal to the surface in question) a step is produced on the crystal surface. This step starts at the dislocation core and increases in height until it reaches the height of one unit cell. The situation is illustrated in figure 2.8.

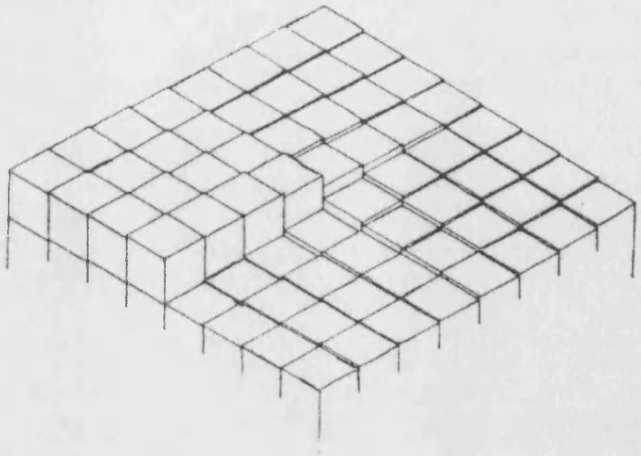

Fig. 2.8 *Screw dislocation emerging on a Kossel crystal face*[18]

The presence of such steps on the surface mean that no nucleation process is required. This is because the step is pinned at its point of emergence. Therefore as growth units are added to the step, at an equal rate per unit length of step, an angular velocity of the step results. The first stages of this occurring are shown schematically for a Kossel crystal in figure 2.9(a-c) below.

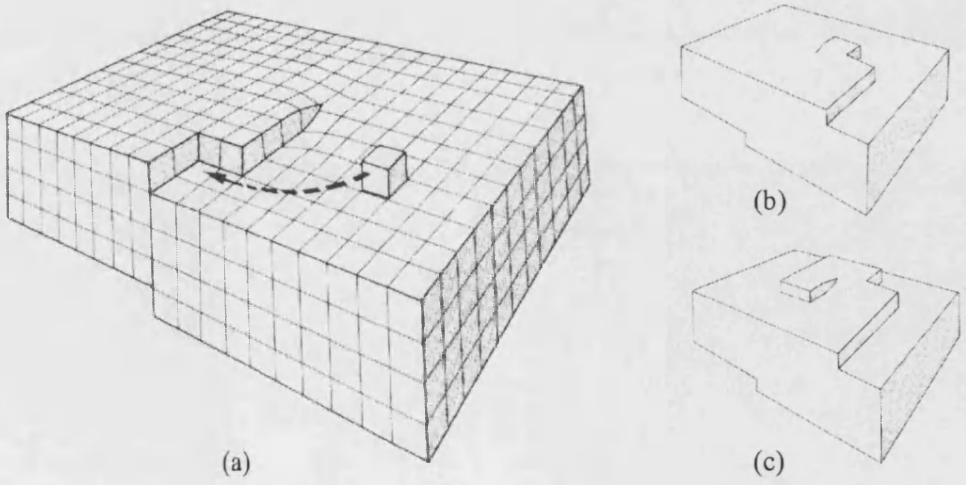

Fig. 2.9 *The first stages in the formation of a growth spiral (b&c) from an emergent screw dislocation (a) on an idealised Kossel crystal surface (modified from Woodruff*[18]*).*

Thus on any crystal surface containing at least one emergent screw dislocation a self perpetuating step is present. BCF show that for growth from the vapour an archimedian spiral is the most probable shape. If viewed from above, such a step appears to wind up around its epicentre as shown in figure 2.10 below.

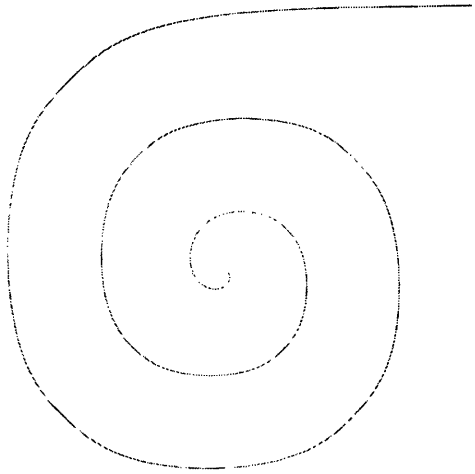

Fig. 2.10 *Growth spiral as calculated from a generalised kinetic equation (modified from Müller-Krumbhaar[19])*

Before continuing it is necessary to qualify the nature of steps on the surfaces of crystals. In the case of a perturbation free step, i.e. with no kink sites, then recall from the model Kossel crystal that once again a nucleation step is required. In this case it is a one dimensional nucleus that must be formed i.e. a single growth unit must join onto the otherwise perturbation free step. Once this has occurred two new kink sites are formed on the step, one each side of the newly added growth unit. For the case of one dimensional nucleation the elimination of the nucleation problem is provided by

thermal energy. Frenkel[20] and Burton & Cabrera[21] have shown that at any temperature reasonably above 0 K, thermal energy provides a large number of kink sites. The reasoning is identical to that used for the calculation of the number of point defects (vacancies) in a crystal lattice above 0 K.

Although no kinetic measurements are made in the work presented here it is worth briefly surveying the crystal growth rate equations derived by BCF, since these are used as the basis for discussions on the growth spiral shape.

Assuming that surface diffusion of adsorbed molecules occurs on the growing crystal surface then, neglecting the influence of movement by the step itself, it may be shown that the velocity of a single straight step on a given crystal surface is given by:

$$\upsilon_{\infty} = 2\sigma X_s \nu \exp\left(\frac{-w}{kT}\right)\beta C_0 \qquad (2.13)$$

where: X_s = displacement of adsorbed molecules

ν = a frequency factor of the order of the atomic frequency of vibration

w = evaporation energy

Note that:

$$X_s^2 = D_s \tau_s \qquad (2.14)$$

where: D_s is the diffusion coefficient

τ_s is the mean life of an adsorbed species

The factor β is introduced to allow for the fact that the exchange between the kinks and the adsorbed layer may not be rapid enough to maintain a surface supersaturation of zero near the step edge. It is given by:

$$\beta = \left(\frac{1 + X_s \tau}{a \tau_s} \right)^{-1} \qquad (2.15)$$

where: τ = relaxation time necessary to re-establish equilibrium near the kink

a = distance between neighbouring equilibrium sites on the surface

The factor C_0 may be readily calculated for two extreme situations. If the displacement of adsorbed molecules (X_s) is much larger than the inter-kink distance (X_0) then C_0 is equal to unity. Conversely, if $X_0 >> X_s$ then C_0 is given by:

$$C_0 = \frac{\pi X_s}{X_0 \ln\left(\frac{2X_s}{\gamma a} \right)} \qquad (2.16)$$

$$X_0 \approx \tfrac{1}{2} a e^{(w_k / kT)} \qquad (2.17)$$

where: γ_e is Eulers constant

w_k is the energy required for kink formation

BCF conclude that for growth from supersaturated vapour it is most likely that $X_s >> X_0$ applies, and therefore C_0 may be neglected. In this case the velocity of a step is found to be independent of orientation thus leading to an archimedian spiral shaped step, as seen in figure 2.10. This is because most growth units may diffuse to a kink site and hence the directions with the lowest kink density (the close packed directions) do not appear as readily.

In the other extreme case, which BCF consider unlikely, $X_s << X_0$ which makes it necessary to consider diffusion of the adsorbed molecules in the edge of the step. Since the mean interkink distance will be a maximum in the close packed directions, it is these steps which will grow most slowly. Hence a polygonised growth spiral will form which is bounded by these directions.

So far only the movement of a single step has been considered. For the (more realistic) case of a train of parallel steps equation 2.11 becomes:

$$\upsilon_\infty = 2\sigma X_s \nu \exp\left(\frac{-w}{kT}\right) \tanh\left(\frac{y_0}{2X_s}\right) \beta C_0 \qquad (2.18)$$

where: y_0 is the distance between successive steps

The growth rate of the crystal face itself i.e. the rate normal to the surface is given by:

$$R = \frac{\omega a}{2\pi} \qquad (2.19)$$

where ω is the angular velocity of the spiral and is given by:

$$\omega = \frac{\upsilon_\infty}{2\rho_c} \qquad (2.20)$$

where: $\rho_c = r_c$ for archimedian spirals and $\frac{1}{2} r_c$ for polygonised spirals.

Combining 2.17 & 2.18 with 2.16 gives:

$$R = \beta C_0 a \nu \exp\left(\frac{-w}{kT}\right)\left[\frac{\sigma X_s}{2\pi\rho_c}\right] \tanh\left[\frac{2\pi\rho_c}{X_s}\right] \qquad (2.21)$$

if $\rho_c = r_c$ then from 2.10:

$$R = \beta C_0 a \nu \exp\left(\frac{-w}{kT}\right)\left[\frac{\sigma^2}{A}\right] \tanh\left[\frac{A}{\sigma}\right] \qquad (2.22)$$

where A is given by:

$$A = \frac{2\pi\alpha V_m}{X_s kT} \qquad (2.23)$$

Consider two cases of σ:

When $\sigma >> A$ then:

$$R = \beta C_0 a \nu \exp\left(\frac{-w}{kT}\right)\sigma \qquad (2.24)$$

since $\tanh(A/\sigma) \rightarrow A/\sigma$.

When $\sigma << A$ then:

$$R = \beta C_0 a \nu \exp\left(\frac{-w}{kT}\right)\frac{\sigma^2}{A} \qquad (2.25)$$

since $\tanh(A/\sigma) \rightarrow 1$.

Equations 2.22 and 2.23 are known as the linear and parabolic laws respectively.

Once again, however, the factor C_0 is difficult to determine for cases other than $X_s >> X_0$ or $X_0 >> X_s$. In the work here we note that these two extremes do not always apply. Therefore for completeness the general solution of C_0 is required. This is given by:

$$\frac{1}{C_0} = 1 + 2b\tanh\left(\frac{y_0}{X_s}\right)\left[\ln\left(\frac{\frac{4bX_s}{a}}{1+(1+b^2)^{\frac{1}{2}}}\right)\right] + \frac{2X_s}{y_0}\tan^{-1} b \qquad (2.26)$$

where: $b = \dfrac{X_0}{2\pi X_s}$

Note that when $y_0 \rightarrow \infty$ and $X_0 >> X_s$ then 2.24 reduces to 2.14 as would be expected.

As a corollary it is worth noting that although the above relates to vapour growth, crystal growth from solution is also discussed in the BCF paper. However the basic tenet which is maintained throughout the argument is that surface diffusion plays no role in the growth mechanism. This assumption has since been convincingly questioned in the light of more recent experimental evidence by a number of authors[22,23,24]. They conclude that whilst the relative importance of surface diffusion may be less for solution growth when compared with vapour growth, it is nonetheless large enough to be of considerable importance. For this reason this section of the BCF paper is omitted here.

Finally it is worth mentioning that in common with the two dimensional nucleation and growth model, the spiral growth model suffers from the fact that many of the required parameters are unknown, and thus a rigorous analysis is usually not possible. For this reason the unknowns are usually grouped into constants and the experimental observation of a change from a parabolic to a linear growth regime is often taken as sufficient evidence for the existence of a spiral mechanism.

2.2.2.1 Spiral Shape

In terms of the study presented here, the spiral shape is of considerable interest, since this is one of the features which is most accessible to an AFM analysis. We have seen that the spiral shape is determined by the interrelationship between X_s and X_0 contained within the factor C_0 and presented in the general form in equation 2.24. It was argued that when $X_s << X_0$ then the spiral would be polygonised in form with the close packed directions bounding the polygon, since the kink density for these directions is a minimum. The idea of close packed directions has been expanded by Hartman and Perdok.[25,26,27]. In order to predict the three dimensional morphology of crystals they identify three different types of growth face in terms of periodic bond chains (PBC's). A PBC is defined as a strong uninterrupted bond between growth units having a periodicity [u,v,w] in the structure. Only those faces with a PBC in two crystallographic orientations (denoted F faces) are predicted to feature in the morphology of the crystal i.e. the crystal will be bounded by F faces. The other two types of faces, namely S and K types have either only one or no PBC's respectively. Therefore it is assumed that these faces have many sites where the direct

incorporation of growth units is possible. This leads to a relatively fast growth rate, and hence disappearance of the faces. Although this approach was originally developed for the prediction of crystal morphology, the essential argument reduces to two dimensions, and hence is applicable to step morphologies.

If we consider the step morphology on an F face then the lowest number of kink sites will occur when the morphology of the polygon lies along the PBC's. Therefore a polygonised spiral is likely to be bounded by the PBC directions present on that face.

2.2.2.2 STEP SPACING

BCF show that in the case of a single, undisturbed archimedian spiral growing under steady state conditions, the form of the spiral is such that successive turns are equidistant. This distance is given by:

$$y_0 = 4\pi r_c \qquad (2.27)$$

Later work by Cabrera & Levine[28] and others[15] has shown that a more accurate relationship is given by:

$$y_0 = 19 r_c \qquad (2.28)$$

These two relationships are essentially similar, as illustrated in figure 2.11 below.

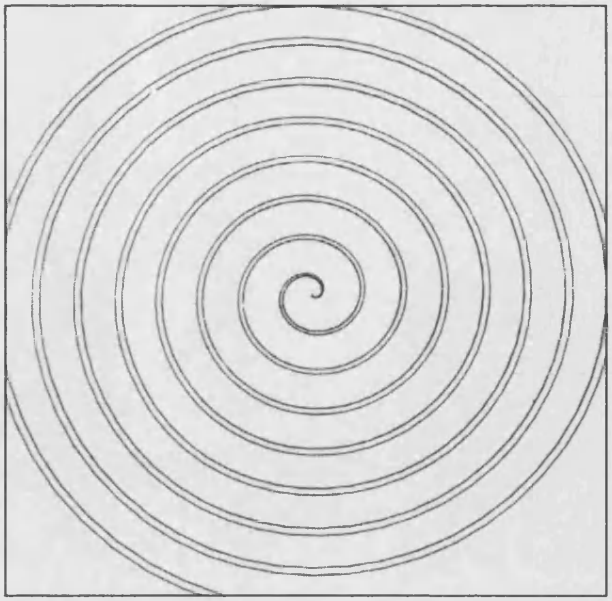

Fig. 2.11 *Comparison of computer calculated spirals on the basis of $4\pi r_c$ (inner spiral) and $19r_c$ (outer spiral) (modified from Sunagawa & Bennema[29])*

With the advent of significantly increased computer processing speeds it has been possible to routinely apply techniques such as Monte Carlo simulations to the crystal growth process. These have confirmed the order of magnitude of equation 2.26. In the case of polygonised spirals the predicted value for the step spacing varies between approximately $6r_c$ and $19r_c$[29,30,31,32].

In practice it is unusual to have only a single undisturbed spiral on a crystal surface and in this case the step spacing is influenced by a number of other factors including:

1. the nature and number of sources giving rise to the spiral
2. the relative dominance of kinetic factors compared with energetic factors
3. the presence of impurities

The first case is considered in more detail below.

When several dislocations interact to form a growth spiral there are a number of general conditions which may occur:

I. two dislocations are a large (>10r_c) distance apart. Here the influence on activity (i.e. number of turns of the spiral per unit time) of one dislocation on the other is very small and becomes negligible at any appreciable distance.

A. when the two dislocations are of opposite sign closed loops of steps will be emitted, as shown schematically in figure 2.12. It is worth noting that if there are two such pairs then the loops will join upon intersection, and hence the number of steps passing a given point on the surface will be identical to the case of a single pair. From this it will be clear that the growth rate of the face will not be affected by the number of such dislocations.

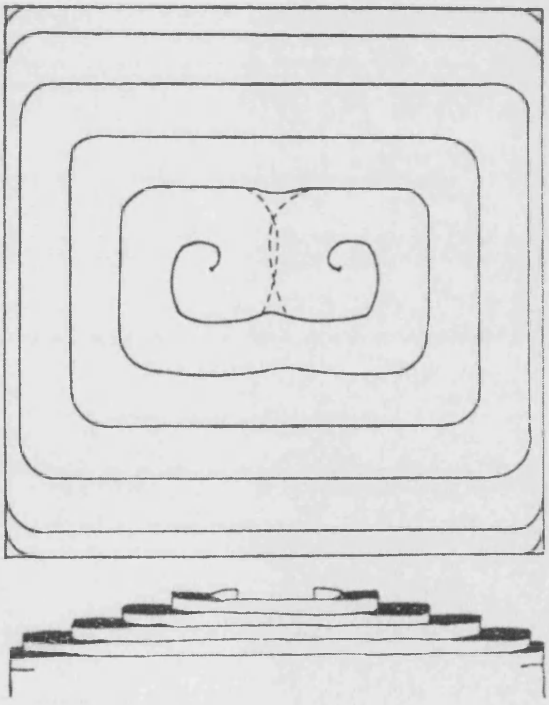

Fig. 2.12 *Closed loops of steps emitted from two sources of opposite sign*[11]

B. for the case of dislocations having like sign, then a locus divides the area of activity of each dislocation in half a shown in figure 2.13. For large inter-dislocation spacings this locus is approximated by a straight line. As the proximity of the dislocations is reduced, however, this locus becomes an S shaped curve. Once again, however, the activity of the pair is almost identical to the activity of a single source.

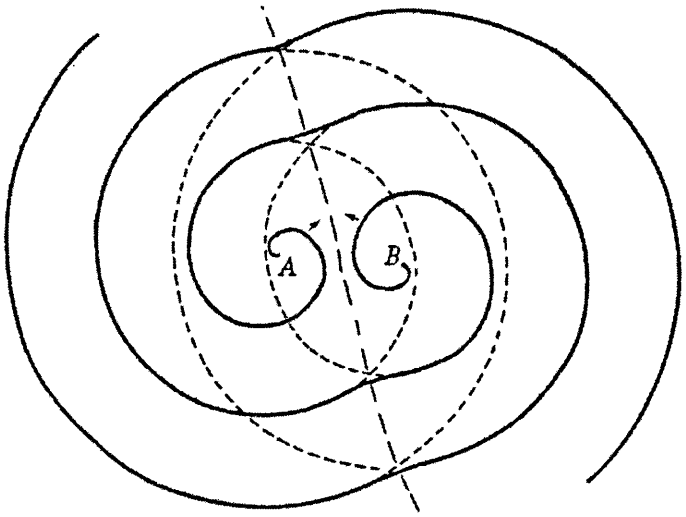

Fig. 2.13 *Two dislocations (denoted A&B) with inter distance > $10r_c$*[11].

II. two dislocations are very close ($<10r_c$) together. In this case there is a significant influence on the activity of the source.

A. for dislocations of opposite sign no growth occurs.

B. for two dislocations of like sign the source activity is increased by a factor of two for dislocations of very close ($<<10r_c$) proximity. At slightly larger distances apart ($<10r_c$) the extra distance which must be travelled by steps around the spiral centres becomes important, and this has a retarding effect on the effective activity of the spiral. In such

a situation the activity lies somewhere between one and two times the activity of a single dislocation. Furthermore there is a significant disruption of the step pattern and spacing as illustrated in figure 2.14 below.

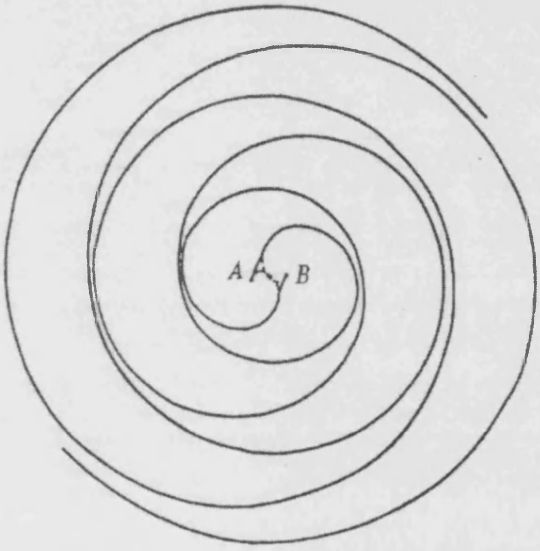

Fig. 2.14 *Two dislocations (denoted A&B) with inter distance < $10r_c$*[11].

It is worth noting that for a large group of closely spaced sources (shown schematically in figure 2.15) the activity will be increased by a factor equal to the number of sources, after taking into account both the cancellation of opposite signed sources and the reduction in activity due to the extra distance travelled by steps when the inter-source distance is not $<<10r_c$.

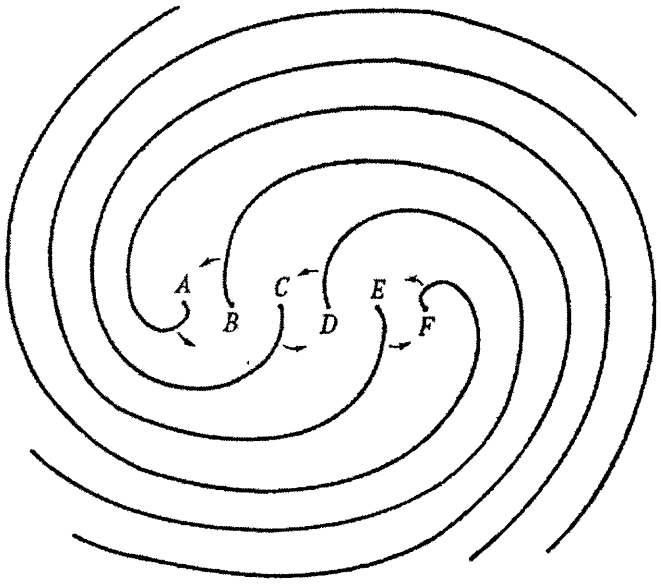

Fig. 2.15 *A group of like signed spirals interacting. In the case of any sources of opposite sign being present the activities are cancelled out*[11].

2.2.3 HOLLOW DISLOCATION CORES

Frank[33] has shown that if the Burgers vector of the dislocation responsible for a growth spiral is sufficiently large then the possibility exists that the energy associated with the dislocation core may be larger than the energy required to form a hollow core surrounding the dislocation. Using an energy balance approach the equilibrium radius of the hollow core may be written as:

$$r_e = \frac{\mu b^2}{8\pi^2 \gamma} \qquad (2.29)$$

where: μ_s= shear modulus

b= Burgers vector

γ= surface energy per unit area

The earliest experimental confirmation of this was cited by Verma[34] in 1953. On SiC crystals, with $\mathbf{b} \approx 15$Å and assuming $\gamma/\mu = 10^{-8}$ cm, he reported holes on dislocation outcrops. From equation 2.27 this is predicted to occur from $\mathbf{b} > 10$ Å.

This relationship has been further studied by van der Hoek et al[35], who showed that the true hollow radius may be smaller than that predicted by Frank. The presence of a hollow radius may also have an influence on the growth kinetics of a dislocation source, since the steps must now spiral around the epicentre of the hollow core.

2.2.4 Normal Growth

So far only singular surfaces have been considered, on which a layer by layer type of growth occurs. It was shown that at low supersaturations this type of growth can only occur if there is an external source of steps. In the BCF model this source is provided by the presence of screw dislocations. At higher supersaturations it becomes energetically feasible for a two-dimensional nucleation and growth mechanism to operate leading to a transition between the two. Initially, it is most likely that both mechanisms operate in the transition zone i.e. inter-step (from the spiral mechanism) nucleation and growth. If a large amount of surface diffusion occurs, then the transition to a two-dimensional nucleation and growth mechanism will be suppressed. As the supersaturation is further increased a roughening transition may occur and a growth region denoted as 'unstable' occurs. In this regime, for example, dendritic growth - as is common in the solidification process of metals, occurs. The layer by layer mechanism is replaced by continuous or 'normal' growth. All arriving

growth units are directly incorporated into the crystal resulting in a rough interface as shown schematically in figure 2.16 below.

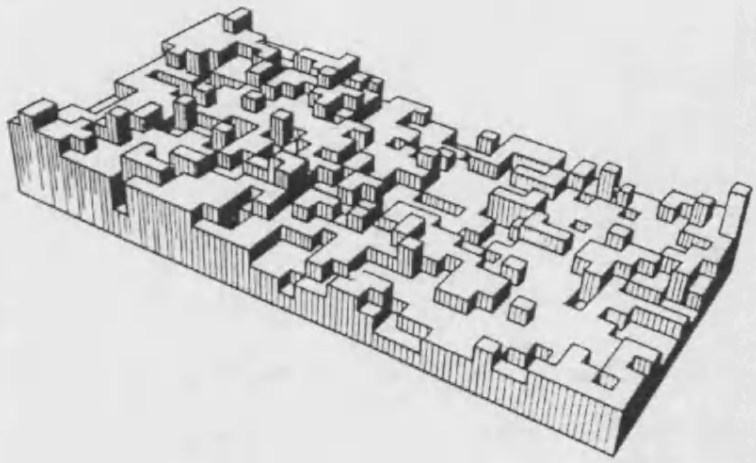

Fig. 2.16 *Schematic diagram of a simulated rough interface[36]. Growth units arriving at the surface may be incorporated directly into the surface.*

In summary, there is therefore the following theoretical sequence of growth mechanisms:

spiral growth → two-dimensional nucleation and growth → normal growth

As the supersaturation increases, the growth mechanism moves from spiral growth to normal growth. It should be noted that the transition to a normal growth mechanism is assumed to occur on a purely kinetic basis here, from a material which at low supersaturations grows by a layer mechanism. This will not be the case for all materials. Jackson[37] has shown that materials may be characterised on the basis of a so-called α factor. This factor is essentially the product of two parameters, one relating to the entropy of melting per mole (a function of the material) and the other relating to the crystal structure and surface under consideration. The α factor may be

used to predict whether materials will fundamentally i.e. also at low supersaturations, grow by a normal mechanism.

2.2.5 Impurity Effects

When studying 'real' crystal growth then the effect of impurities needs to be considered.

The mechanism of impurity effects on step growth was first suggested by Cabrera and Vermilyea[38]. They assumed that many impurities would be absorbed on the surface. As a first approximation they assumed a square lattice distribution over the surface, and immobility of the adsorbed impurities. In this case the lattice acts as periodic step pinning sites - an approaching step has to squeeze through the lattice leading to a curvature of the steps. The effect of this curvature on the velocity of the step may be approximated from the Gibbs-Thompson effect. As might be expected, the tendency is for the velocity of the steps to be reduced. At a certain point, when the lattice spacing of the impurity network becomes less than the critical radius of a two-dimensional nucleus, the velocity of the step is reduced to zero and growth stops altogether. This effect has been experimentally observed on many crystal systems at low supersaturations and is known as the 'dead zone'.

On a macroscopic level the effects of impurities have been suggested to be the cause of so-called macro-steps. These steps are frequently visible under optical light microscopes or even the naked eye. Although their formation is not fully understood, it has been suggested that impurities may cause bunching of the monoatomic steps, due to variability in their velocity. The cause of such a variation may be better

appreciated if one realises that simply due to statistical effects different steps will have different numbers of adsorbed impurities and hence slightly different velocities. Since the number of impurities that a step encounters is dependent on the size of the terrace in front of it, it follows that steps which are already travelling slowly (i.e. have a relatively large terrace in front of them) will be further reduced in velocity. A combination of many such steps has been studied by Frank[39] and Cabrera & Vermilyea[38] using traffic flow theory developed by Lighthill & Whitman[40,41]. They conclude that the formation of macro-steps may occur under such conditions.

A second theoretical explanation has been proposed by Amelinckx[42], who considered the case of a helical dislocation giving rise to a spiral. The helical nature of the spiral causes the centre to 'wobble' as the crystal grows. This may be shown to give rise to a periodic step bunching, resulting in the formation of a macro-spiral. The predicted form is illustrated below.

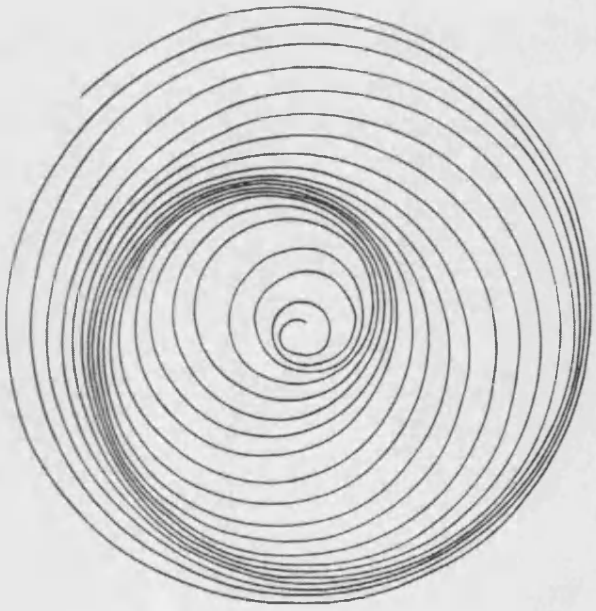

Fig. 2.17 *Macrosteps resulting from the mechanism suggested by Amelinkcx[42].*

The main criticism of this kind of spiral is that there seems little experimental justification for it - helical dislocations are not commonly encountered in practice, whereas macro spirals are relatively common.

2.3 Atomic Force Microscopy (AFM)

Atomic Force Microscopy or AFM as it is commonly termed, belongs to the category of microscopes known as scanning probe microscopes. As is apparent from the name, this category of microscope consists of a probe of some type which scans across, and in close proximity to, the sample. The development of such microscopes is a relatively recent innovation, which began with the invention of the scanning tunnelling microscope[43] (STM) in 1982. In the STM the spatial variation of a tunnelling current between a tip and sample (in close proximity) is used to generate an image of the sample surface. Although the use of a tunnelling current allows very high resolutions, it suffers from the disadvantage that only conducting surfaces may be imaged. It is basically for this reason that the AFM was developed[44]. In AFM a sharp tip is scanned across the sample surface, and the measurement of the repulsive force between the tip and sample allows a spatial map of the surface to be constructed. Because of is wide applicability AFM is the most commonly used of the SPM techniques.

Figure 2.18 below shows a schematic diagram of a typical AFM. The tip is initially brought into close proximity with the surface via some coarse mechanical means, and is subsequently brought into contact with the surface via a software controlled motor. The sample is mounted on a piezoelectric scanner which can move in both the x and

y planes (for scanning of the sample) and the z direction (normal to the sample surface). Deflection of the cantilever is usually measured by an optical lever system. A laser beam is reflected via the back of the cantilever to a position sensitive photodetector, capable of sub-nanometer movement detection. Thus if the lever is constructed such that sub-angstrom movements of the cantilever are slightly amplified, these may be registered.

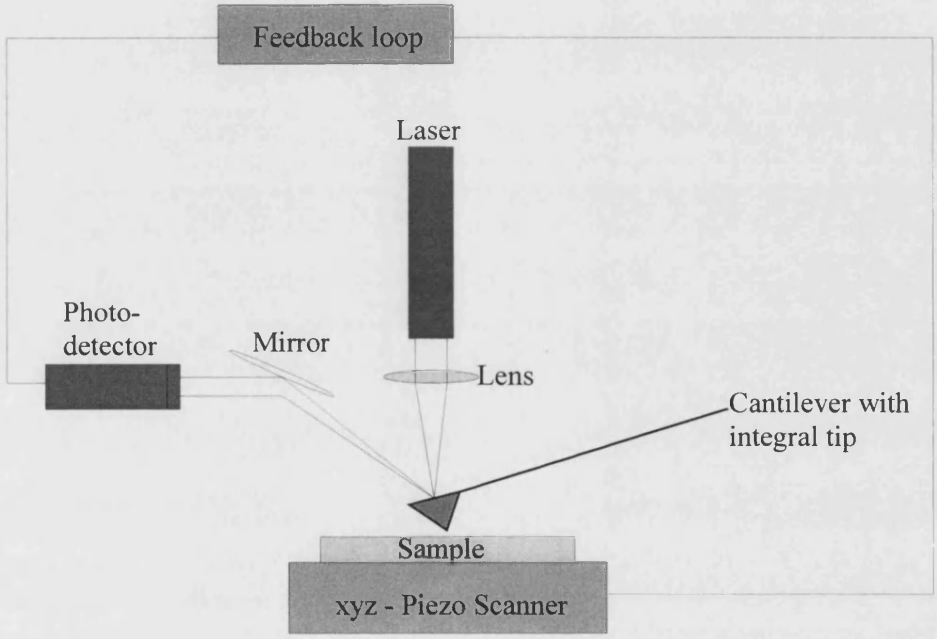

Fig. 2.18 *Schematic diagram of a generic AFM*

During AFM there are commonly three types of forces present, namely van der Waals; a capillary force due to any adsorbed moisture on the surface and the force due to the deformation of the cantilever. From the shape of the van der Waals force-

distance curve, shown in figure 2.19, the two main modes of AFM operation may be appreciated.

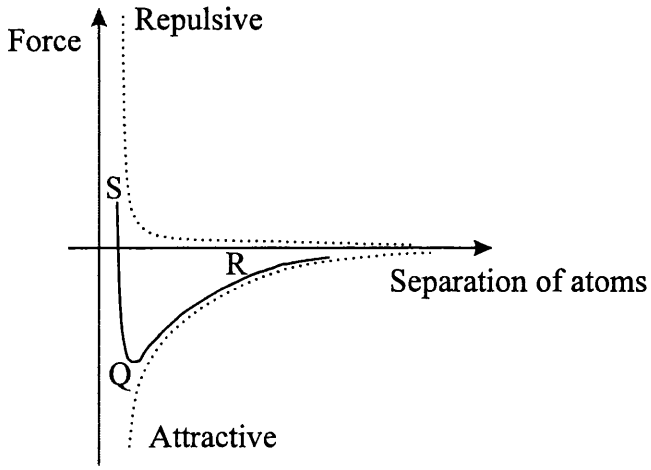

Fig. 2.19 *Schematic figure of a Lennard-Jones potential showing the force distance curve resulting from a higher order repulsive curve summed with a lower order attractive curve. The curve also illustrates the contact (S-Q) and non-contact (Q-R) operating zones of the AFM.*

In contact mode the tip is in close (sub nanometer) contact with the surface, and there exists a repulsive force between the two. Due to the extreme steepness of the curve in this region (S-P in figure 2.19), any attempt to bring the tip closer to the surface results in the bending of the cantilever to which the tip is attached. In the other mode of operation, namely non-contact mode, the tip is held between 1 and 10 nanometers from the surface. As is seen from the force-distance curve, the force between the sample and tip is attractive in this mode.

The role of capillary forces is important when considering any study not performed in an ultra high vacuum. If the sample is in contact with air then there almost always

exists an adsorbed layer of moisture on the sample surface. The effect of this layer on the force-distance curve is shown schematically below.

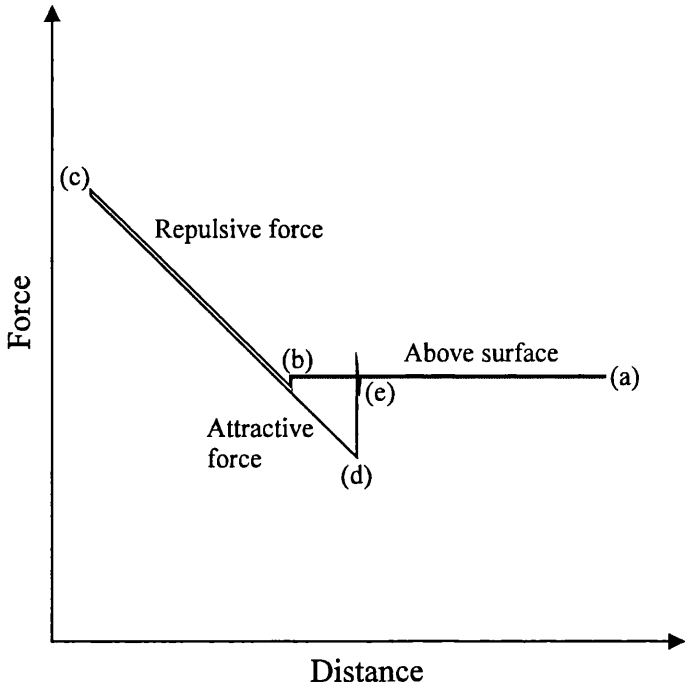

Fig. 2.20 *Force - distance plot for an AFM probe and a solid surface.*

In UHV the tip is brought close to the surface (a-b) until the attractive force causes the tip to be deflected towards the surface (b) and into the equilibrium position. Any further attempt to reduce the tip-sample distance pushes the tip into the very steep region of the van der Waals curve, and thus causes the cantilever to deflect (b-c). This deflection is approximately linear with distance, and the relationship between the force and cantilever deflection is given by:

$$F = k_s D \qquad (2.30)$$

where: F is the force

k_s is the spring constant

D is the cantilever deflection

On retraction of the tip a small amount of hysteresis occurs due to the tip moving into the non-contact mode (i.e. the cantilever is bent down). At a certain point (the pull-out point) the tip springs back from the surface (d-e). If a layer of adsorbed moisture is now considered to be present on the surface of sample then the force distance relationship of the tip and sample is modified by the fact that there is a large increase in the amount of hysteresis. This is due to the capillary force which strongly attracts the tip. Depending on the thickness of the adsorbed layer, or the presence of contaminants the shape of the hysteresis may be further effected, for example multiple pull outs may be observed. By varying the equilibrium setting of the tip on the force distance plot (called the set point) it is possible to optimise the imaging conditions for the sample. For example on soft samples such as biological tissue a high surface pressure exerted by the tip can destroy the sample. In this case it may desirable to use a negative set point to minimise the force. In practice care needs to be taken that the set point is not too close to the pull-out point, or the tip will retract from the sample during imaging. In the case of imaging crystal surfaces the set point can be slightly negative, without damaging the surface. Having discussed the various tip-sample interactions, the two imaging modes used in the work here, are now presented.

Once the tip has been brought into contact with the sample at the desired setpoint, the sample is scanned beneath the tip in a raster fashion by the xy piezos. Any undulations on the surface result in the deflection of the tip, and hence a change in the current detected by the position sensitive photodetector (PSPD). The spatial

variation of this current may be used to generate a map of the surface. This is the variable force mode of the AFM. At the moment of the current change being detected in the PSPD, the feedback system adjusts the height of the z piezo to bring the force back to the set-point value. The spatial map of the feedback voltage to the z piezo may be used to generate a constant force image of the surface, subject to the resolution limit of the z piezo. The two imaging methods each have different advantages. If height information is required on the sample surface then the constant force mode must be used. If on the other hand high scan rates, or high contrast of small features is required then often the variable force mode is used. In practice it is common to obtain both types of image simultaneously thus providing the benefits of both modes. It should be noted that many other imaging modes such as lateral force and tapping mode (particularly suitable for fragile biological material) are possible, and indeed are an active area of AFM research and development. However, since only the contact mode is used in the work here, these other modes are not covered here.

2.3.1 TIP - CANTILEVER

The fabrication of a tip-cantilever combination with a small and sharp enough tip is one of the technological achievements which allowed the AFM to be developed, and continues to be an area where many improvements are made. The basic manufacturing sequence for a silicon nitride tip is as follows:

1. A silicon wafer with a thermally grown layer of silicon dioxide is photolithographically etched to produce small squares.

2. Chemical etching of the Si produces pyramidal etch pits.
3. The silicon dioxide is removed and a thin layer of silicon nitride (Si_3N_4) is deposited on the surface according to the dimensions required
4. Once again a photolithographic process is used to create the shape of the cantilever.
5. The rear of the cantilever is coated with gold in order to optimise reflection of the laser beam.

The spring constant of the cantilever is also determined during the manufacturing process. A large variety of force constants are available, depending on the specific application and imaging mode required. For contact mode imaging of most surfaces, cantilevers with low spring constants are preferred since they do not damage the surface - values ranging between 0.05 and 0.5 N/m are typical. An example of a standard silicon nitride tip is shown in figure 2.21 below.

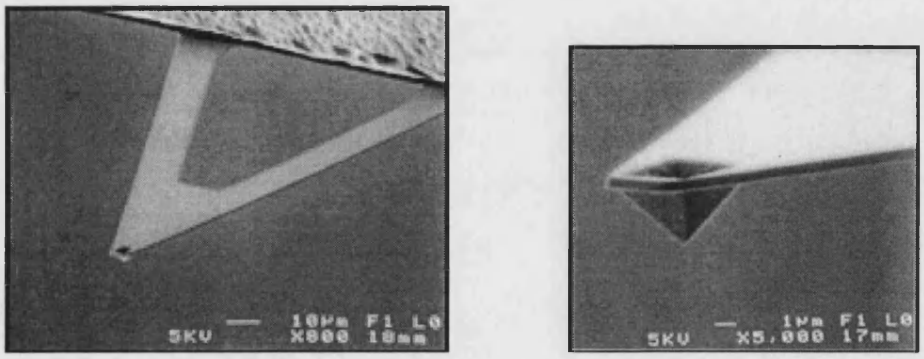

(a) (b)

Fig. 2.21 *SEM images of a Si_3N_4 probe illustrating the tip-cantilever combination (a) and the pyramidal tip (b) (Digital Instruments[45]).*

An important feature of the tip is its sharpness, which determines the available resolution. Rayleighs criterion may be adapted to this situation as shown schematically in figure 2.22.

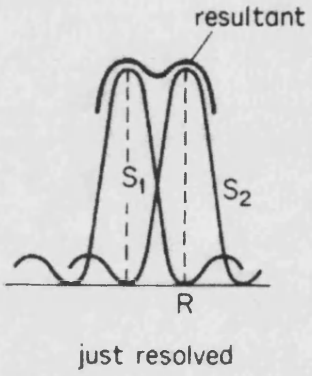

Fig. 2.22 *Resolution according to Rayleighs criterion: the resultant curve must dip at least 10% of the height of the features for them to be 'just resolved'.*

If the tip drops an amount of 10% of the total height of two neighbouring features, whilst travelling between the features, then these are considered to be resolved. Using the latest high resolution tips (see figure 2.23 for an example of a chemically sharpened tip) this translates to a lateral resolution of better than 20Å.

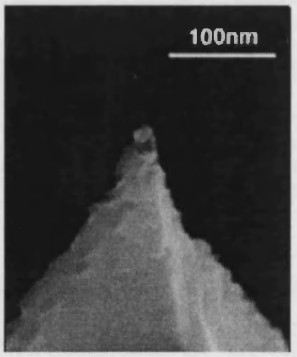

Fig. 2.23 *Chemically etched tip with a radius of around 50Å (Digital Instruments[45])*

Tip sharpness also gives rise to one of the most common imaging artefacts, namely tip imaging. This occurs when the aspect ratio of features on the surface is higher than that of the tip itself. In this case an image of the tip is effectively produced. Therefore pyramidal features observed on a surface should be treated with caution - particularly if the base - apex angle lies near the manufacturers specification of the tip in use.

2.3.2 THE PIEZOELECTRIC SCANNER

The role of the piezoelectric scanner is twofold. Firstly the scanner is used to control the value of the set-point between the sample and tip (z direction). Secondly the scanner is used to scan the sample beneath the tip (x-y plane). There are two basic designs of scanner. The first involves three piezoelectric ceramics, such as zirconium titanate oriented orthogonally. The second consists of a hollow tube divided into four segments. From the combined effect of voltages on these four piezos a fully functional scanner is achieved (see schematic in figure 2.27). Due to their compactness and light weight, tube scanners are commonly used in high resolution applications.

Although piezoelectric materials are essential to modern SPM's due to their sub angstrom resolution, fast reaction to applied voltage and light weight, many of the most common image distortions seen on AFM's are due to the non ideal characteristics which they exhibit. The most important of these are discussed below.

The mechanical deformation of a piezoelectric material by an applied electric field may be separated into two regimes. Initially the reaction time is fast and a rapid

extension of the piezo occurs. Subsequently, however, a small amount of extension occurs much more slowly. This effect is termed scanner creep and causes a distortion on images, in particular on vertical features. A common example of a sample exhibiting periodic vertical features is a semi-conductor grid. Due to the uniformity of such grids they are frequently used as calibration devices for AFM's and are therefore useful samples on which to illustrate image artefacts. In figure 2.24 below the effect of creep on the imaging of such a surface is isolated.

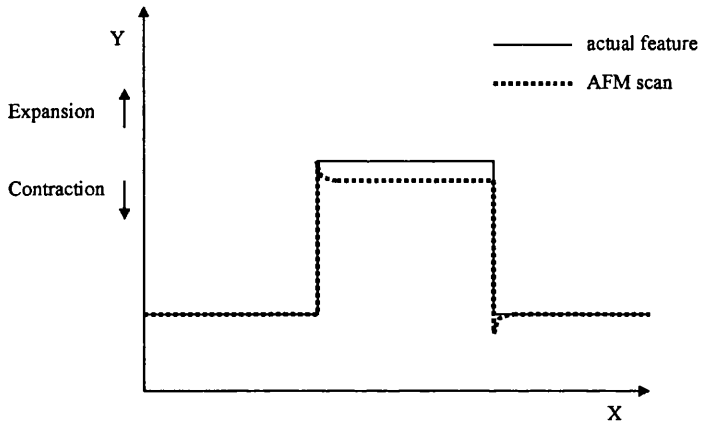

Fig. 2.24 *Effect of scanner creep on a periodic feature.*

Piezoeletric materials do not exhibit an exactly linear relationship between the applied voltage and the extension (i.e. $s \approx kE$, where s is the strain and E is the applied electric field).

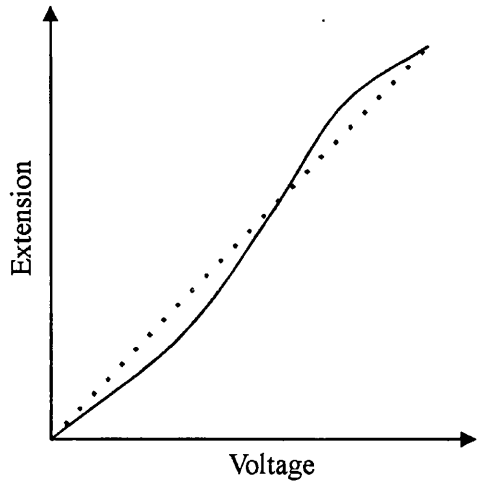

Fig. 2.25 *Non-linear behaviour of scanner.*

As shown in figure 2.25 above, the relationship has the form of a curve with an inflection. This has the effect that once calibrated, the height measurement will only be correct for surface features close to the calibrated height. For features with significantly different heights, over or underestimates of the height will be recorded. In addition to the non-linearity, piezoelectric materials also display hysteresis of up to 15%. Depending on whether the scanner is calibrated for extension or contraction, the height of a uniform object will therefore either be initially underestimated or finally overestimated: the situation is illustrated in figure 2.26.

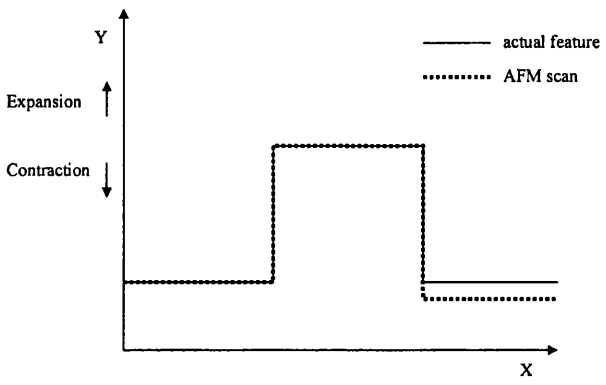

Fig. 2.26 *Effect of scanner hysteresis on a periodic feature.*

In the case of a tube scanner there is an additional image artefact which will be introduced. This is due the method by which movement in the xy plane is produced - contraction of one set of piezos together with expansion of the other two (see figure 2.27 (a). The result is that a bowed surface is scanned rather than a plane. The effect of this on the image is readily visualised, and is illustrated in figure 2.27 (b).

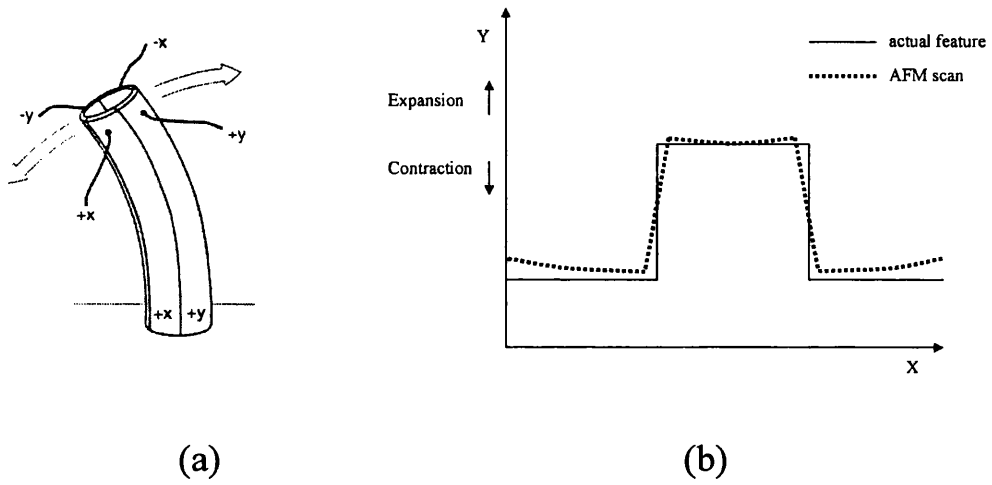

Fig. 2.27 *Figure (a) demonstrates the functioning of the tube scanner, whilst in (b) the effect of cross-coupling on a periodic feature is shown.*

Finally it should be noted that time and temperature will also both affect the scanner. During production of the piezos the dipole moments are aligned at a temperature of around 250°C. Subsequently to this there is a slow randomisation of the dipoles at room temperature, which increases markedly for higher temperatures (Curie temperatures of around 180°C are typical). Therefore exposure of the scanner to high temperatures should be avoided, as should prolonged periods of non-use (the voltage applied during normal use helps to maintain the dipole moments).

In the discussion above the focus has been on the effect of non-ideal behaviour of the piezos in the z direction. It will be appreciated that similar problems are also encountered in the xy plane during scanning. For example creep will cause drift of the image subsequent to moving the scanner to a new area on the sample. In order to minimise the effect of hysteresis in the xy plane during scanning, the spatial map of the surface is produced from only one direction of the scan (i.e. either the +x or -x direction). Because of this it is possible to choose the image from either the forward or reverse scan. Depending on what is being imaged, one of these directions may provide higher contrast for the features of interest.

In order to illustrate some of the effects discussed above, it is useful to show a practical example. Figure 2.28 shows an AFM scan of a semiconductor grid. The scan area seen here is 20 μm. The image was recorded using a Topometrix Explorer, with a tube scanner. On such samples it is also possible to gain an insight into the vertical resolution of the instrument. In the case of both the Topometrix Explorer and the Nanoscope III this was found to be of the order of 0.25 nm.

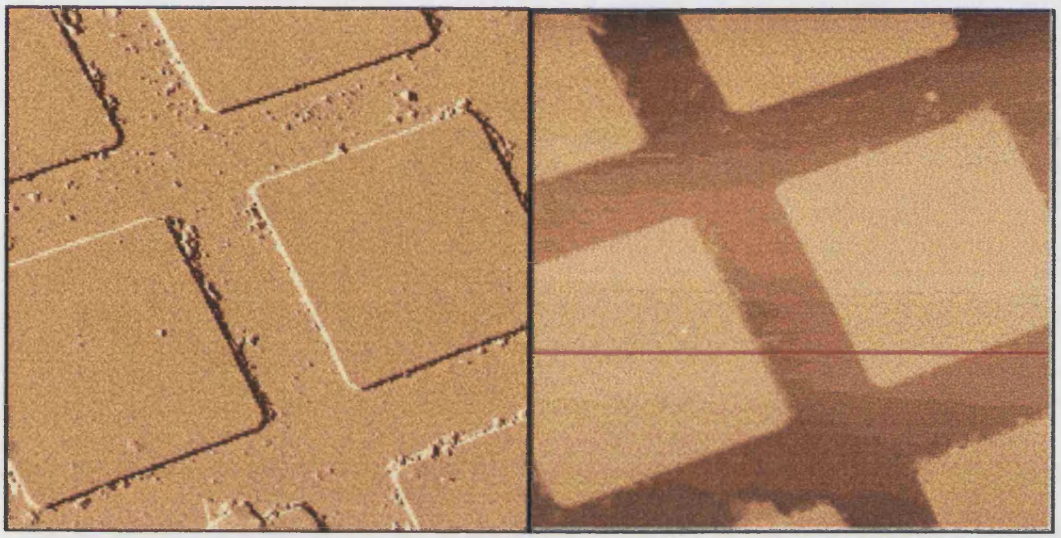

(a) (b)

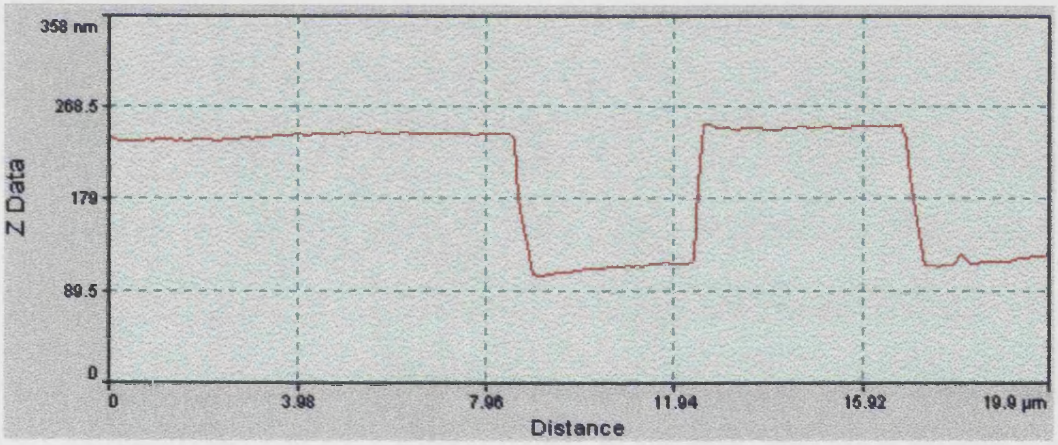

(c)

Fig. 2.22 *The combined effect of cross-coupling, scanner hystersis and creep are seen in the line scan in (c) corresponding to the red line on (b). In (a) the improved contrast of the variable force image is illustrated.*

2.4 X-RAY TOPOGRAPHY

X-ray topography (XRT) is a diffraction technique, which provides a means for the direct observation of strain fields within a crystal. A projected volume image of a crystal is produced by a topographical mapping of X-ray intensities.

There are a number of different experimental set-ups with which X-ray topographs may be recorded using laboratory X-ray sources. In the work here, however, the synchrotron radiation source stationed in Daresbury, UK was used. The use of synchrotron radiation has not been covered extensively for X-ray topography work[46], however, it shares many of the essential features of the more commonly used laboratory sources. Therefore the discussion below begins with an outline of the image formation mechanism for laboratory sources, followed by an overview of the important differences when dealing with a white synchrotron radiation source.

2.4.1 IMAGE FORMATION OF STRAIN FIELDS

Strain fields within crystals may be visualised using X-ray topography, since they produce a contrast variation with respect to non-strained regions of the crystal. In order to understand the origin of the image contrasts, a brief discussion of the two ways in which an image may be formed is given. These are termed the dynamical image and the kinematical image respectively.

The kinematic or direct image occurs when the absorption of a perfect crystal is low. In terms of crystal thickness this is often defined as approximately[47]:

$$\mu_0 t < 1 \qquad (2.31)$$

where: μ_0 is the linear absorption coefficient

t is the crystal thickness

For thin crystals the image contrast may be understood in terms of the kinematical theory of X-ray diffraction. This is essentially an extension to three dimensions of the optical theory developed for one dimensional diffraction gratings.

Because of the low absorption a large amount of the energy of the beam will pass through the crystal. Once again, therefore in the case of a perfect crystal a featureless grey image would be produced on the X-ray topograph. If defects are present in the crystal then because in these regions the Bragg condition is slightly different, extra intensity from the incident beam will be diffracted. This extra intensity is provided from the fact that the divergence of the incident beam is 3 to 4 minutes of arc compared with the diffracted divergence of 3 to 10 seconds of arc.

The dynamical image becomes more dominant when dealing with thicker crystals. A convenient definition of a thick crystal in X-ray terms is if the following condition is satisfied:

$$\mu_0 t > 10 \qquad (2.32)$$

For a crystal of this thickness, most of the radiation will be absorbed by the crystal. The exception is if the Bragg condition is met:

$$\lambda = 2d \sin\theta \qquad (2.33)$$

where: λ is the wavelength

d is the interplanar spacing

θ is the angle of incidence

In this case a significant amount of the beam energy may pass through the crystal unattenuated. This is because two standing wavefields are generated within the

crystal, with a wavelength equal to the interplanar spacing. One wavefield has its nodes situated on the lattice points (termed the β wave) and is therefore strongly absorbed. The other wavefield, however, has its nodes situated midway between the lattice points (the α wave) and will therefore have a far lower absorption (approximately one order of magnitude less than μ_o). The wavefield has both a forward diffracted and diffracted component, so that a 'fan' shape is produced from the point of entry of the beam into the crystal. This is sometimes called the Borrmann fan. The angle of the 'fan', is the angle between the diffracted and forward diffracted beams and is equal to twice the Bragg angle.

In the case of a perfect, thick crystal the recorded image will therefore consist of an even, light grey contrast on the photographic emulsion. If, however, imperfect regions are present within the crystal then the wave field will collapse in the vicinity of the defective region. The result is that these areas will show strongly reduced (usually zero) contrast and produce a white region on the X-ray topograph.

Lang[48] has stated that the two most important formulae for practical X-ray topography (apart from Bragg's law) are the extinction distance:

$$\xi_g = \frac{\pi V \cos\theta_b}{\lambda |F_a|} \qquad (2.34)$$

and the rocking curve width:

$$W_0 = \frac{2d}{\xi_g} \qquad (2.35)$$

where: λ = wavelength of the radiation

F_a = structure factor of the reflection

V = unit cell volume

θ_b = Bragg angle

d = interplanar spacing

The extinction distance is useful in determining whether defect contrast will be sufficient. For specimens with a thickness below approximately $^1/_3$ to $^1/_4$ of ξ_g, diffraction contrast is not usually acceptable.

The rocking curve width is useful in determining suitable parameters to optimise the spatial resolution. For a high spatial resolution a large rocking curve width (low strain sensitivity) is required. This equates to a large structure factor, high wavelength and low order reflection.

2.4.2 Pendellosung Fringes

A further consequence which follows from the dynamical theory of X-rays is that interference may occur between the α and β wavefields. This will only occur if the crystal is highly perfect and there are is little disturbance to the wavefields. In this case interference fringes may be seen on the X-ray topographs.

2.4.3 Application to White Synchrotron Radiation

There are a number of important differences between the synchrotron source and a laboratory source when considering the mechanism of image formation. In summary these may be listed as follows:

- The photon flux from the synchrotron source is orders of magnitude higher than for standard laboratory sources (with the exclusion of rotating anode generators)

- A continuous power spectrum is delivered from the synchrotron source.
- The beam divergence is very low (approx. 10^{-5})

From these difference several important points arise with respect to X-ray topography. Firstly, due to the much higher power and large area of the beam, it is possible to image entire crystals (with dimensions of 1-2 cm) in a single exposure of between 1-30 mins depending on the beam current and film type. Secondly, the kinematical image is formed by misoriented regions within the lattice surrounding the defect diffracting wavelengths which do not participate in the diffraction from the perfect crystal. This follows from the fact that a continuous power spectrum is delivered by the synchrotron source. Therefore, as was the case for laboratory sources, the kinematical image of a defect is registered as a region of increased contrast.

2.4.4 Characterising Growth Defects within Crystals

Generally a diffraction contrast image will be produced if there exists, within a crystal, a region where:

$$\mathbf{g}.\mathbf{u}(r) \neq 0 \qquad (2.36)$$

Where: **g** is the diffraction vector

u(r) is a displacement vector

The displacement vector may be due to features such as growth striations, stacking faults, growth sector boundaries and dislocations. Since the characterisation work is mainly concerned with dislocations, due to their role in the crystal growth process, the rest of the description is focussed on them.

From (2.36) it follows that dislocations will appear invisible if:

$$\mathbf{g}.\mathbf{u}(\mathbf{r}) = 0 \qquad (2.37)$$

This simply means that the displacement vector normal to the reflecting planes is zero, and is satisfied for screw dislocations when:

$$\mathbf{g}.\mathbf{b} = 0 \qquad (2.38)$$

where: **b** is the Burgers vector of the dislocation

and for edge dislocations when:

$$\mathbf{g}.(\mathbf{b}\Lambda\mathbf{l}) = 0 \qquad (2.39)$$

where: **l** is the line direction of the dislocation

In the case of mixed dislocations there is always a component of strain non-perpendicular to the diffracting planes, however, contrast will be minimised when the dominant strain vector is normal to the diffracting planes.

From the above analysis it follows that if two reflections may be obtained in which a given dislocation is invisible, the intersection of these two planes uniquely define the Burgers vector of the dislocation.

3. LITERATURE REVIEW

3.1 POTASSIUM HYDROGEN PHTHALATE (KAP)

Potassium Hydrogen Phthalate K·C_6H_4·COOH·COO (also known as potassium acid phthalate, and abbreviated as KAP) belongs to a series of alkali acid phthalates which crystallise in the orthorhombic system. KAP has been studied by a number of groups, mainly due to its suitability as a model compound. However, it has also found limited practical use, for example in X-ray monochromators[49,50,51], and as a piezoelectric material[52]

The structure of KAP has been determined by Okaya[53] as a noncentrosymmetric $P2_1ab$ space group, with lattice parameters a=6.466 Å, b=9.609 Å and c=13.857 Å, and four molecules per unit cell. For practical reasons Jetten[54] exchanged the crystallographic axes giving a=9.609 Å, b=13.857 Å, and c=6.466 Å and space group $Pca2_1$, which will also be used in the work here. KAP crystallised from aqueous solution is dominated by the (010) face, giving rise to a platelet morphology. The other faces present occur in the following order of importance: {110}, {111}, {121}, {210}, {120} & {102}[55].

The solubility of KAP in water has been covered by numerous authors[56-60]. The most recent data given by Šolc[58] agrees well with that of Hendrixson[59], and is the solubility equation used in the work here (see section 4).

KAP has been the subject of a comprehensive PBC analysis by both Hottenhuis[61] and Jetten[62]. A summary of the main findings is given below.

A PBC analysis of the morphological importance of the F faces gives the following order[62]: (010), {110}, {200}, {210}, {111}. Comparing this with the experimentally observed order of importance given above reveals that whilst the most important face, the (010) face, and the {110} face are correctly predicted, a number of other faces are not. The {120} and {121} are not even F faces according to the analysis, but are of the S type. Possible reasons for this discrepancy are given below.

The popularity of KAP as a model compound for crystal growth studies is due mainly to the very well developed step system on the (010) face. The fact that these steps often bunch to form macro-steps, means that they may be observed relatively easily using interference techniques such as differential interference microscopy (DICM). The first studies of the step morphology were by Enckevoort and Jetten[63], followed by numerous others[64,65,66]. The typical step pattern observed is shown schematically below in figure 3.1. together with a DICM image of the (010) face of a KAP crystal.

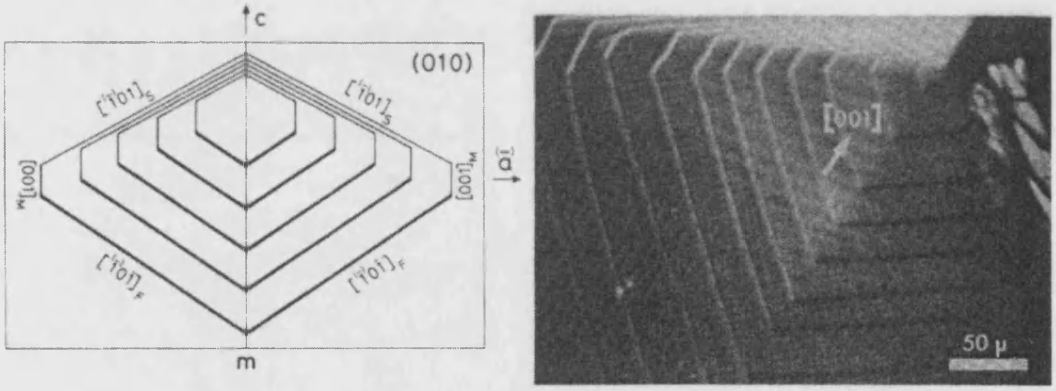

Fig. 3.1 *Schematic diagram of the (010) face of KAP and DICM image for comparison[61].*

As described in the theory section, a PBC analysis may also be used on a particular face to predict the bounding directions of a growth spiral if this is polygonised in form. For KAP this analysis correctly predicts the appearance of the [101] type steps on the (010) face as those having the highest bond energy[61]. The [001] step direction is, however, not predicted. In fact, in terms of the energy associated with the bonds per molecule in the [001] direction and [100] direction, the [100] direction is preferred. This is in contradiction with experiment, as the [100] step direction has never been observed. It would appear therefore that some factor external to the simple PBC analysis is present. One known limitation of the standard PBC analysis is the assumption that the surface structure is essentially similar to the bulk. For many materials, however, this may not be correct due to the missing interactions with half of the bulk, and new interactions with the medium now in contact with the surface. This phenomenon is known as surface relaxation, and may result in the formation of new PBC's not apparent from the more simple approach. A further problem rather peculiar to KAP is the large number of different bonds type present. Coulombic forces exist between the ions, hydrogen bonding is present between the ionised and un-ionised carboxyl groups of neighbouring molecules and finally van der Waals forces are also present. This rather complicates the PBC analysis, with the result that certain simplifying assumptions need to be made. The final limiting factor in the traditional PBC analysis is the neglect of impurity influences. From the above it therefore seems quite likely that either an oversimplification in the PBC analysis or surface reconstruction, combined with an impurity effect may lead to an extra stabilising effect of the [001] steps.

One of the most prominent features of the observed growth spirals on the (010) face of KAP is that the growth hillocks are not only polygonised but also anisotropic. The anisotropy is such that growth rates in the [001] and [00$\bar{1}$] directions are not equivalent. Hottenhuis[61] has suggested a growth rate discrepancy of the [101] steps in the fast and slow directions of about a factor of ten, whilst Jetten[62]has suggested a factor of approximately five.

A reason for the anisotropy has been suggested by Jetten[63]. If the dissociated KAP ions (K^+ and HP^-) are considered to enter the structure as individual growth units then a discrepancy may exist between the relative adsorption rate of these two species. K^+ will be surrounded by 4 water molecules in aqueous solution and has a solvation enthalpy of -84 kcal/mol[67]. This is likely to be higher than the hydration enthalpy for the HP^- species, since the charge will be delocalised over the ion. Therefore it is possible that the incorporation of the K^+ ion in the lattice is the rate determining step for growth of the crystal. If this is considered to be the case, the growth behaviour of the spiral can be reduced to a consideration of the likely rates of incorporation of the K^+ ion. Since KAP is non-centrosymmetric it follows that the bonds formed on a face (hkl) and ($\bar{h}\bar{k}\bar{l}$) will not be equivalent if h,k&l are non zero. The implication of this is that opposite faces e.g. the (1$\bar{2}$1) and ($\bar{1}$2$\bar{1}$) faces on the crystal will have different growth rates. This is also true for the relative growth rates of a unit cell height polygon on the surface of the crystal. On the (010) face of KAP the difference in energy associated with a bond on the [001] and [00$\bar{1}$] direction is equal to 10.8 Kcal/mol.

The use of in-situ methods has allowed the step kinetics of the different step directions to be studied[68-72]. At low supersaturations (1-4%) the velocity of the fast steps varied between 0.7 and 2.2 μm/s, whilst the slow steps did not move at all. At higher supersaturations (5-7%) the slow steps had velocities of 0.2-0.4 μm/s and the fast steps 2.5-3.6 μm/s[70]. Because more data points are available for the fast step direction the kinetic coefficient may be estimated in this direction to be approximately 50μm/s.

The polygonised step morphology shown in figure 3.1, has been shown to be susceptible to the presence of impurities, which has led to a number of impurity studies[61,73]. In particular the influence of a number of different cations on the shape of the spiral has been studied. In all cases the tendency of the impurity cations was to reduce the amount of polygonisation. In the case of some cations, such as Cr^{3+}, the spiral became completely round.

Several in-situ studies have also investigated the influence on the growth spiral due to impacting with a glass rod[74,75,76].

As already discussed, the role of defects in the crystal growth process are of a paramount importance. There exist a limited number of studies on the growth defects of KAP. These may be divided into two groups - etching studies[63,77]and X-Ray topography studies[78-82].

From the etching studies[63,77] it is tentatively suggested that dominant hillocks on the (010) face of KAP are associated with multiple dislocations whereas minor hillocks are due to only a single dislocation. It was also noted that as the (010) surface was etched back, it frequently occurred that two etch pits became progressively closer together. This suggests a V orientation of the dislocations.

The defect studies utilising X-Ray topography[78-82] cover the general defect structure, however, no significant amount of dislocation characterisation is present. In general the crystals were noted to be of a relatively low defect density.

3.2 AFM STUDIES OF CRYSTAL GROWTH

Since its introduction, AFM has not been applied to a very large number of studies for crystal growth from solution. The reason for this lies in the fact that in-situ studies require very low growth rates due to the slow scanning speed of current AFMs. If an ex-situ approach is adopted, then to make use of the higher resolution capabilities a concurrent increase in the degree of surface protection during removal is required.

Because of this, in-situ studies are typically restricted to materials which are barely soluble[83-86], or high molecular weight materials, such as proteins, which have low step kinetic coefficients[87-92]. The amount of work on small molecule materials is limited[93,94,95], with the possible exception of KDP[96,97,98]. Of the different materials studied, it is primarily the work on KDP which is of relevance to the work here. Many of the dislocation cores observed on the {101} face of KDP were found to be hollow[97]. Theoretical calculations on the basis of equation 2.27 in section 2.1.3 confirmed the likelihood of this occurrence, provided the Burgers vector was larger than single unit cell height. Furthermore, the measured core radius was found to be similar to that predicted theoretically. From ex-situ experiments it was found that over a large range of supersaturations (between 3 and 30%) there was very little

change in the terrace widths. This is in conflict with the BCF theory, since from equations 2.10 and 2.25:

$$y_0 \propto \frac{1}{\ln\left(\frac{C_B}{C_E}\right)} \qquad (3.1)$$

Using a rate model which takes the modified period of step rotation about a hollow core into account, good agreement with the experimental results was found.

As far as the material KAP is concerned there is only a single study using scanning force microscopy[99], which however studies the layer structure of the compound and in no way relates to the crystal growth process.

In this study we have chosen to study KAP in detail with a combination of X-Ray topography and AFM. Existing DICM surface topography work provides a useful low resolution comparison for images, as well as an experimental background for the use of the newer AFM. More detailed use of X-Ray topography than previously allows better characterisation of defect structure which may then be coupled with AFM analysis.

4. EXPERIMENTAL METHODS

4.1 CRYSTAL GROWTH OF POTASSIUM HYDROGEN PHTHALATE (KAP)

The solubility curve of KAP as described by Šolc[58] was used for the preparation of all KAP solutions used in this study. The equation is:

$$C(T) = 9.283 - 0.059T + 0.0058T^2 \qquad (4.1)$$

where: c(T) is the amount of KAP per 100 cm^3 of water

T is the temperature in °C

A graphical representation of this relationship is given in figure 4.1 below:

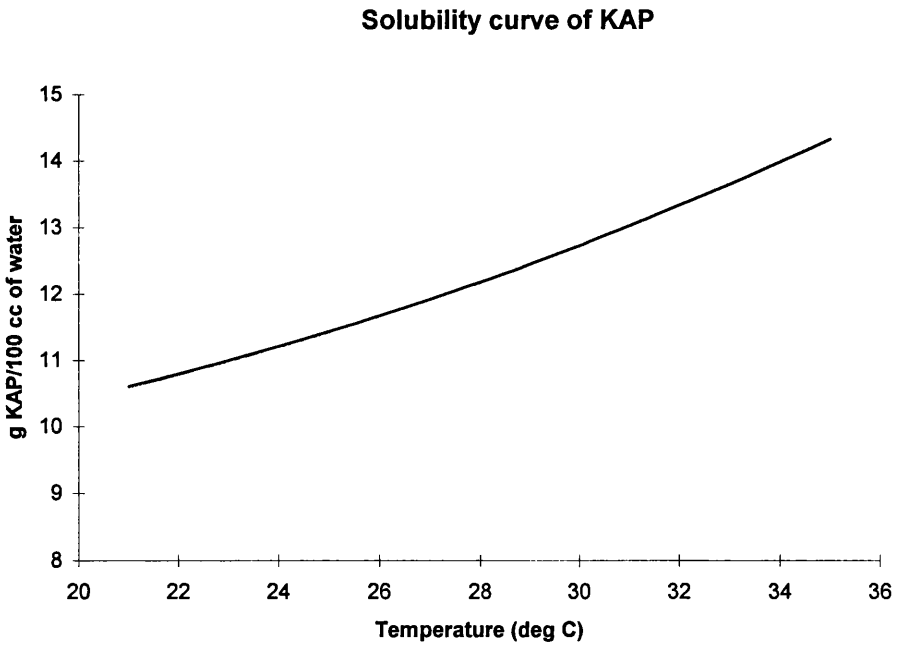

Fig. 4.1 *Solubility of KAP in water as given by Solc et al*[51]

4.1.1 Growth by Spontaneous Nucleation and Evaporation Induced Growth

For experimental work using X-ray topography in particular, but in some instances also AFM, relatively large crystals were used. These typically had a largest dimension ranging from about 0.5 cm to 3 cm.

A solution of recrystallised commercial KAP (BDH, Analar grade) in distilled water was prepared with a saturation temperature of 35°C. To ensure the complete dissolution of KAP the solution was heated to a temperature of 50°C whilst stirring with a magnetic stirrer. After stirring for a period of several hours the solution was filtered at 50°C into crystallising dishes through a 40μm sintered glass filter. The crystallizing dishes were subsequently covered with polyethylene film in which several small perforations were made to allow slow evaporation of the solution. The crystallising dished were all placed in an incubator regulated at a temperature of 35°C. Typically nucleation of crystals would occur after 1-4 days. Due to the evaporation of the solution through the perforated holes the solution was maintained in a metastable condition and growth occurred in an uncontrolled, but slow manner. Of the various crystals present in a given crystallising dish usually only a small fraction, if any, were of suitably high quality to be used in further experimental work. These crystals were removed from solution with extreme care using specially fabricated balsa wood implements. Prior to removal of the crystals from solution a thin (0.5 cm) layer of n-hexane (pre-heated to 35°C) was introduced onto the surface of the solution. The crystals were therefore withdrawn through this layer, thus ensuring complete separation from solution before exposure to air. This common protection method has been used previously to protect KAP crystals surfaces[62].

Immediately after withdrawal through the n-hexane layer the crystals were further rinsed with n-hexane. In some cases a jet of n-hexane was directed on the crystal surfaces during the withdrawal through the n-hexane layer.

An example of a large crystal produced in this manner is given in figure 4.2 below. The largest dimension is approx. 3 cm.

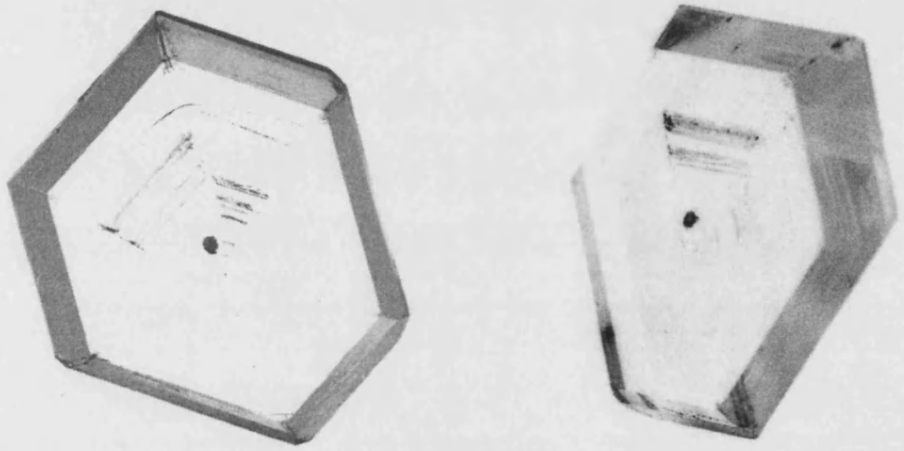

(a) (b)

Fig. 4.2 *KAP seed crystal grown by spontaneous nucleation and growth. The large face in figure (a) is the (010) face. In figure (b) the platelet habit of KAP is shown.*

4.1.2 CRYSTALS GROWN BY TEMPERATURE LOWERING (LOW SUPERSATURATIONS)

For crystals grown in the undercooling range 0.5-5°C, a growth cell was used with a volume of 800 ml. The cell was surrounded by a jacket of water thermostatted by a Haake DC-5 controller mounted in an refrigeration bath. The temperature accuracy of the bath was ± 0.05°C (manufacturers specification). The bath was stirred using a magnetic stirrer with a rotation speed of 60 RPM. Above the solution a layer of approx. 3cm of n-hexane was present. This had the function of eliminating

concentration changes due to water evaporation, and protection of the crystal(s) during removal from solution. The set-up is illustrated schematically in figure 4.3 below.

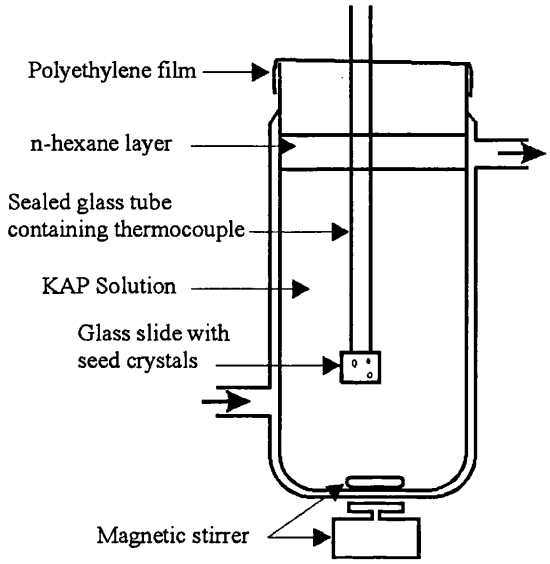

Fig. 4.3 *Schematic diagram of the growth cell used for low supersaturation growth of KAP micro-crystals*

Seed crystals for the growth of the micro-crystals were prepared by introducing a droplet of saturated solution (approx. 30%) onto a small (5 mm side) square of glass cut from a microscope cover slip. After periods of typically 30 seconds, depending on ambient conditions, micro-crystals nucleated on the glass slide. The number of nuclei varied between approx. ten to several hundred. Slides with a relatively low (ten - thirty) number of nuclei were typically selected for further crystal growth. Such slides were glued to a glass rod using a cyano-acrylate adhesive in preparation for subsequent growth.

A typical growth run was started by heating the solution in the growth vessel to a temperature approx. 10 degrees above the saturation point, in order to ensure the removal of any undissolved nuclei. After stirring at this temperature for approximately 30 minutes the bath temperature was set to the appropriate undercooling temperature. Whilst the bath was cooling to this temperature the seed crystals were introduced at a temperature just *above* the saturation point of the solution. In this manner a small amount of dissolution was effected on the micro-crystal seeds. The seeds were then left to grow for a period of time dependent on the undercooling (see table 4.1). Due to the relatively large volume of the growth cell relative to the micro crystals, the supersaturation change within the cell during growth was estimated to be less than 1%, taking into account the number of micro crystals growing on a typical slide. Subsequently the grown crystals were removed from solution via the layer of n-hexane. In some instances an n-hexane jet was directed at the crystal surface in addition to withdrawing through the n-hexane layer. The jet was produced by squeezing a standard polymer solvent bottle, equipped with a polymer nozzle. In addition to using n-hexane, experiments were also performed using other solvents in order to protect the surface. The method of protection was as described for n-hexane. The following solvents were used:

n-octane; n-decane; benzene; cyclohexane.

In other instances no solvent layer was used to protect the surfaces. Instead the crystals were withdrawn through a jet of compressed air (approx. 50 psi).

Supersaturation (%)	0.5	1	1.5	3	5	10	14
Growth time (mins)	180	120	120	30	15	2-5	1-5

Table 4.1 *Overview of growth run times for various supersaturations*

4.1.3 CRYSTALS GROWN BY TEMPERATURE LOWERING (HIGH SUPERSATURATIONS)

For crystal growth of micro crystals at the higher end of the supersaturation scale (5%-30%), a large volume cell is not practical, due to large amounts of secondary nucleation occurring on the crystals during removal (leading to agitation of the solution) from the growth cell. In order to solve this problem a small growth cell was developed (Volume - 0.035 cm^3). The temperature of the cell was controlled by maintaining thermal contact with a heater element via a thermal conducting paste. A Zeica thermal imaging camera was used to determine the temperature profile of the growth cell on the heating element. The temperature difference between the surface of the growth cell and the surface of the heating element was found to be better than 0.1°C. Thermal equilibrium between the growth cell and the heating unit occurred within several minutes.

The production of seed crystals was achieved either in the same manner as described previously - for supersaturations of up to 9% - or nucleated within the cell during the growth run itself for higher supersaturations.

Protection of the crystal surfaces occurred in the same manner as described for the crystals grown at low supersaturations

4.2 X-RAY TOPOGRAPHY

X-Ray topographs of a large number of evaporation grown KAP crystals were studied.

The X-Ray source used was station 7.6 situated in Daresbury laboratory (DRAL).

The preparation of crystals for XRT was as follows:

- Usually crystals grown by the spontaneous nucleation and growth method described above have a significant amount of strain associated with the surface region. This may be removed by polishing the crystals in a suitable solvent. For KAP this was performed on several crystals by polishing the crystals, using light finger pressure, on a damp cotton cloth, spread over a sheet of glass. Subsequent to this treatment, the crystals were etched by immersion in water to remove any remaining surface strain.
- Some crystals were used in the 'as grown' condition, i.e. without the polishing step.
- In a few cases the crystals were cleaved prior to the XRT. This was achieved with a sharp razor blade, cleaving parallel to the large (010) face. This was followed by a polishing step as described previously.
- The crystal, prepared by one of the above methods, was then clamped between two sheets of amorphous polymer film in a sample holder.

The diffraction geometry of the crystal was the Laue (transmission) geometry, and is shown schematically in figure 4.4 below.

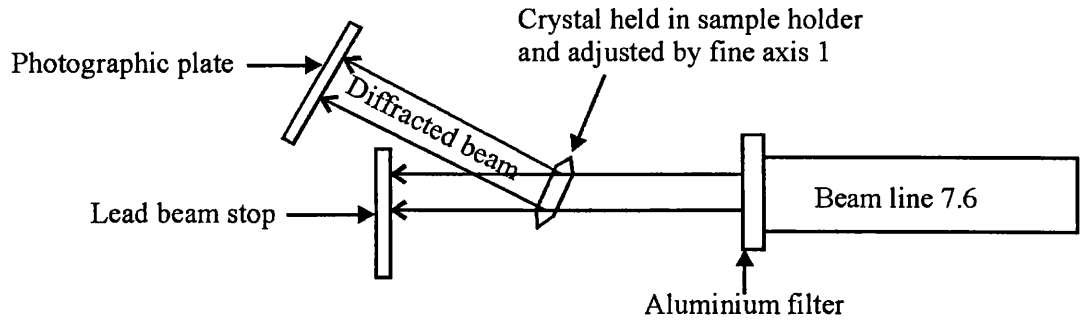

Fig. 4.4 *Schematic diagram of the diffraction geometry used during the X-Ray topography of KAP.*

The crystal was mounted in the beam path at the correct angle (interplanar angle + Bragg angle) to diffract X-Rays of 0.9 Å wavelength. This wavelength was selected since the cutoff wavelength of the synchrotron source is approximately 0.45 Å, and therefore higher order harmonics are eliminated. An aluminium filter was placed between the source and the crystal in order to protect the crystal from damage by long wavelengths. These are absorbed by the aluminium. Photographic plates (Ilford L4 nuclear plates) were mounted on the detector arm at twice the Bragg angle and set normal to the diffracted beam (since the emulsion has a finite (25μm) thickness).

Exposure and development times of the nuclear plates were adjusted experimentally according to the crystal thickness and beam current (300 mA at injection decaying to circa 150 mA), but were typically 20 mins and 10 mins respectively.

The thickness of the KAP crystals varied between approximately 1 and 3 mm. Since KAP has a linear absorption coefficient of 11.5 cm^{-1} at 0.9 Å, this corresponds to a μt product for the samples in this study of between approximately 1 and 3.

4.3 Atomic Force Microscopy (AFM)

Two different commercial AFM's were used for work here, namely the Nanoscope III SPM controller with a multimode AFM head produced by Digital Instruments and a Topometrix TMX 2010 scanning probe microscope with a Topometrix Discoverer AFM stage. These are shown in figure 4.5 below.

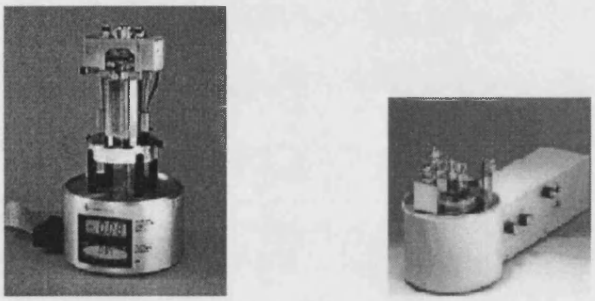

(a) (b)

Fig. 4.5 *The two commercial atomic force microscopes used in this work. In figure (a) is the Digital Instruments Nanoscope III and (b) the Topometrix TMX 2010 scanning probe microscope.*

In practice the two AFM's differ in detail, but are broadly similar to operate.

In order to prepare the samples for imaging the following procedure was followed:

1. The sample (usually a glass slide containing many KAP micro-crystals) was mounted on metal disk, which was fixed to top of the scanner via a magnet.
2. The cantilever was brought close to the sample surface via a mechanical coarse adjustment method. On the Topometrix, the tips used were silicon nitride 'v' shaped cantilevers with a nominal force constant of ≈ 0.03 N/m. The length of the

arms was 200μm. On the Nanoscope the tips used were silicon probes with a nominal force constant of ≈ 0.2 N/m. The probe length was 450 μm.

3. This was followed by a software controlled tip approach, until the tip was in contact with surface (for contact mode). The proximity of tip was controlled by the z-set point. In this work the set point was usually set to zero, but was occasionally lower depending on specific tip behaviour.
4. The size of the scan area was set. The maximum and minimum scan areas are dependent on the range of scanner used. For the topometrix three scanners were used, namely: 8μm, 70μm & 75μm. These figures refer to the maximum x-y scan area of the scanners. Since most crystals viewed were of the order of 500μm, and it was desirable to image relatively large areas of the surface, in most cases the larger scanners were used. For some higher resolution work, however, the 8μm scanner was also used. In the case of the Nanoscope a large (120 μm) scanner was used in all cases. This scanner proved to be superior to the topometrix scanners, and was therefore also used for the higher resolutions.
5. The scan speed was set. For imaging of the surface in variable force mode, relatively high scan speeds may be set (approx. 20 times the scan area), however when height information (constant force mode) is required a lower (approx. 1-5 times the scan area) scan speed is required, due to the time dependency of the response to the feedback loop which adjusts the z-piezo height.
6. PID settings. Proportional, Integral and Differential settings are the final step in tuning the quality of the image. The optimum setting of these is determined

experimentally, and is very dependent on the nature of the surface. As a general starting point the following settings were used:

P=2.5; I=0.1; D=0

7. Image Analysis. Within the software of the AFM package a number of image manipulation algorithms are available. However in order to avoid excessive altering of the image in all cases only a histogram adjust and levelling of the image was performed (if necessary).

In order to ensure that the image obtained was free from artefacts the following procedures were routinely carried out:

- Repeating of the scan in order to check for discrepancies.
- Altering of the scan direction to check for consistency of imaged features.
- Changing of the scan size in order to verify correct scaling of the features.
- Rotation of the sample to check spatial alignment of features.
- Variation of the scan speed (useful for checking quasi-periodic features).

5. RESULTS AND DISCUSSION

5.1 CHARACTERISATION OF DEFECTS USING X-RAY TOPOGRAPHY

5.1.1 INTRODUCTION

As already discussed in the literature review, one aspect of KAP that has received relatively little experimental attention is the dislocation density and character[63,77-82]. In view of the fundamental role which modern crystal growth theories have assigned to the influence of defects on growth behaviour, this aspect of the growth characterisation is essential in order to allow a complete understanding of the surface growth features. One of the most effective methods for a thorough characterisation of the defect structure of low defect crystals is X-ray topography. As discussed above, however, the work on KAP has mainly been performed using etching techniques which offer limited scope for detailed analysis of dislocations types.

In the work presented here many different X-ray topograph reflections of a variety of solution grown KAP crystals were studied. This has made it possible to determine the general defect structure present in solution grown KAP crystals as well as characterising most of the commonly seen dislocation types. In particular, it has been possible to provide strong evidence concerning the character of the dislocation types emerging on the large (010) face. It is this face which has been central in most of the studies concerning KAP, and indeed is also the face on which all the AFM studies contained within this thesis were performed.

5.1.2 Results and Discussion

All of the X-ray topographs shown in this study indicate that the selected crystals of KAP were of very high quality.

A good illustration of this fact is the X-ray topograph shown in figure 5.1.1. A first glance immediately reveals the low defect density. This is particularly true, since this topograph is of an entire 'as grown' crystal which has not been sliced or prepared in any way.

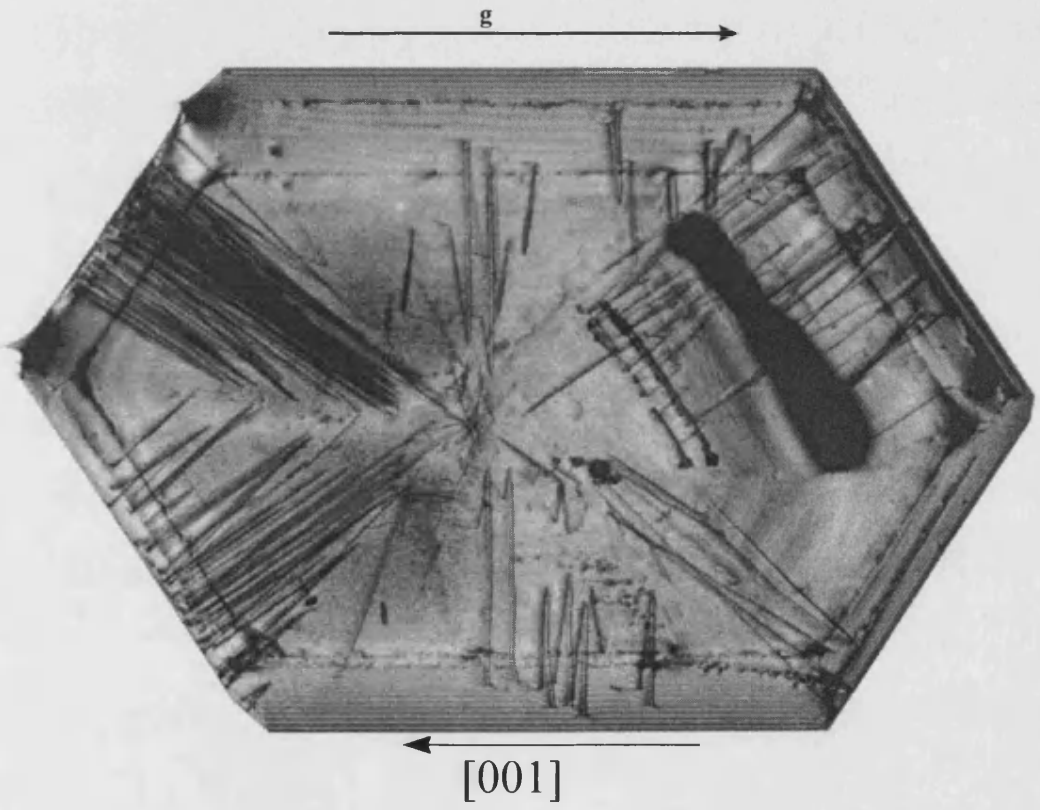

Fig. 5.1.1 *$01\bar{2}$ reflection of an entire, untreated, solution grown KAP crystal. The largest dimension is approx. 15 mm.*

Before a more detailed discussion of the various growth characteristics is entered, it useful to compare the X-ray topograph in figure 5.1.1, with a schematic drawing of a KAP crystal. This allows familiarisation of the relation between the various growth sectors present within KAP and the topographs.

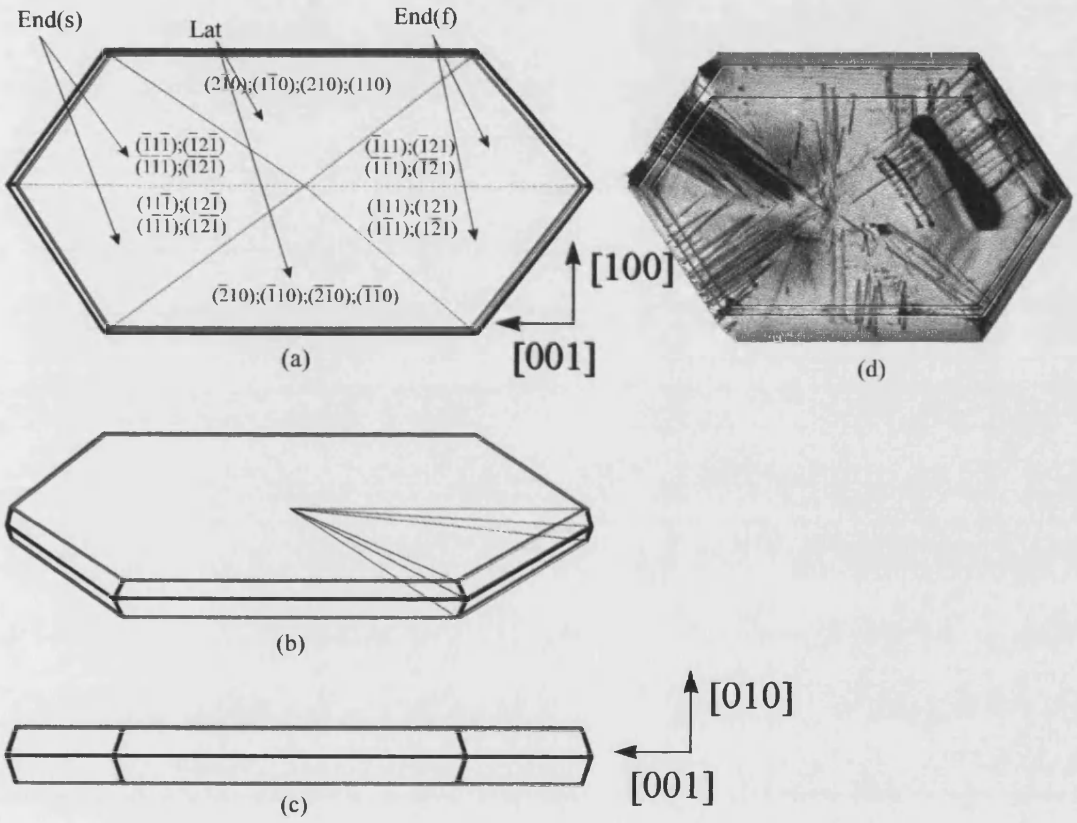

Fig. 5.1.2 *Figures (a-c) show several schematic diagrams of a typical KAP crystal. Figure (b) illustrates how more than one growth sector lie above one another in the projected topographs. In order to facilitate the discussion of the topographs several sectors have therefore been grouped together as labelled in figure (a). Figure (d) shows the topograph from figure 5.1.1 as a reference. Note also that the slice plane of all crystals in this study was (010).*

As already stated the KAP crystal in figure 5.1.1 and 5.1.2(d) was topographed in the as grown condition without any subsequent processing such as polishing. This gives

rise to an interesting effect. With reference to figure 5.1.2(a), it is clear that when viewed from above, the outline of the crystal will extend further than the edges of the (010) sector due to the protrusion of the side faces. On the unpolished samples the outline of the (010) face is actually visible, due to a small amount of strain being associated with the edge of the face. This may be seen in figure 5.1.1 where the outline of the (010) face is visible at both the top and bottom of the crystal, thus giving a 3D effect to the topograph. The effect is more clearly illustrated in figure 5.1.2(d), where the same colour coding of the edges is shown in the topograph as is used on the schematic diagrams.

Because of the platelet morphology of KAP many of the growth sectors are impossible to distinguish in the diffraction geometry which was chosen. With reference to figure 5.1.2 (b) it can be seen that several growth sectors lie one above the other in the plane of the crystal. In order to facilitate the discussion of these topographs the growth sectors have been grouped together. This is illustrated in figure 5.1.2(a), and it is relative to this figure that all vectors will be labelled. The two Lat sectors are symmetrically equivalent and therefore have the same label. The two End sectors, however, are not equivalent due to the non-centro symmetric character of KAP. To differentiate between these sectors the suffixes s and f have been used. These denote the s(low) and f(ast) step directions of steps on the (010) face as previously described by Jetten et al.[63]. The relationship is further illustrated in figure 5.1.3. In practice the slope difference is large enough to allow the respective ends of the crystal to be determined by eye.

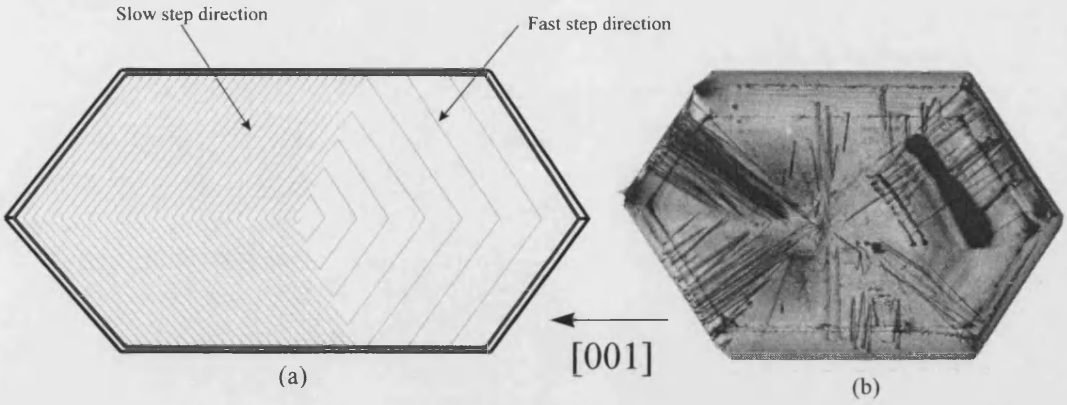

Fig. 5.1.3 *The slow and fast step directions on the (010) face as they relate to the topographs.*

5.1.2.1 INCLUSIONS

Inclusions are visible on all the topographs of KAP. They occur particularly frequently in the End(f) sector (Figure 5.1.3(b) above shows a typical example). In the upper half of the End(f) sector two inclusions may be seen lying parallel to the step direction on the (010) face. Once again it should be stressed that since topographs simply record strain, the size of the inclusions, as recorded on the topograph, need not be related to the physical dimensions. In this example the two inclusions were observed, by optical means, to be of similar physical dimensions. The strain associated with the one lying nearer the crystal edge, however, is significantly higher than the that lying nearer the crystal centre. Such large inclusions lying parallel to the step directions have been commonly suggested to be due to incorporation of solution within the crystal. An overview of a possible mechanism is given in the sequence of schematic diagrams shown in figure 5.1.4(a-f).

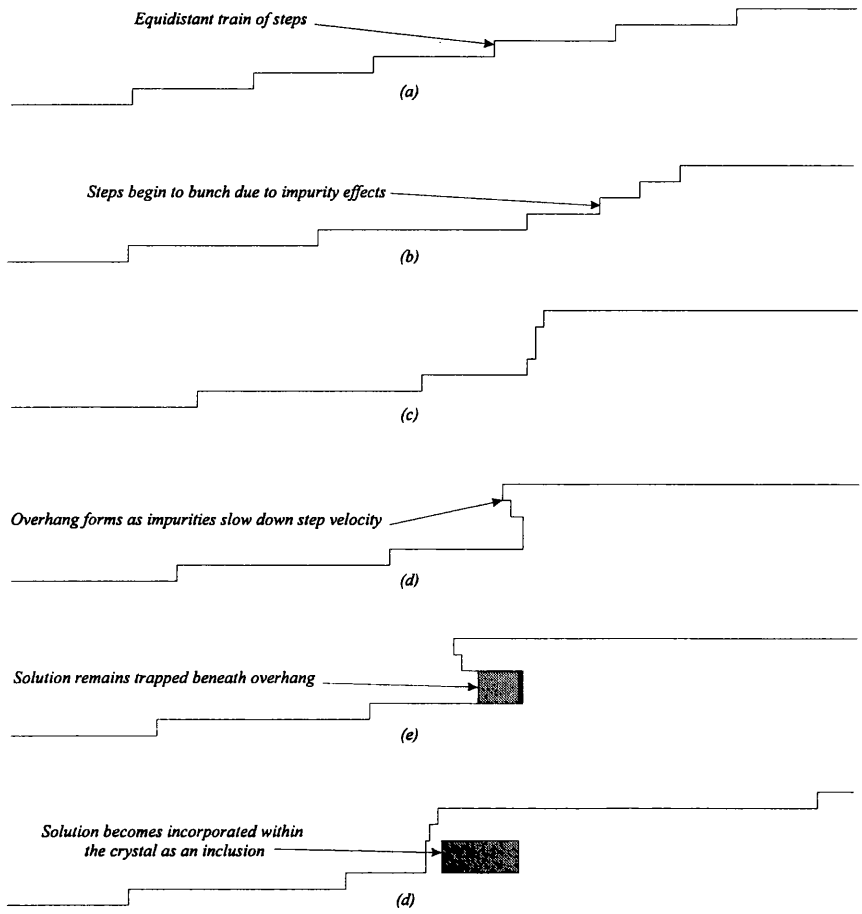

Fig. 5.1.4 *Schematic sequence showing a possible mechanism for impurity incorporation within a crystal. In this case the particular example of the impurity is the solution itself.*

An interesting observation from the topographs is the fact that the large inclusions lie in the End(f) sector, which is associated with the direction of the faster moving steps. In the End(s) sector large inclusions of this type were never observed. Below, in the work using AFM this relation is explored in more detail.

5.1.2.2 GROWTH BANDS

Growth bands are also an impurity related phenomenon. They occur due to local variations in the amount of incorporated impurities. This may be caused for example by fluctuations in growth conditions such as temperature and supersaturations. Once again the crystal used previously may be shown as a general illustration. Figure 5.1.5, below enlarges a region where the growth bands are particularly prominent.

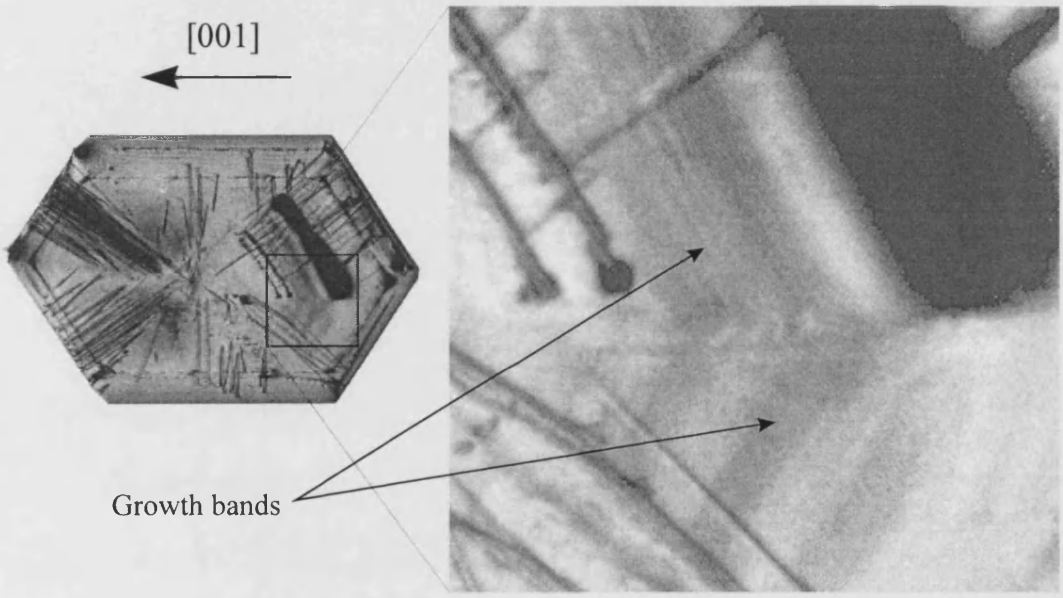

Fig. 5.1.5 *Close-up of End(f) sector to illustrate the occurrence of growth bands.*

The change in direction of the growth bands occurs at the growth sector boundary between two sectors. To understand which growth sector boundary is observed it is worth recalling that that the End(f) sector is made up of a several growth sectors. These may be divided into three major sub groups, namely the large (010) sector which lies above all other sectors, and the upper and lower halves of the End(f)

sector. It is the growth sector boundary between these two zones which is visible. On some crystals it was possible to assign a dominant strain vector associated with the growth bands. This was done on the basis of the **g.b**=0 condition as described in the theory section.

5.1.2.3 GROWTH SECTOR BOUNDARIES

Due to the strain which is often associated with growth sector boundaries it is common to be able to observe them 'directly' on X-ray topographs, rather than indirectly as seen above. In all the crystals studied here, however, hardly any indication of growth sector boundaries was visible, indicating a low level of strain misorientation between them. To illustrate this, figure 5.1.6 shows a similar region as seen in figure 5.1.5, but within a different crystal. This topograph was taken using the most strain sensitive of the reflections used in this study, the $00\bar{4}$ reflection.

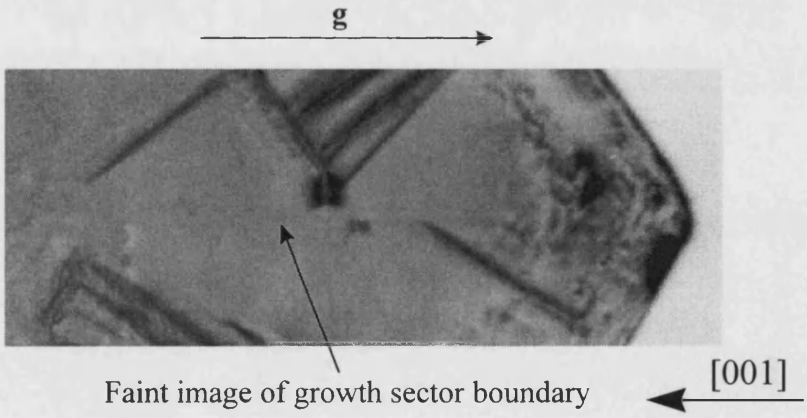

Fig. 5.1.6 *$00\bar{4}$ reflection of a the End(f) sector. The growth sector boundary is not visible. The field of view is approx. 8 mm.*

5.1.2.4 PENDELLOSUNG FRINGES

From section 2.2 recall that pendellosung fringes are interference fringes which occur only in crystals of extremely high perfection. These fringes are seen at the edges of all the KAP crystals examined here. Once again an example of the fringes may be seen in figure 5.1.1. The relevant region is enlarged below in figure 5.1.7.

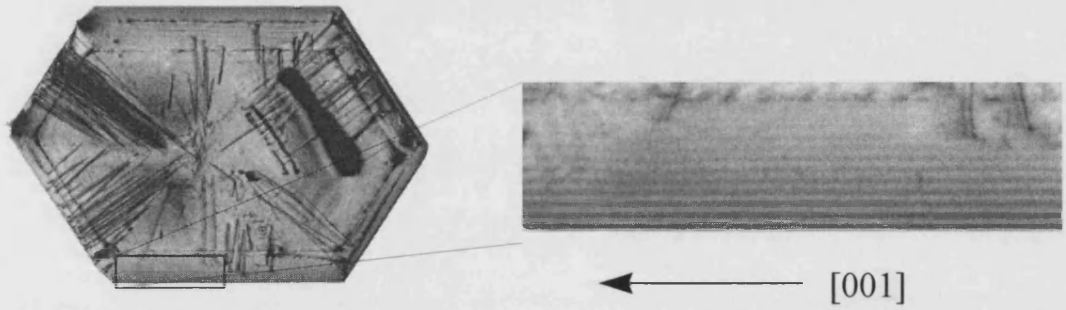

Fig. 5.1.7 *Example of pendellosung fringes.*

5.1.2.5 DISLOCATIONS

As stated in the introduction it is the dislocations present within crystals which play a crucial role in the growth process. Therefore, having established the general features which are present within solution grown KAP crystals, the remainder of the discussion now focuses on the important subject of dislocations.

Firstly a division has to be made between two unrelated sources of dislocations. The first source, and for the work here of lower interest, are mechanical dislocations. Mechanical dislocations may be introduced into a material when it is stressed above a certain, material dependent, level. Since their production is determined primarily by energetic considerations they tend to have the shortest Burgers vector possible within

the particular crystal system. This is particularly true since the strain energy associated with a dislocation has a proportional relationship with $\mathbf{b}^2$.

The second group of dislocations are known as growth dislocations. These dislocations are formed within the crystal during the growth process. Typical characteristics of these dislocations are that they are straight and lie parallel or at small angles with respect to the normal of the corresponding sector. It is an experimental observation that growth dislocations are not confined to only the lowest Burgers vectors within a crystal system. This may be due to the possibility that their formation is not solely determined by energetics, but also by the nature and geometry of the crystallographic region in which they are produced.

Usually mechanical dislocations do not play a role in the growth process since they are mostly introduced 'after the event' or post-growth. This need not always be the case however. In some instances seed crystals may contain mechanically induced dislocations which can act as growth centres during further growth. In other instances crystals may be intentionally or unintentionally strained during the growth process, thus producing mechanical dislocations, which in turn may influence the growth process.

In the work here extreme care was taken with the crystals in order to minimise the introduction of any mechanical dislocations after the growth process. In order to verify this, as well as investigate in more detail the difference between these two groups of dislocations, mechanical dislocations were generated within a KAP crystal subsequent to growth using a razor blade. In the crystal structure of KAP the expected slip direction is the short <001> vector (0.6466 nm) and the slip plane the (010) plane. Because the (010) plane is a cleavage plane for KAP, the most

straightforward method of straining the crystal is to cleave it along this plane. Figure 5.1.8 shows a topograph of an uppermost cleaved slice (i.e. the slice containing the growth surface of the crystal). Also shown is the cleaving geometry.

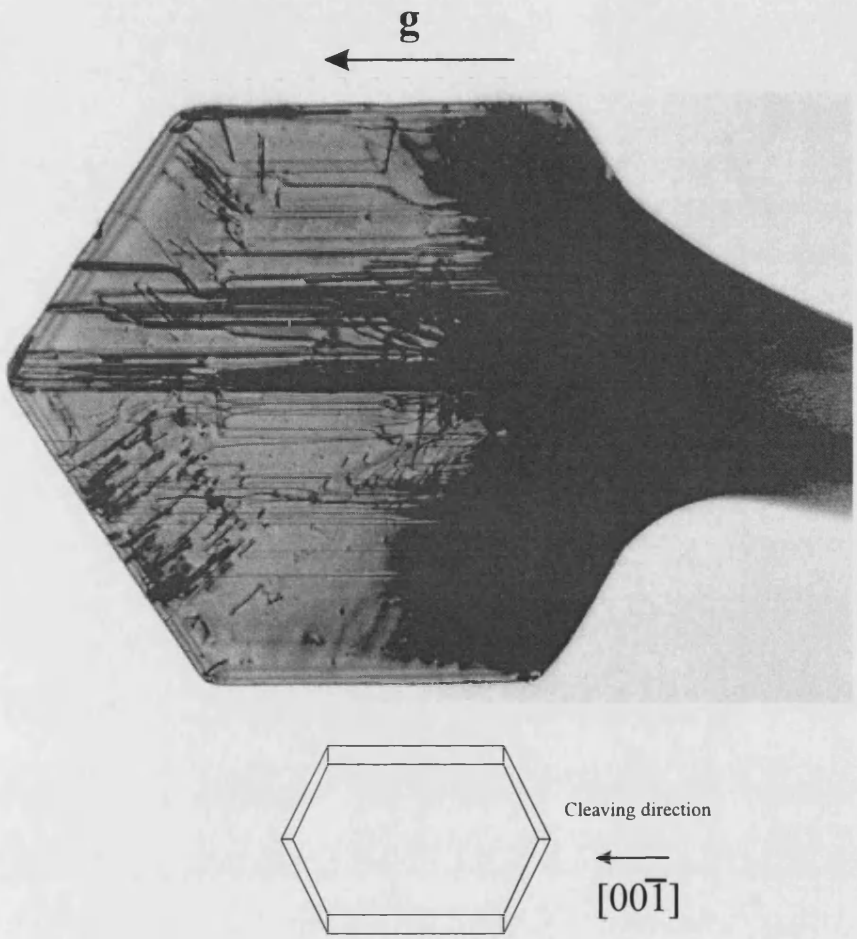

Fig. 5.1.8 *$01\bar{2}$ reflection of a KAP crystal subsequent to cleaving in the direction indicated on the schematic diagram. The largest dimension of the crystal is approx. 15mm.*

Although the Schmid factor, and therefore the critical resolved shear stress, is theoretically zero for the above slip plane and slip direction and cleaving geometry, it is unlikely that this is the case in practice - the cleaving geometry will not be perfectly parallel to the (010) face.

In figure 5.1.8 the very dark region on the right side of the topograph indicates that a large amount of strain has been introduced into the crystal. Due to this induced strain the outline of the crystal in this region is no longer visible. The effect which is seen is due to the fact that the now deformed lattice diffracts a large number of different wavelengths from the synchrotron source, and thus gives rise to a 'tail' effect. The actual crystal slice appeared undamaged to the eye. Moving further toward the left side of the crystal it may be seen that where the strain damage is low enough to view the defect structure, a large number of straight (or nearly straight) lines lie parallel to the cleaving direction (the slip direction). Inspection of the topographs shown previously will reveal that this type of damage is not present in as grown crystals. These lines are therefore very likely to be the strain fields of mechanically induced dislocations. In some cases the lines are not completely straight, but show a bend or kink before continuing in the same direction. This may be caused by obstacles, such as inclusions, forcing the dislocations to change direction temporarily. Cross slip, i.e. movement onto a new slip plane may also not be ruled out, however, it is unclear which other plane would serve as the new slip plane.

Assuming that KAP is likely to contain only one slip direction, it is relatively straightforward to cleave a thin section from the top of the crystal without introducing any mechanical dislocations. This provides useful information concerning the growth dislocations, as will be discussed later, however, the result is also shown here in order to allow direct comparison with figure 5.1.8. In this case the cleaving direction is <100> as shown in figure 5.1.9.

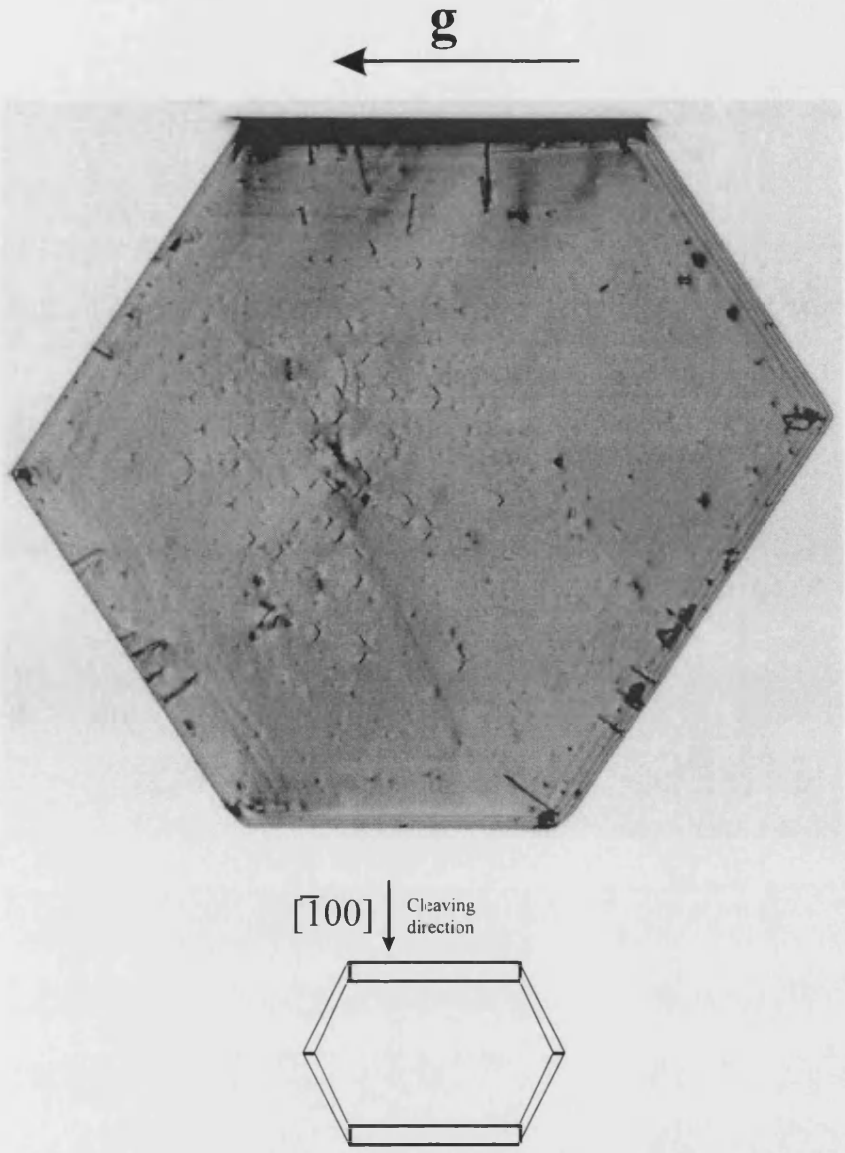

Fig. 5.1.9 *$01\bar{2}$ reflection of a KAP crystal subsequent to cleaving in the direction indicated on the schematic diagram.*

In contrast to figure 5.1.8, the topographed section in figure 5.1.9 shows very little damage, and no evidence of mechanically induced dislocations. In fact the only dislocations which remain are those which lie nearest the surface of the (010) face. The slice is approximately 1 mm thick and the largest dimension is approx 15 mm.

5.1.2.6 GROWTH DISLOCATIONS

Apart from the instances described above, where mechanical dislocations were deliberately introduced into crystals, all the dislocations observed in KAP had the characteristics typically associated with growth dislocations[100]. This may be verified, once again, using the crystal shown in figure 5.1.1 or figure 5.1.10 below.

The density of the dislocations shows a variation between sectors. The lowest dislocation density is found in the Lat sectors. In some crystals this sector was almost free of dislocations, an example of which is given in figure 5.1.10. Note once again that this crystal was topographed in the 'as grown' condition.

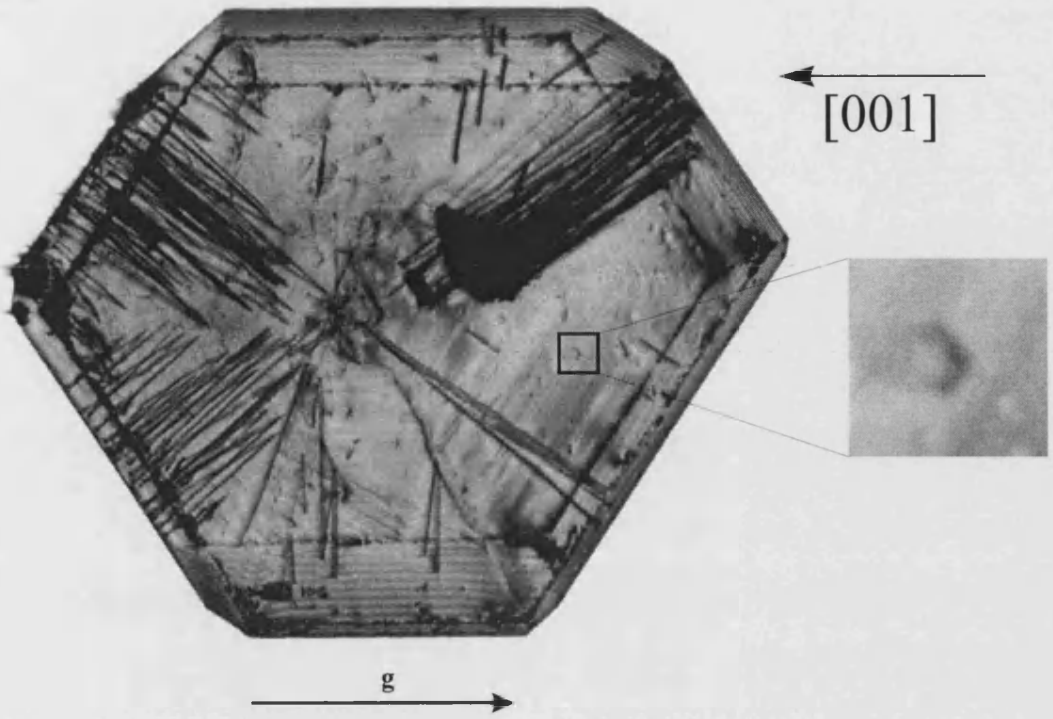

Fig. 5.1.10 *$01\bar{2}$ reflection of an unprepared KAP crystal. Note the low overall defect density, particularly the Lat sectors. The largest dimension of the crystal is approx. 10 mm.*

The two End sectors have a somewhat higher, and broadly similar dislocation density. In the End(f) sector, dislocations tend to form at the large inclusions which are uniquely present in this sector (see figures 5.1.10 & 5.1.1). Because of this, the dislocation density in these sectors is predominantly determined by the size and number of these inclusions. In the End(s) sector where no large inclusions were observed, the dislocation density was usually found to be slightly higher than in End(f). The origin of these dislocations is not clearly visible, but may possibly be attributed to be small or point inclusions which are beyond the resolution of X-ray topography.

In all three growth sectors a common feature of the dislocations is that they frequently nucleate in pairs. This gives rise to a V shape. Possible explanations for this phenomenon are discussed later.

It is worth noting that all of the dislocations discussed so far lie in sectors beneath the (010) sector (refer to figure 5.1.2). For this reason they terminate on the side faces. Dislocations in the (010) sector are less obviously visible. This is due to the fact that the line direction must lie almost parallel to the diffracting planes. Hence the projected line direction will be very short and appear to both begin and terminate within the crystal. An example of a dislocation in the (010) sector is magnified in figure 5.1.11. Once again it is noteworthy that the dislocation has a V shape.

5.1.2.7 Characterisation of Growth Dislocations

In order to begin the process of characterising dislocations in terms of their Burgers vector it is useful to make some realistic assumptions concerning the magnitude of the possible Burgers vectors. The most energetically likely dislocations in a crystal structure are those with the shortest Burgers vectors. On this basis table 5.1.1 gives a list of the most likely Burgers of the dislocations occuring in KAP. It is worth recalling that in the case of growth, as opposed to mechanically induced dislocations, it is possible that energetic considerations alone will not determine the Burgers vector but also the nature of the defect giving rise to the dislocation. For practical purposes in the study here it has been arbitrarily assumed that dislocations with a Burgers vector larger than [111] do not occur.

Burgers vector (**b**)	$\|\mathbf{b}\|$ (Å)	$\|\mathbf{b}\|^2$ (Å^2)
<001>	6.466	41.81
<100>	9.609	92.33
<101>	11.582	134.14
<010>	13.857	192.02
<011>	15.291	233.81
<110>	16.823	283.01
<111>	18.06	326.16

Table 5.1.1 *The shortest Burgers vectors in KAP together with b^2 which is proportional to the strain energy associated with the dislocation core.*

Dislocations may be characterised in terms of their Burgers vector by using the **g.b**=0 condition as described in the theory section. To recap briefly: a pure screw dislocation will be invisible when **g.b**=0 and a pure edge dislocation will be invisible when **g.bxl**=0. This theoretical prediction has to be somewhat qualified for practical use when analysing topographs. Firstly, some dislocations may have a character with both an edge component and a screw component. These dislocations are termed 'mixed', and produce a strain field in all directions. Therefore the strain would be expected to be at a minimum for **g.b**=0, resulting in a reduction in contrast of the dislocation rather than complete invisibility. The second possibility is decoration of the dislocation by solvent or other impurities. The strain field due to these can cause the dislocation to be visible in all reflections. Although it would again be expected that such dislocations be less prominent in reflections where **g.b**=0, this is not a prerequisite.

From the above conditions it follows that to uniquely determine the Burgers vector of a dislocation, invisibility is required in two non parallel reflections (two planes define a vector). Using the short-list of Burgers vectors given in table 5.1.1 it is therefore

necessary to decide on a number of reflections which satisfy the **g.b**=0 in at least two different reflections, for all the Burgers vectors under investigation. The choice of reflections is also limited by the desired geometry of the X-ray topograph and the availability of suitably strong X-ray reflections. After taking these factors into consideration table 5.1.2 shows the list of reflections which were used, together with the invisibility conditions of the various Burgers vectors under investigation.

g vector	$01\bar{2}$	012	004	$\bar{2}00$	022	$0\bar{2}2$	$\bar{3}20$	112	$\bar{1}12$	$1\bar{1}2$	$\bar{1}\bar{1}2$	$11\bar{1}$	$1\bar{1}\bar{1}$	$\bar{1}1\bar{1}$	$\bar{1}\bar{1}\bar{1}$
b vector															
<100>	☒	☒	☒	☑	☒	☒	☑	☑	☑	☑	☑	☑	☑	☑	☑
<010>	☑	☑	☒	☒	☑	☑	☑	☑	☑	☑	☑	☑	☑	☑	☑
<001>	☑	☑	☑	☒	☑	☑	☒	☑	☑	☑	☑	☑	☑	☑	☑
$<0\bar{1}1>$	☑	☑	☑	☒	☑	☒	☑	☑	☑	☑	☑	☒	☑	☑	☒
$<0\bar{1}\bar{1}>$	☑	☑	☑	☒	☒	☑	☑	☑	☑	☑	☑	☑	☒	☒	☑
$<\bar{1}01>$	☑	☑	☑	☑	☑	☑	☑	☑	☑	☑	☑	☒	☒	☑	☑
$<\bar{1}01>$	☑	☑	☑	☑	☑	☑	☑	☑	☑	☑	☑	☑	☑	☒	☒
$<\bar{1}10>$	☑	☑	☒	☑	☑	☑	☑	☑	☒	☒	☑	☑	☒	☑	☒
$<\bar{1}10>$	☑	☑	☒	☑	☑	☑	☑	☒	☑	☑	☒	☒	☑	☒	☑
$<\bar{1}11>$	☑	☑	☑	☑	☑	☒	☑	☑	☑	☑	☒	☑	☑	☑	☑
$<\bar{1}11>$	☑	☑	☑	☑	☑	☒	☑	☑	☑	☒	☑	☑	☑	☑	☑
$<\bar{1}\bar{1}1>$	☑	☑	☑	☑	☒	☑	☑	☒	☑	☑	☑	☑	☑	☑	☑
$<1\bar{1}1>$	☑	☑	☑	☑	☒	☑	☑	☑	☒	☑	☑	☑	☑	☑	☑

☒ **g.b**=0 ; ☑ **g.b**≠0

Table 5.1.2 *Invisibility conditions for low index Burgers vectors in KAP crystals.*

Further information concerning the Burgers vector of the dislocation may be deduced from the line direction when used in conjunction with the minimum energy approach as described by Klapper[100]. In summary, some general observations follow from this theory:

(i) If the Burgers vector **b** is parallel to the growth normal **n** then the line direction **l** is parallel to **n**.

(ii) If **b** is perpendicular to **n** then **l** is also parallel to **n** provided that **n** is parallel to a twofold symmetry axis.

(iii) Usually **l** lies between and is coplanar with **b** and **n**.

From this it follows that dislocations with **b.n**=0 will be of either pure edge or pure screw character and dislocations with **b.n**≠0 will be predominantly of mixed character. A comparison of table 5.1.1 and the possible growth sectors listed in figure 2(a) show that for KAP most dislocations will be of mixed character, with a few exceptions in the (010) and (110) growth sectors.

For the purpose of this analysis the dislocations were split into two groups namely:

(i) Dislocations which could be completely characterised by the **g.b**=0 condition.

(ii) Dislocations where additional information was necessary for complete characterisation.

5.1.2.8 Dislocations Characterised using the Invisibility Criterion

The <001> Burgers Vector

Although, as already stated, energy may not be the only consideration for determining what types of dislocation will form during the growth process, it remains an important factor. This is particularly true for KAP since the shortest Burgers vector (the <001> direction) is considerably shorter than the <100> Burgers vector, which is the second most favourable. Therefore, within the limitations of an energetic approach, it would be expected that the <001> dislocation be particularly common. Inspection of the topographs verifies the prominence of this dislocation type - it is seen in all sectors. This fact is substantiated below in a sector by sector analysis.

Firstly it is necessary to establish two reflections in which the <001> Burgers vector will be invisible. Reference to table 5.1.2 reveals this to be the $\bar{3}20$ and $\bar{2}00$ reflections. Figure 5.1.11 shows one of these reflections (the $\bar{3}20$) together with the $01\bar{2}$ reflection. The region shown lies in the End(s) sector.

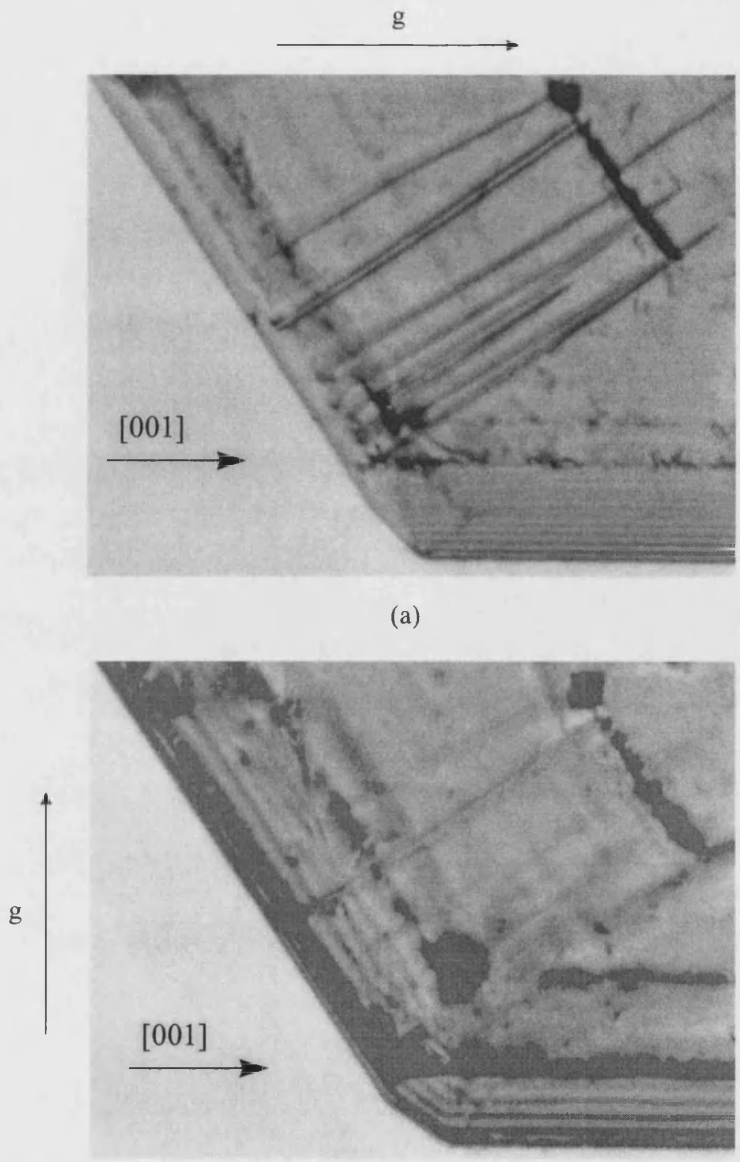

Fig. 5.1.11 *Figure (a) shows the $01\bar{2}$ reflection and figure (b) the $\bar{3}20$ reflection of a KAP crystal. All the dislocations show a substantial reduction in contrast. The field of view is approx. 7 mm.*

In figure 5.1.11(a) a group of dislocations have nucleated at an inclusion. Several others have also nucleated prior to the formation of the inclusion, and therefore may be seen in the top right of the figure, above the inclusion. With reference to table

5.1.2 it is clear that dislocations with an [001] Burgers vector will be visible in the $01\bar{2}$ reflection. In figure 5.1.11(b) all of the dislocations are either invisible or are strongly reduced in contrast. This was also the case in the $00\bar{2}$ reflection, which is not shown here. The conclusion therefore, is that all of the dislocations have a Burgers vector of [001]. If the dislocations seen in figure 5.1.11(b) are analysed more closely, it can be seen that they do not all have the same projected line direction. This is illustrated in figure 5.1.12 where the dislocations are colour coded into two main groups, with approximately the same line direction.

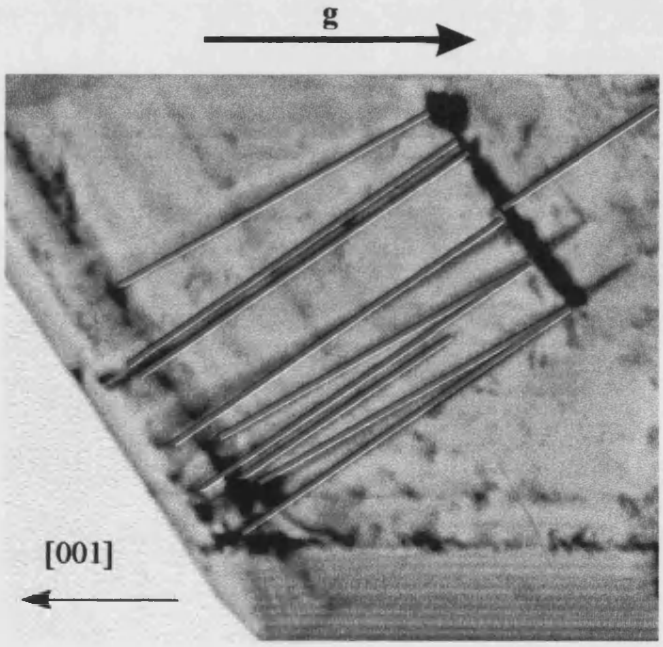

Fig. 5.1.12 *This figure is the same reflection as shown in figure 5.1.11(a). The two basic line directions which are present are highlighted in red and blue. The field of view is approx. 5mm.*

In some cases the dislocations appear to nucleate individually, whilst in other cases two dislocations nucleate at a single point, therefore giving rise to a 'V' shape. Each

arm of the 'V' lies in one of the two major direction groups. From the fact that all of the dislocations have the same Burgers vector it follows that within the same sector they should have an identical line direction. The observation that this is not the case therefore suggests that the dislocations lie in different growth sectors. In order to explain this, it is necessary to recall that each of the sectors described in this analysis, i.e. End(s), End(f) etc. consists of a number of growth sectors lying above one another. This was shown in figure 5.1.2(a). In figure 5.1.2(c), which shows a side view of the crystal, a schematic representation is given in which contains only two faces at the edge. In reality this will not be the case, and depending on the number of sectors present in the particular crystal, the side may be visualised more accurately as shown in figure 5.1.13. Nonetheless, the basic fact remains that whilst a small difference in angles may be present between the {111} and {121} type faces, it will not be nearly as large as the angle difference between faces lying on opposite sides of the crystal.

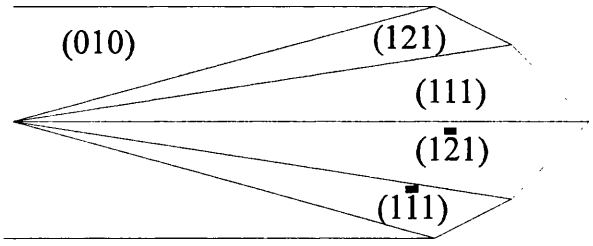

Fig. 5.1.13 *Schematic diagram of a KAP crystal edge.*

The implication for the projected line directions of dislocations within these sectors is that they will fall into two major groups, as is seen experimentally. This, however, does not account for the fact that a 'V' shape arises. This can only be explained if the

nucleation point of the dislocation pair is on the growth sector boundary. If this were the case then the possibility would arise that two dislocations could nucleate at the same point, but subsequently exist in two different sectors. There is also a strong theoretical justification for the occurrence of dislocations at growth sector boundaries - the boundary is an area where crystal imperfections have an increased likelihood of occurrence.

An additional piece of evidence which supports the general assumption that different arms of the V lie in different growth sectors is given in figure 5.1.14.

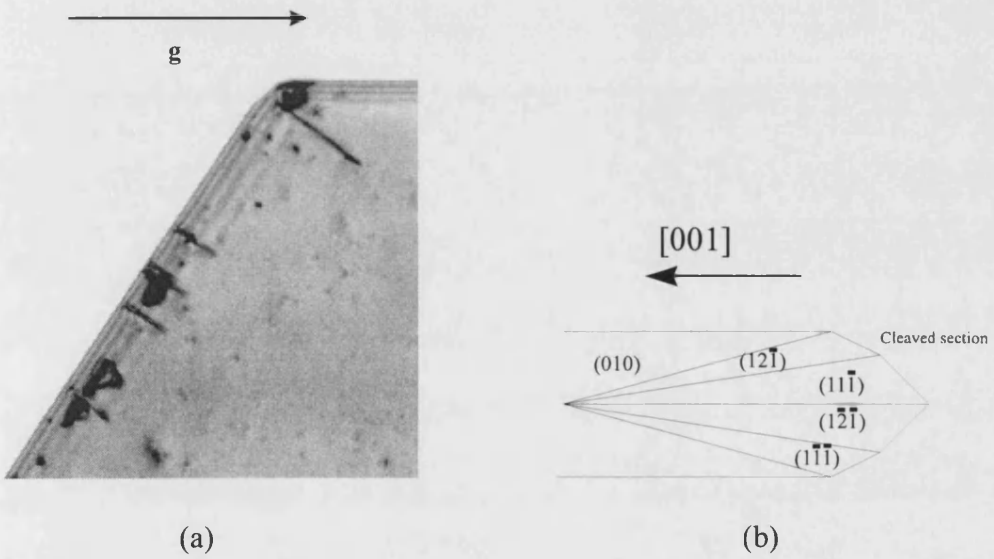

(a) (b)

Fig. 5.1.14 *Figure (a) shows an $01\bar{2}$ topograph of a section of the End(f) sector of a KAP crystal cleaved from the surface, as indicated in figure (b). Most of the crystal consists of the (010) sector, apart from near the edge. Here short segments of dislocations may be seen. Note that whilst in topographs of complete crystals, several line directions are seen in the End(s) sectors, here only one direction exists. The field of view is approx. 6 mm*

Figure 5.1.14(a) shows a cleaved section of crystal, taken from the top of the crystal. This is illustrated using the schematic diagram as seen in figure 5.1.13 and reproduced here as figure 5.1.14(b). The cleaved slice therefore contains a reduced number of growth sectors, namely the (010) sector and the uppermost sectors within the End(s), End(f) and Lat sector groups. The region depicted here is from the End(s) side of the crystal. Whereas previously two different line direction groups were visible, here only one direction occurs in the End(s) sector. The indication is therefore that by removing the dislocations in the lower sectors, only one projected line direction of the <001> type Burgers vector remains, as would be theoretically expected (Note that the dislocations in this sector appear much shorter than in the uncleaved crystals. With reference to figure 5.1.14(b) it will be appreciated that this is due to the fact that a substantial amount of the sector is removed during cleaving).

A further feature of interest arises from the fact that 'V' shaped dislocations with the <001> Burgers vector must lie in two growth sectors. This is the observation that frequently the V's are seen to nucleate on the inclusions which are encountered in the End(s) sectors. This may be seen in figure 5.1.11 and is also shown in figure 5.1.15 below.

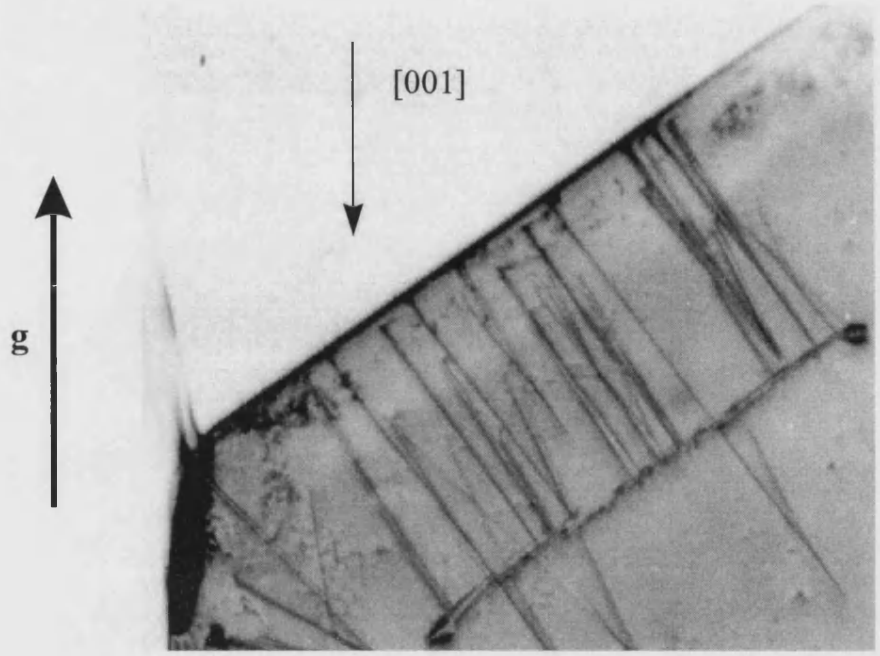

Fig. 5.1.15 *$02\bar{2}$ topograph of the End(f) sector of a KAP crystal. Of the many dislocations which nucleate on the inclusion, some occur as 'V' shapes. The field of view is approx. 5 mm.*

From the preceding argument this implies that the inclusions also occur on the growth sector boundary. Once again the theoretical justification is strong - there is an increased likelihood of faults at the growth sector boundaries, in which the incorporation of solution may occur.

So far the discussion has focused exclusively on the occurrence of <001> dislocations within the End(f) sector. The other sectors are now considered. In the End(s) sector it will be remembered that the occurrence of inclusions was not common. Nonetheless a dislocation density comparable to that seen in the End(f) sectors occurs. Figure 5.1.16 below shows a comparison of two topographs of the End(s) region of a crystal. Once again the $\bar{3}20$ reflection is used to illustrate the invisibility of dislocations with the <001> Burgers vector.

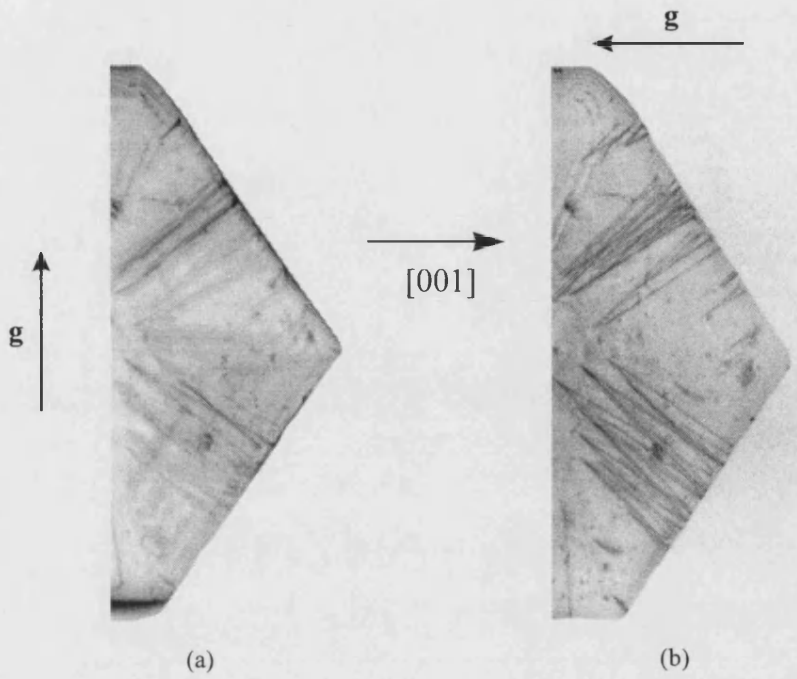

Fig. 5.1.16 *Figure (a) shows the $\bar{3}20$ reflection and figure (b) the $02\bar{2}$ reflection. Many of the dislocations seen in figure (b) show a strong reduction in contrast in figure (a). The largest dimension of the crystal is approx. 10 mm.*

Many, but not all, of the dislocations show a decrease in contrast between the two reflections. Once again it is worth noting the relative frequency of 'V' shaped dislocations which are invisible, and therefore have the <001> Burgers vector. These must all have nucleated as a pair on the growth sector boundary.

The highest quality growth sectors observed were the Lat sectors. In all the topographs examined these sectors consistently had the lowest dislocation density. Furthermore, in these sectors the <001> type dislocations did not nucleate frequently. Although nucleation is the most common source of growth dislocations within a particular growth sector, it is not the only one. A second possibility is the bending of dislocations between sectors. This occurs when a dislocation intersects with a growth

sector boundary during crystal growth. The dislocation cannot continue in its current sector and therefore is forced to cross the boundary, into the new sector. However, this also has implications for the line direction, which once again must adopt a minimum energy position. This gives rise to a sharp direction change in the line direction as it bends between the two sectors. Several examples of this are illustrated in figure 5.1.17 below.

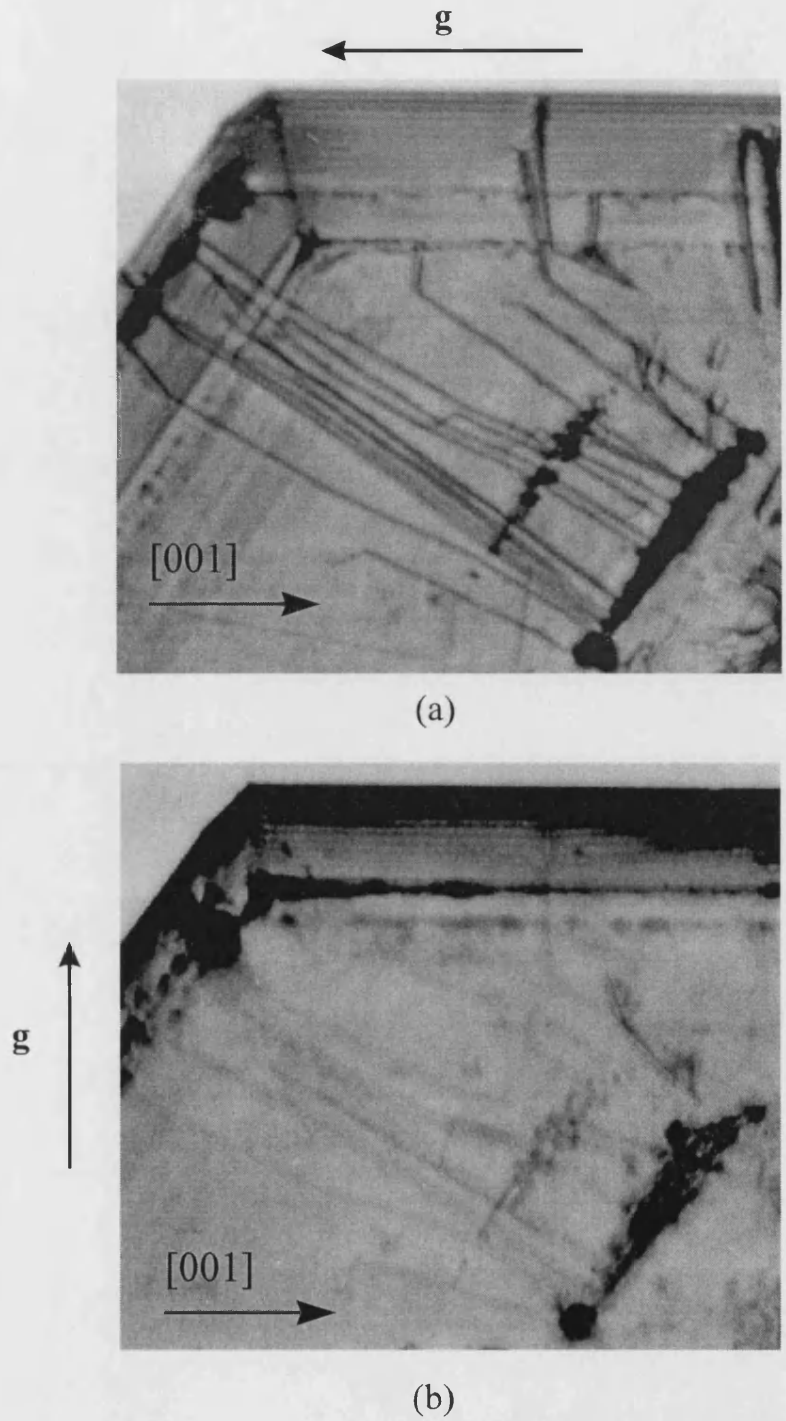

Fig. 5.1.17 *Figure (a) shows the $01\bar{2}$, and figure (b) the $\bar{3}20$ reflection of the upper region of an End(f) sector and a Lat sector. In the bottom right of the figure is an inclusion which forms the nucleation site of many dislocations. Several of these may be seen to bend into other sectors. The field of view is approx. 7 mm.*

Within figure 5.1.17 a large amount of information is present. Firstly it should be noted that all the dislocations seen in the $01\bar{2}$ reflection show a strong reduction in contrast in the $\bar{3}20$ reflection. This was also the case for the $\bar{2}00$ reflection (not shown here), once again implying the <001> Burgers vector for all the dislocations.

In the bottom right-hand corner of the image an inclusion is present from which most of the dislocations seen in the image have nucleated. The uppermost dislocation on this inclusion nucleates within the End(f) sector, but has bent into the Lat sector during growth of the crystal. Several other dislocations also bend into other sectors. For example the dislocation at the bottom of the inclusion bends near the end, and appears to terminate in the centre of the crystal. This indicates that it has bent into the (010) sector and terminates on the surface of the large (010) face.

From this figure it is therefore possible to confirm the existence of the <001> Burgers vector dislocation in both the Lat and (010) sectors.

Although other dislocation types were observed in the low defect lat sectors it was not possible to determine the Burgers vectors. No significant reduction in contrast of these dislocations was seen in any of the reflections studied, presumably for the reasons given previously.

The <101> Burgers vector

Dislocations with the <101> Burgers vector were observed in both the End(s) and End(f) sectors. A good illustration of a particular dislocation with this Burgers vector is shown in the series of figures (5.1.18 a-e) below.

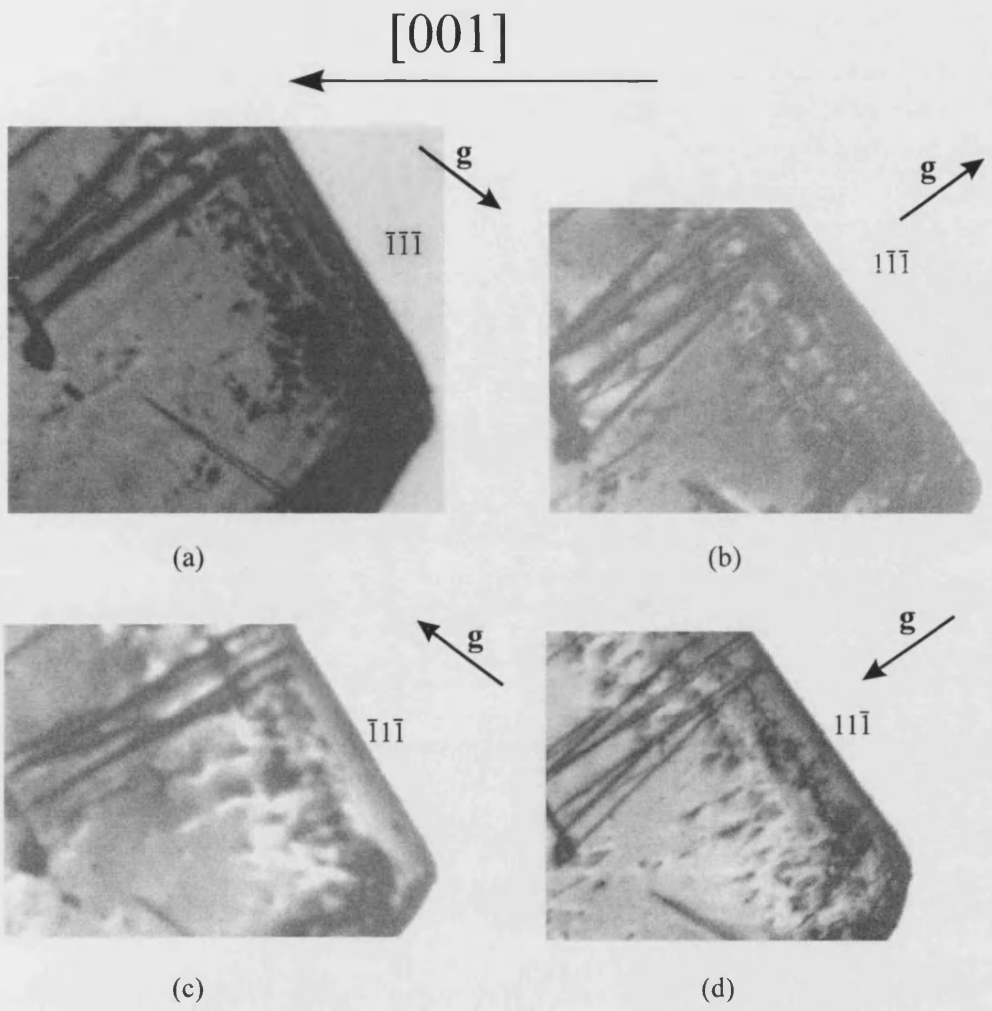

Fig. 5.1.18 *Region within an End(f) sector of a crystal. On the left of the images the end of an inclusion may be seen, from which a number of dislocations have nucleated. On the very edge of this inclusion is a dislocation with the <101> Burgers vector. The field of view is approx. 4 mm.*

Of the many dislocations which have nucleated from an inclusion in the End(f) sector, the one lying nearest to the bottom of the inclusion in figures 5.1.18(b) and 5.1.18(d) is almost completely invisible in the $\bar{1}\,1\,\bar{1}$ and $\bar{1}\,\bar{1}\,\bar{1}$ reflections. Therefore it has the $<\bar{1}01>$ Burgers vector.

For the case of the End(s) sector a more general example of dislocation invisibility is given. This is illustrated in figures 5.1.19(a) to 5.1.19(d).

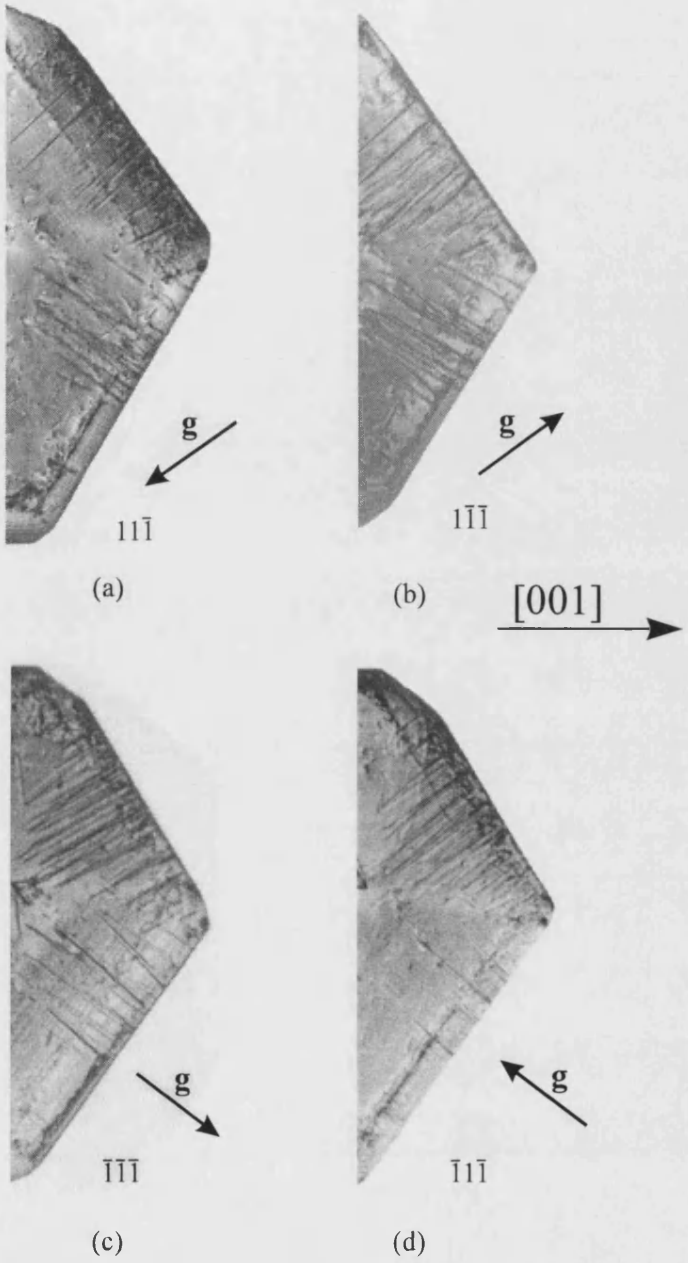

Fig. 5.1.19 *The series of figures illustrate the general invisibility of a number of dislocations in the End(s) sector which have the [101] type Burgers vector. A comparison of the upper half of the sector in figures (a) & (b) with (c) & (d) reveals a considerable decrease in contrast for a number of dislocations in (a) & (b). From table 5.1.2 this implies the <101> Burgers vector for these dislocations. In the bottom half of the sector the contrast variation is reversed, with a number of dislocations invisible in figures (c) & (d). These therefore have the <$\bar{1}$01> Burgers vector. The largest visible dimension of the crystal is approx. 11 mm.*

As already established above, many of the dislocations in the End(s) sector are of the <001> type. From figure 5.1.19 it may be seen that nearly all of the remaining dislocations are likely to have the [101] type Burgers vector.

5.1.2.9 Dislocations Characterised using other Information

For the reasons given above, the growth sector of most interest to those studying KAP as a model compound for crystal growth from solution is (010). The remainder of the discussion is therefore concerned with the dislocation types occurring in this sector. Although we have already seen that the <001> Burgers vector occurs in this sector, it is not particularly common, and is usually the result of <001> dislocations which originated in one of the lower sectors and were forced to change sectors during the growth process. These are the 'bending' dislocations discussed above. Furthermore the <001> dislocation in the (010) growth sector will be expected to be a pure edge dislocation and will therefore not produce a step on the surface of the (010) face. Thus it appears unlikely that this dislocation type can be involved in the growth spirals observed on this face. As discussed, the occurrence of spirals is associated with the presence of screw (or mixed) dislocations.

The other type of dislocation which is observed in the (010) sector is far more common. It was already illustrated in figure 5.1.10 and has the appearance of a V shape. Figure 5.1.20 below shows the central region of a topograph of a crystal containing a relatively high number of these dislocation types.

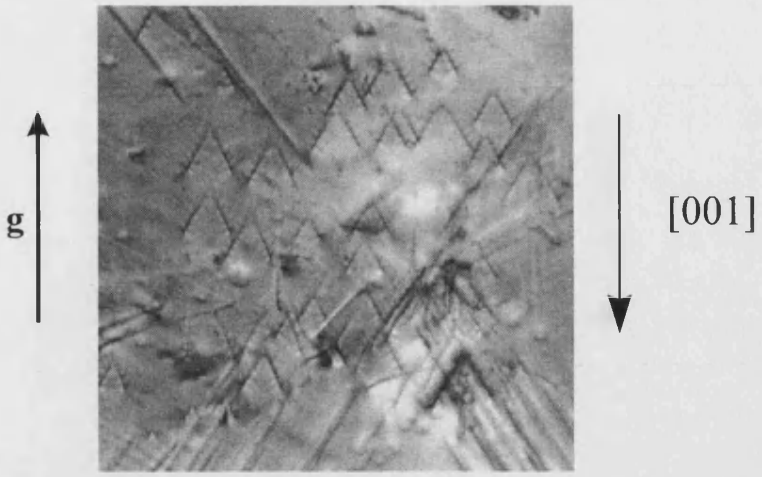

Fig. 5.1.20 *022 reflection of the central region of a KAP crystal. Note the prominence of the 'V' type dislocations. The field of view is approx. 5 mm.*

It was found that although these dislocations showed some contrast variation between reflections, this information on its own was not sufficient for a conclusive characterisation. In order to achieve this a more detailed investigation of the available information is necessary.

The first question to answer is the cause of the 'V' shape. In the case of the End sectors a convincing argument could be given that the two 'arms' of the 'V' lay in different growth sectors. For the V's under consideration here, however, this is not the case. The fact that both arms lie in the same growth sector may easily be shown by looking at a slice of a crystal which is taken from the growth surface. The central region of such a slice is shown in figure 5.1.21.

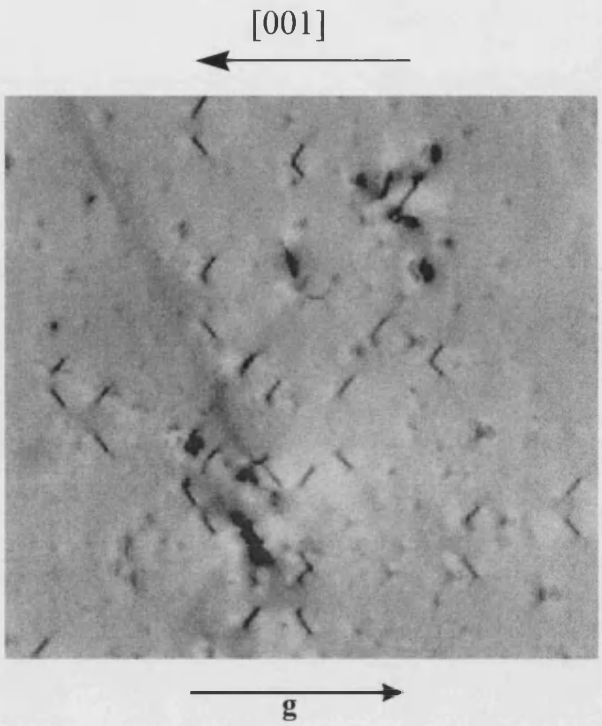

Fig. 5.1.21 *$01\bar{2}$ reflection of the central region of the top surface of a cleaved crystal. The 'V's seen in the previous figure have the bottom removed. This implies that the dislocation pair lie in the same sector. The field of view is approx. 5 mm.*

Because the dislocation pair lie in the same sector they cannot both be perpendicular to the (010). Therefore it is possible to eliminate a number of Burgers vectors. All of the following Burgers vectors would be expected to be pure edge: <001>, <100>, <101>. The <010> Burgers vector would be expected to be pure screw. Therefore these dislocations, which would all lie perpendicular to the (010) face, may be eliminated. The remaining possibilities are: <011>; <110> and <111>.

Figure 5.1.22 below shows a number of different reflections of the 'V' dislocations. From the various pieces of information contained within these figures it is possible to characterise the dislocations.

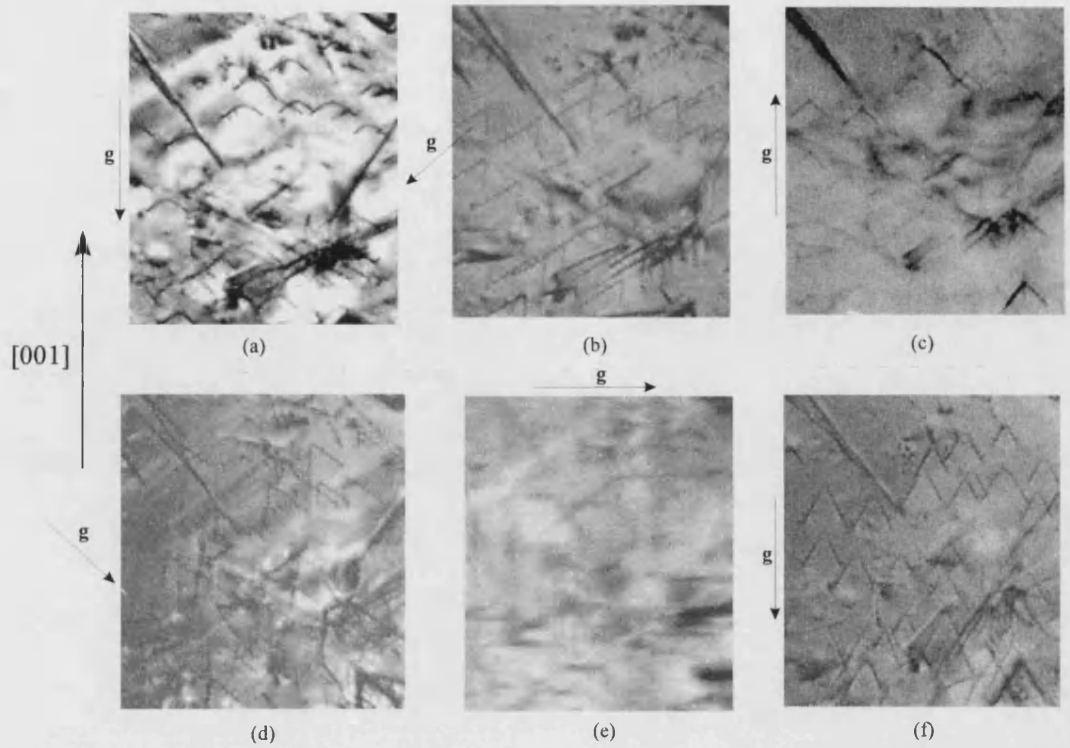

Fig. 5.1.22 *(a) $01\bar{2}$ reflection (b) $11\bar{1}$ (c) $00\bar{4}$ (d) $\bar{1}\bar{1}\bar{1}$ (e) $\bar{3}20$ (f) $02\bar{2}$. All images have the V oriented in the same direction. The field of view is approx. 4 mm.*

The first point to note is the relative lengths of the arms of the 'V's. Ignoring figure (e) for the moment it is apparent that the two arms have the same length in all reflections apart from the <111>. In the case of the <111> types, although the length of the arms are different, the angle between the V's is constant. This was also true for the other <111> types which are not shown here. The combination of these two points suggests that the 'V's lie in the (001) plane. If this is the case then the Burgers vector must also lie in (001) plane. From the possible vectors given above this implies that **b**=<110>. If this is tentatively assumed to be true then the logical consequences may be investigated and compared with the experimental evidence. To assist in the discussion a schematic figure (5.1.23) of the <110> dislocation pair is shown within a KAP crystal.

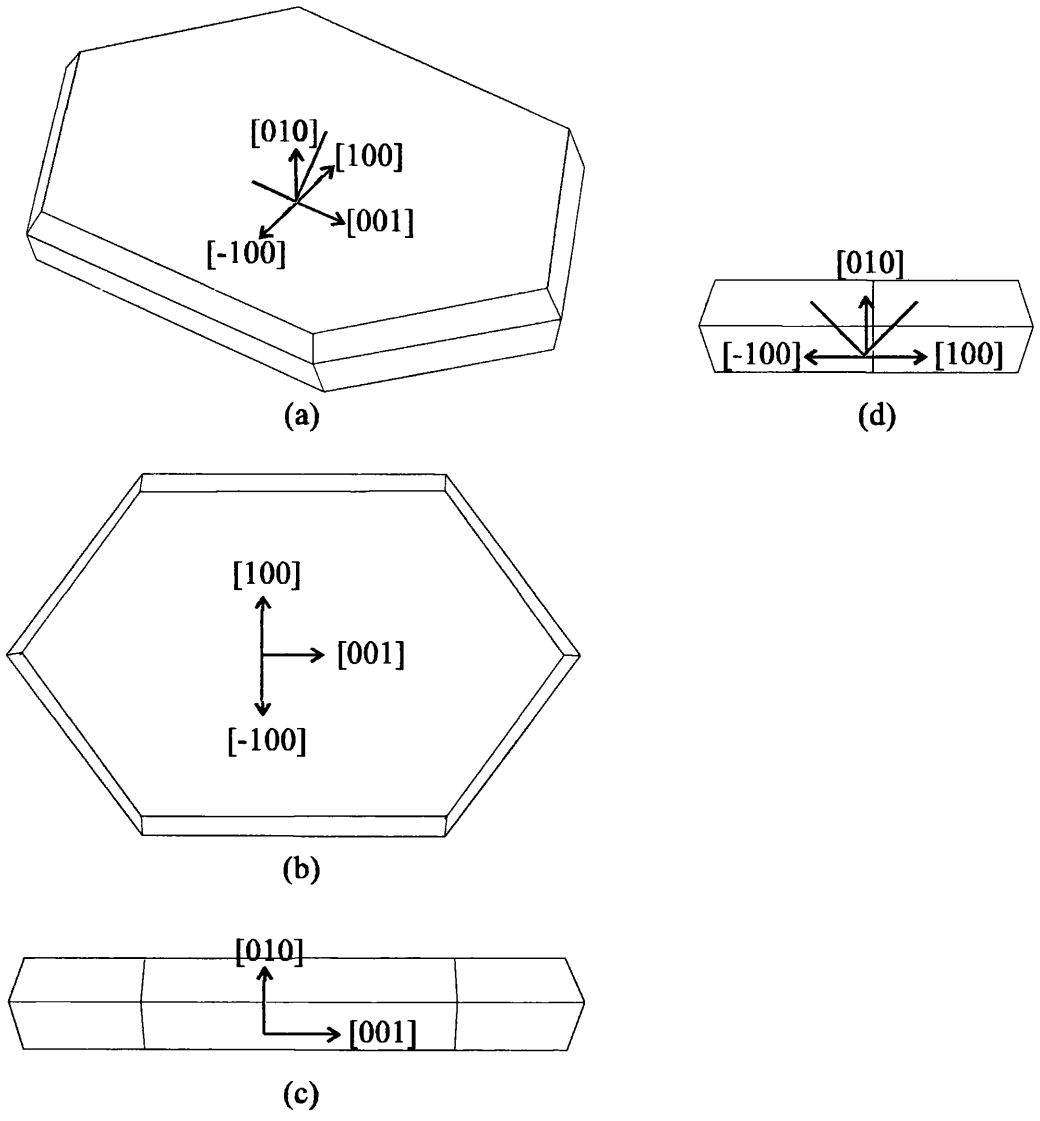

Fig. 5.1.23 *Schematic diagram of the <110> type Burgers vector (shown in red) within a KAP crystal.*

By referring to figure 5.1.23 it is more easy to visualise the orientation of the 'V's as they appear in different reflections. The combination of images (a) and (d) illustrate how the symmetrical 'V' shape arises in reflections $01\bar{2}$, $02\bar{2}$ and $00\bar{4}$. From figure (a) it is also clear that an asymmetric orientation of the crystal, such as is the case for

the 111 reflection, will lead to different lengths of the arms of the 'V'. In figure (b) the crystal orientation is such that the 'V' appears as a straight line. This will be true for all reflections lying perpendicular to (001). From table 5.1.2, this corresponds to $\bar{3}20$ and $\bar{2}00$. The $\bar{3}20$ reflection is shown in figure (e) to illustrate this point. No 'V's are visible in this reflection.

In figure 5.1.21(a),(c) & (f) there is a discrepancy in the orientation of the 'V's with respect to **g**. In the $00\bar{4}$ reflection the 'V' is inverted. This may also be explained if the 'V' lies in the (001) plane. Because the 001 and $00\bar{4}$ planes are parallel, then any image will be inverted. This is shown in figure 5.1.24 below.

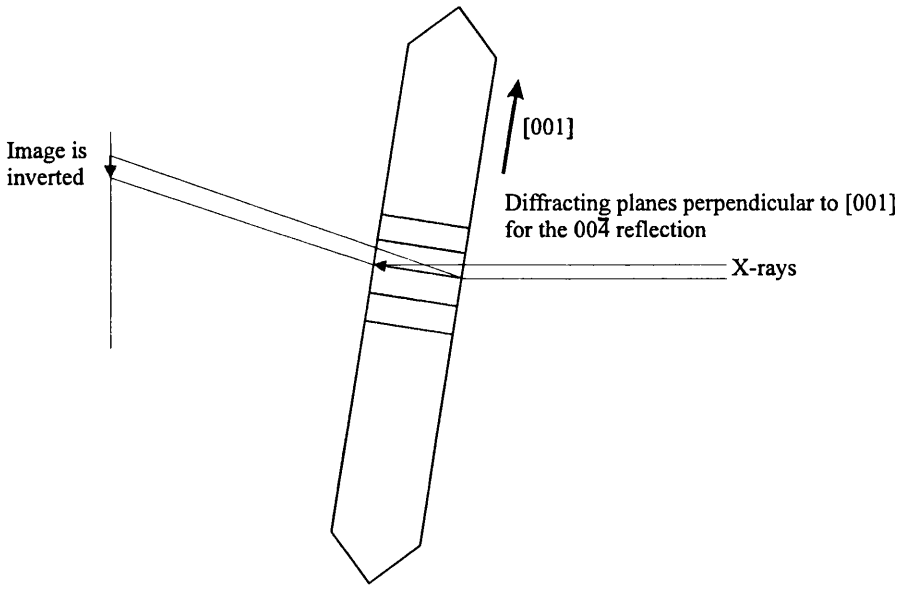

Fig. 5.1.24 *If the line directions of the dislocations lie in the same plane as the diffracting planes then the image will be inverted.*

When a reflection is used which lies out of plane i.e. not parallel to (001), then the image remains upright. This is shown in figure 5.1.25.

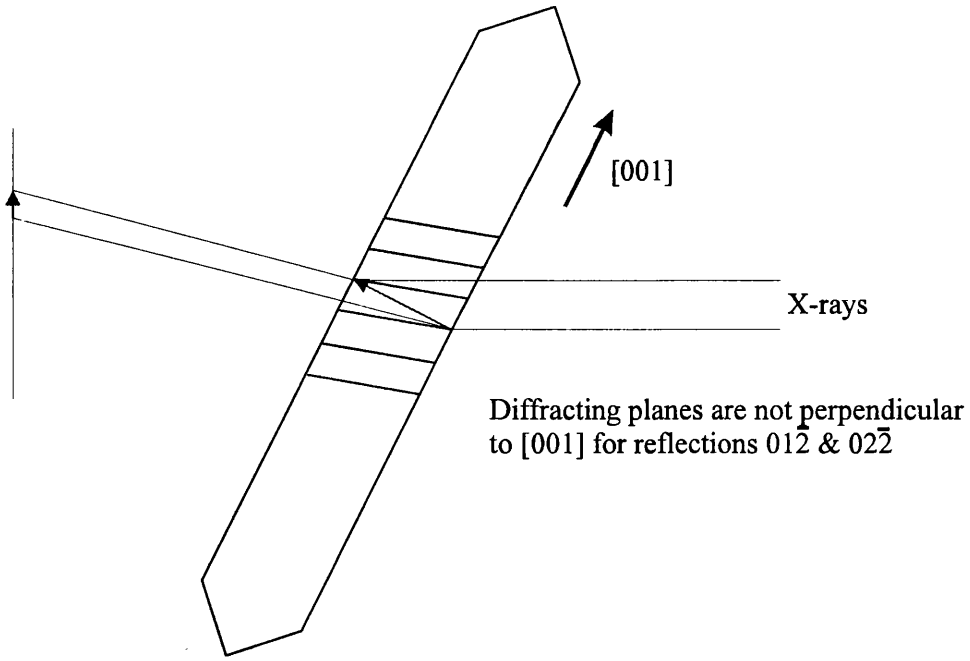

Fig. 5.1.25 *If the diffracting planes and the plane containing the dislocations do not coincide, then the image will not be inverted.*

Furthermore as the angle between the reflecting planes and the (001) increases, the projected image length will be increased. For the 'V' shapes this is most easily recognisable as a decrease in the angle between the arms of the 'V'. This is also confirmed experimentally - compare the 'V' angles in figure 5.1.21 (a) and (f).

The general conclusion from the above observations is that the 'V' dislocations are very likely to be of the type **b**=<110>.

5.1.2.10 SUMMARY

Table 5.1.4 shows a summary of all the dislocations characterised in this study. From a crystal growth point of view the sector of greatest interest is the (010) sector. It is

on this face that the remainder of the studies reported here were performed. From table 5.1.4 it may be seen that one of the two Burgers vectors observed in this sector is pure edge. No step will therefore be produced on the surface due to this dislocation, making it unlikely to be involved in the growth of this face. The other Burgers observed is the <110>. This is a mixed dislocation with a component of **b** normal to the surface, and therefore will produce a step on the surface. It is this dislocation that is therefore most likely to determine the growth behaviour.

Growth sector	Burgers vector (b)	Likely character
End(f)	<001>	mixed
	<101>	mixed
End(s)	<001>	mixed
	<101>	mixed
Lat	<001>	mixed
(010)	<001>	edge
	<110>	mixed

Table 5.1.4. *Observed dislocation types in KAP*

5.2 Surface Damage on the (010) Face of KAP During Removal From Solution

The relatively large number of studies which have been performed on KAP grown from aqueous solution are testimony to its suitability as a model compound for the study of crystal growth from solution. This is particularly due to the very well formed step system on the large (010) face. Frequently the presence of the polygonised growth spirals may be observed with the naked eye. For this reason optical methods such as DICM and interferometry have been used successfully to study various aspects of the growth behaviour[63]. Nonetheless, whilst the use of these optical techniques has provided many insights into the nature of the spirals, an obvious limitation has been the relatively poor resolutions attainable. The lateral resolution in particular is poor, meaning that only steps with a large inter-spacing may be viewed. In practice this translates to crystals grown at low supersaturations. The height resolution of optical techniques, whilst considerably higher than the lateral resolution, is still not ideal for viewing very small step heights. This has meant that direct observation of the unit cell step heights on KAP has not been possible.

In order to overcome these problems the growth spirals on the (010) face of KAP were studied using atomic force microscopy (Nanoscope III and Topometrix explorer). One of the oft-cited benefits of atomic force microscopy is the ability to perform in-situ work. In various areas (biological systems in particular) this capability has proven invaluable, however, in the case of crystal growth the problem of relatively high growth rates set against a low scanning speed of currently available

microscopes, means that only very slow growing crystals can be imaged dynamically. It is for this basic reason that most in-situ crystal growth studies have focused on conditions where slow step growth occurs. Examples of such systems are sparingly soluble salts such as calcite and large molecular structures such as proteins. Whilst the potential benefits of in-situ work to the science of crystal growth are clear, here we are particularly interested in the growth behaviour over a wide range of supersaturations. For this reason an ex-situ approach was adopted. The major concern with such an approach is the possibility of changes occurring on the crystal surface during removal from solution, particularly since the resolving capabilities of the AFM are so high. An extensive preliminary feasibility study was therefore carried out to investigate the extent and nature of surface damage during or subsequent to removal of the KAP crystals from solution. As a starting point, the surface protection method which has been used to protect a variety of non-organic crystals was used. This relatively common method involves withdrawing the crystal from the mother solution through a layer of n-hexane, followed by immediate rinsing with n-hexane. Full details are given in the experimental section.

5.2.1 Observed Degradation Features on (010) Face of KAP Removed from Solution.

5.2.1.1 Damage Giving Rise to Rough Appearance of Surfaces.

Figures 5.2.1 and 5.2.2 below show examples of AFM scans of crystals which were separated from the growth solution by withdrawal through a layer of n-hexane. The

crystals were grown by spontaneous nucleation followed with growth by evaporation, as described in section 4.1.1.

When studied by DICM these surfaces appeared well protected, and growth hillocks were discernible. When viewed under AFM, however, it is clear that a varying degree of success has been achieved during the protection process.

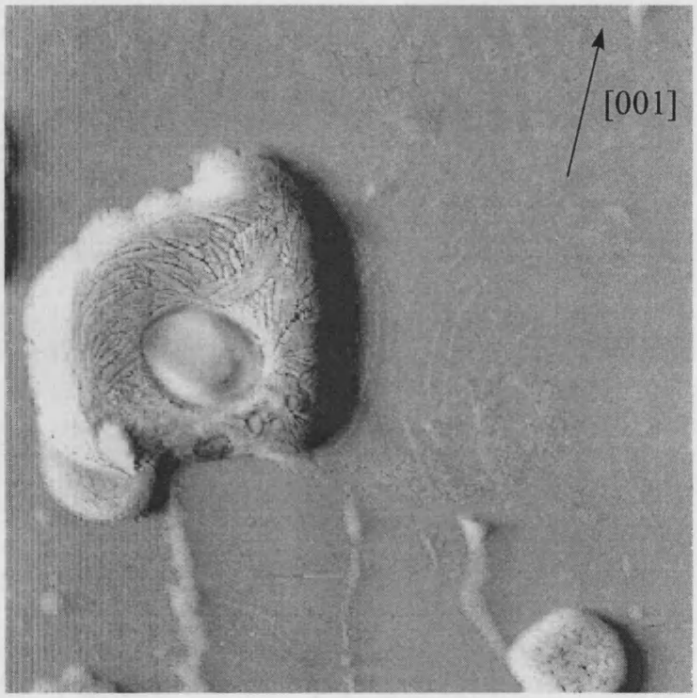

Fig. 5.2.1 *50 μm AFM image of a KAP surface protected by withdrawal through a layer of n-hexane. No recognisable growth features are visible.*

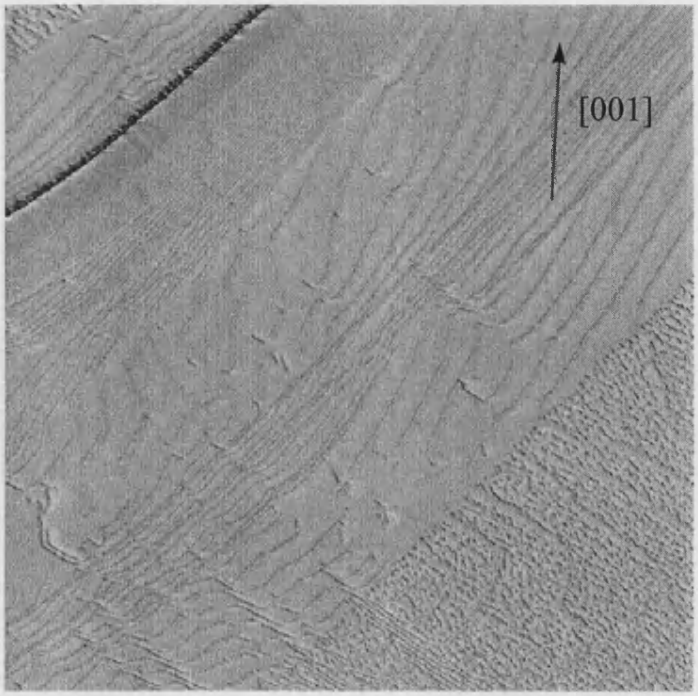

Fig. 5.2.2 *10 μm AFM image of a KAP surface protected by withdrawal through a layer of n-hexane. Trains of steps in different orientations are visible.*

In figure 5.2.1 no discernible features are visible. Figure 5.2.2 shows a surface where trains of steps may be seen, but no particular order is visible. On this image the steps terraces are also damaged, particularly those in the lower right section of the image. Apart from the poor protection of the surfaces, a further problem is the very small size of the scan area in relation to the area of the crystal face. In the case of small crystals having an area of around 1 cm^2, less than 1‰ of the surface is visible in the largest scan size (75 μm^2). This fact gives rise to two issues. Firstly there is the experimental difficulty of (re)locating particular regions of interest on the surface. Secondly, and more importantly, interpretation of features observed on the surface become less representative as the ratio (scanned area)/ (crystal face area) decreases. In order to tackle this problem a crystal growth approach was developed for the

growth of micro sized crystals. The methodology and equipment are described fully in section 4.

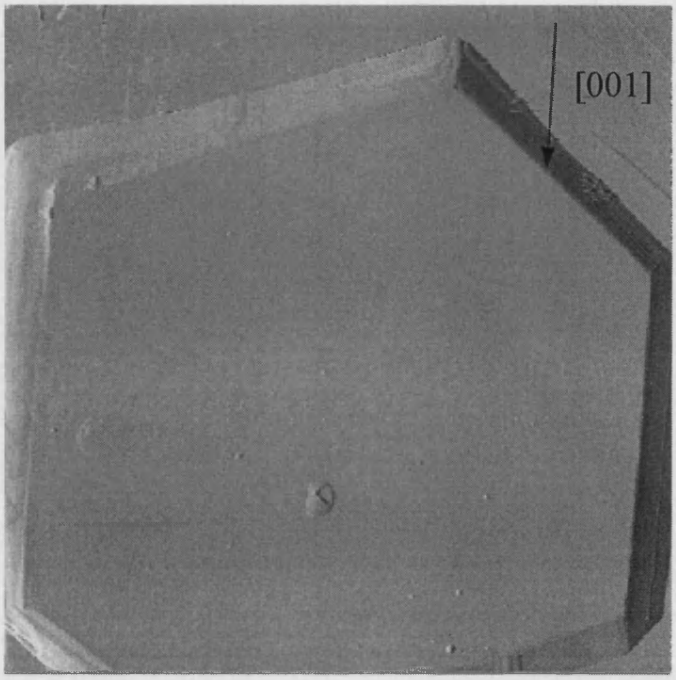

Fig. 5.3.3 *50 μm AFM image of almost an entire KAP micro crystal grown at a supersaturation of approx. 30%. Constant force mode reveals the crystal height to be approximately 1.5 μm.*

Figure 5.2.3 above shows an example of a complete micro crystal grown by this method. Although no growth steps are visible on the crystal due to the several orders of magnitude difference in the height of the micro crystal and the height of unit cell steps, the figure does serve to illustrate the relative ease with which the entire surface may be inspected. Note also the damage which is visible near the centre of the crystal. This is similar in appearance to that already shown in figure 5.2.1. Figure 5.2.4 below shows an AFM scan on the surface of a similarly sized crystal, also protected by withdrawal through a layer of n-hexane, and reveals what appears to be

the centre of a growth spiral. The surface also has a damaged appearance, presumably associated with the protection method, which rules out a more thorough analysis or description. A further problem associated with the protection of the surfaces, as illustrated above, was the large variability in the degree of surface protection.

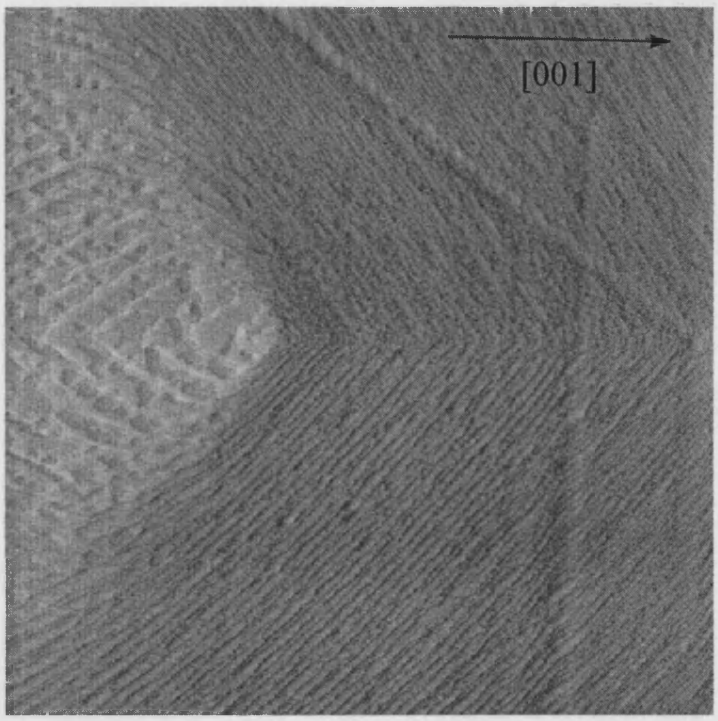

Fig. 5.2.4 *10 μm AFM image of what appears to be the centre of a growth spiral on a crystal grown at a supersaturation of approx. 30%. Extensive damage is evident on the growth terraces.*

In an attempt to improve on the protection method, crystals were removed through an n-hexane layer, whilst simultaneously spraying the crystal surface with a jet of n-hexane. This was observed to give improved results. An example of a surface protected in this manner shown in figure 5.2.5. In this image the centre of a growth spiral is visible. Although there is extensive damage to the terraces it is clear that the

general features of the spiral correspond well with those reported in previous DICM studies.

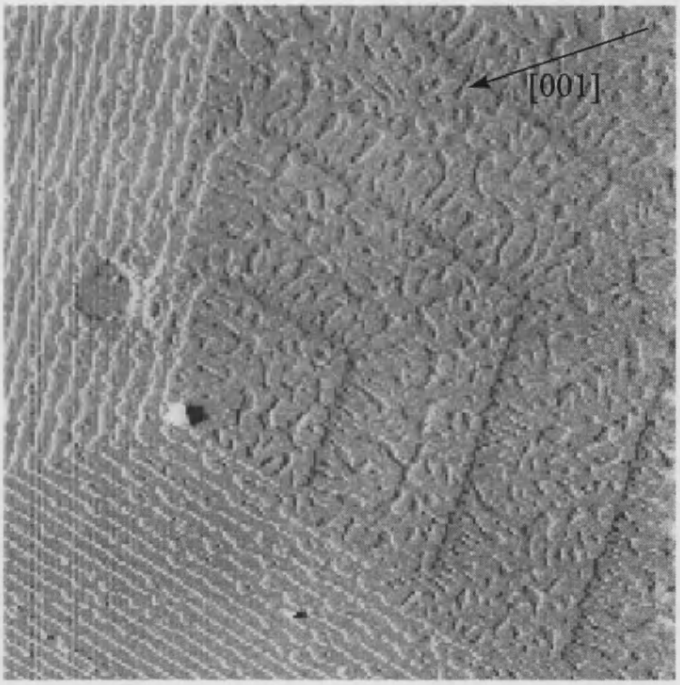

Fig. 5.2.5 *10 μm AFM image of a KAP (grown at low σ) surface protected via withdrawal through a simultaneous layer and jet of n-hexane. The shape of the spiral corresponds well with previous studies[63]. Damage in the form of extensive 'pitting' is visible on the terraces.*

The damage observed on the terraces of the KAP gives the impression of a surface on which dissolution has occurred. The use of constant force microscopy on the surface revealed the 'pitting' to invariably have a depth of 1.2 ± 0.2 nm. This corresponds with the height of one KAP unit cell in the c direction (1.386 nm). In the next section the origin of this damage is studied in more detail, with a view to further improvement of the protection method.

5.2.1.2 Investigation of Improved Surface Protection Method.

As stated above, the damage apparent on the (010) face of KAP protected by a jet of n-hexane and studied using AFM gives the visual impression of a surface on which dissolution has taken place. In order to study this possibility in more detail, it is first necessary to establish the different media with which the crystal comes into contact during, and subsequent to, the removal process. A list is given below:

- supersaturated KAP solution
- n-hexane
- air under normal atmospheric conditions

Dealing with these points in order, we start with the growth solution itself. For the entire period of time that the KAP crystals are in contact with the solution, i.e. from the moment of nucleation to the point of removal from solution, the solution is maintained in a supersaturated condition. Clearly this must be so, or no crystal growth would occur. Subsequent to removal, any droplets of solution which adhere to the surface will become even more supersaturated as water evaporates from the droplet. On this basis, it therefore seems reasonable to exclude the growth solution as a possible cause of dissolution of the crystal surface.

A medium which might more plausibly be considered to cause dissolution is the humidity content of air. Typically, crystals were imaged within one hour of removal from solution, therefore allowing a large time for dissolution to occur. In order to test this possibility a crystal was imaged, then left for several weeks in a relatively humid environment before re-imaging. No perceivable difference was apparent between the two images. This fact was later confirmed by numerous experiments, where crystals were stored under normal atmospheric conditions for considerable time periods

(many months) with no perceivable changes in the surface condition between imaging.

The final medium considered is n-hexane. Although n-hexane is selected for the fact that KAP is not soluble in it, at the molecular scale resolved by the AFM even the smallest amount of solubility would be detectable. During the protection process the crystal passes through a direct jet of n-hexane for a brief (1-2 seconds) period. For the purpose of solubility testing it is therefore sufficient to submerge an already protected crystal in a bath of n-hexane for several minutes (two orders of magnitude longer exposure than for the standard protection method). The result of this experiment was once again negative - no change in the crystal surface was observed.

As a final test a number of solvents other than n-hexane were used to protect the surface. A full list of all solvents used is given in the experimental section, however two examples are shown in figure 5.2.6 below.

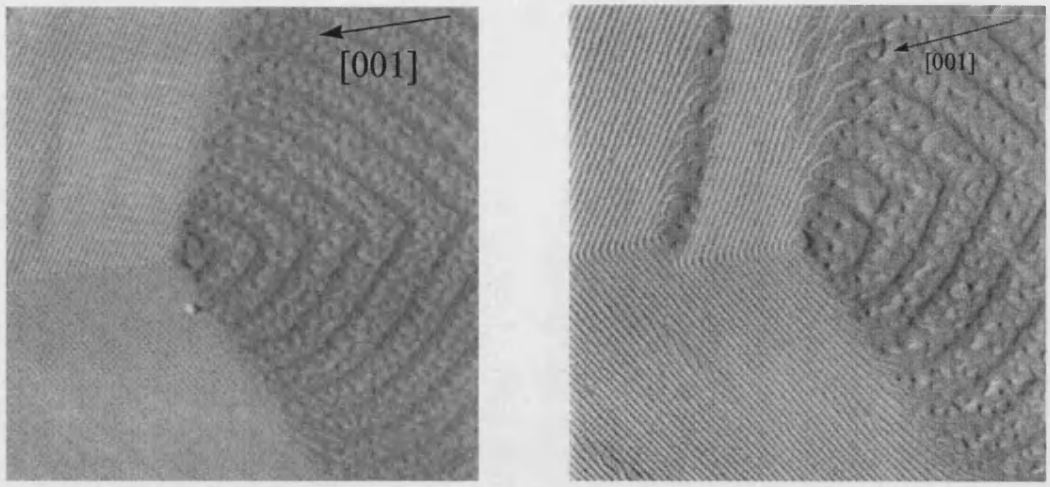

(a) *(b)*

Fig. 5.2.6 *Two AFM images (both 6 μm) of KAP (grown at a supersaturation of approx. 30%) crystal surfaces. Figure (a) was protected using n-octane and (b) using cyclohexane. On both crystals similar damage is visible on the large terraces.*

From these results it may be concluded that none of the media with which the crystal comes into contact is likely to cause dissolution, therefore ruling out this mechanism as the cause for the damaged appearance of the protected crystal surfaces.

A further variable with which to alter the removal process of KAP is the rate at which the solution is removed. Already some empirical evidence indicates that this may be of beneficial influence - increasing the removal rate by direct spraying of n-hexane rather than slow withdrawal through a layer produced improved results (compare figures 5.2.4 & 5.2.5).

In order to optimise only the removal rate of solution a jet of compressed air was used, without any n-hexane. The air typically had a pressure of 50 psi. A surface protected in this manner is shown in figure 5.2.7. In comparison with all previous protected KAP surfaces, a significant improvement in the appearance of the spiral is seen.

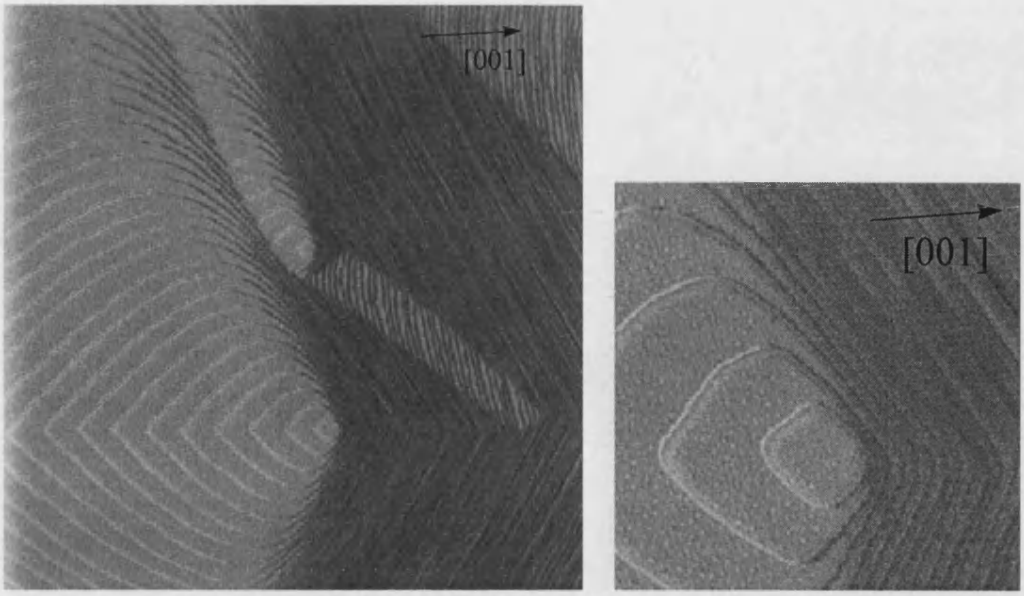

(a) *(b)*

Fig. 5.2.7 *AFM images of a KAP (grown at a supersaturation of approx. 30%) surface protected by removal through an air jet at a pressure of 50 psi. Figure (a) shows a 10μm area scan. Figure (b) is a 2μm area scan of the lower hillock. Note the undamaged appearance of the terraces.*

5.2.1.3 Damage Giving Rise to the Formation of Hexagonal Features on the (010) Face of KAP.

On a small percentage of the n-hexane protected KAP crystal surfaces, hexagonal 'pits' were observed. A typical example is shown in figure 5.2.8. The image shows a region of the surface which lies on the [101]f side of the hillock, which is characterised by a larger step spacing than the [101]s side (see figure 5.1.3). These steps may be seen between the hexagonal features. The sharp change of direction in the steps, visible in the bottom right corner of the image, is due to the polygonised shape of the growth hillock.

Fig. 5.2.8 *20 μm AFM image of a KAP crystal surface protected with a jet of n-hexane. Many hexagonal features are visible.*

At the interface between the steps and the hexagonal features it can be seen that the steps continue into the hexagonal area, but change direction in an inconsistent manner. In the centre of each hexagon lies a deposited mound of material. From constant force mode measurements the height, and hence the volume of these mounds may be determined. These were generally found to range between 3×10^{-20} m^3 and 1×10^{-19} m^3. Because this surface has been protected using n-hexane, there is the familiar damage on the terraces between the steps. Inside the hexagonal regions, however, the crystal surface appears completely smooth and free of damage. A final point of interest is the fact that all the boundaries of all the hexagons lie in approximately the same orientations. When compared with orientation of the entire

(010) face, it was observed that these also concurred to a large extent i.e. the edges of the hexagons are approximately oriented in the PBC directions.

5.2.1.4 Damage Having the Appearance of the Deposition of Material on the (010) Face of KAP.

On nearly all of the protected surfaces observed, regardless of protection method, some degree of debris was observed. The term debris is used here to indicate that this form of surface damage had the characteristics of contamination external to the entire crystal growth and removal process. Such contamination may, for example, be caused by atmospheric dust. This is quite possible, since on both the AFM instruments used, the sample was not held within a sealed container during imaging. In all cases no visible damage was apparent to growth features, such as steps, in the vicinity of the debris. This is well illustrated in figure 5.2.9.

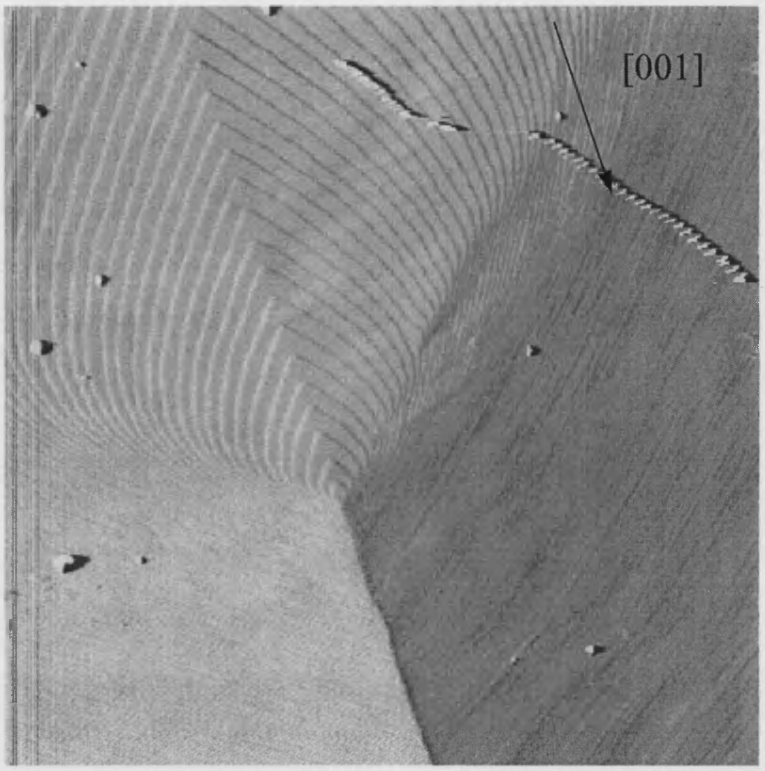

Fig. 5.2.9 *20 μm AFM image of a KAP crystal illustrating the presence of both immobile and mobile surface debris. The mobile debris is pushed to the edge of the image by the scanning tip.*

Two types of debris may be seen in figure 5.2.9. The first type remains adhered to the surface during the AFM scan, and therefore appears as a small deposit in the image. Several of these may be seen on figure 5.2.9. The second type is more loosely attached to the surface, and therefore is physically moved by the interaction with the scanning tip. Since the tip scans from the top of the image to the bottom, and from the left of the image to the right, the debris is pushed downward and to the right with each new scan. This causes the appearance of a jagged line on the image as is seen in the top right hand corner of figure 5.2.9.

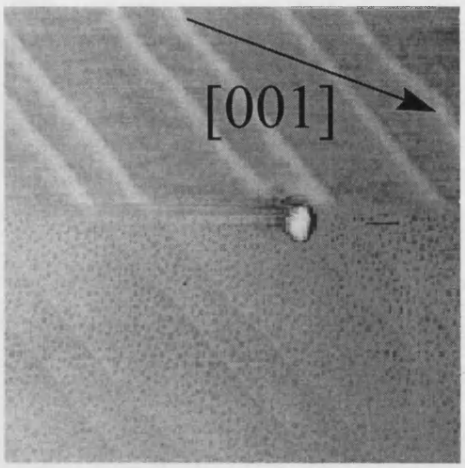

Fig. 5.2.10 *3 μm AFM image of a KAP crystal surface with a small piece of adsorbed debris. After scanning over the debris the tip is improved, resulting in a clearer image.*

In some instances the presence of debris proves to be useful due to the 'sharpening' effect that it may have on the tip. A good example of this is given in figure 5.2.10. Here a blunt tip, with a poor resolution strikes a piece of debris mid-scan. A noticeable improvement in resolution is apparent in the area of the image lying below the interaction with the debris.

5.2.2 Possible Damage Mechanisms Incurred on (010) Face of KAP During Removal from Solution.

Firstly, the damage visible on the terraces of spirals on the (010) face is discussed. This damage was particularly noticeable on KAP surfaces protected using n-hexane (see figs. 5.2.1-3).

Since we have already shown that KAP has no solubility in n-hexane, and remains unaffected by atmospheric moisture, it appears that only one inherent mechanism

remains to account for any surface damage. This is the deposition of KAP on the surface during removal from solution. Although it was observed in figure 5.2.5 that the terraces appear pitted, the possibility of deposition may not be ruled out on this basis alone, and is therefore considered in more detail here. The most likely mechanism for deposition of material on the surface is as follows: during the removal of the crystal from solution, at some point a very thin layer of adsorbed solution will be all that remains on the surface. As this last layer rapidly evaporates, a huge increase in the supersaturation results. This supersaturation is sufficiently high to cause inter-step two-dimensional nucleation and growth. The growth is terminated very rapidly due to the limited amount of dissolved material available. In this manner a widespread coverage of two-dimensional nuclei could occur on the surface. Since the edge of each newly formed two-dimensional nucleus would constitute the energetically most favourable site for growth units within its diffusion field, the resulting deposition would most likely be of unit cell height rather than a nuclei on nuclei process. For such a mechanism, the rate of removal of solution would be the major factor affecting the rate of increase in supersaturation of the adsorbed layer. Higher supersaturations would lead to a higher nucleation rate, and therefore the presence of more two-dimensional nuclei per unit area. Because of the fact that the AFM tip is relatively coarse in comparison with the unit cell height features it is imaging, this leads to the possibility that a surface which is nominally rougher than another surface, nonetheless appears smoother when imaged using the AFM. The situation is outlined schematically in figure 5.2.11 below.

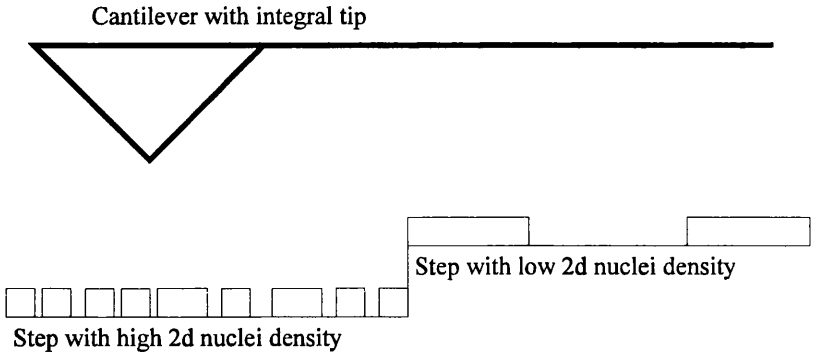

Fig. 5.2.11 *Schematic diagram showing the comparison between steps containing different sizes and densities of two-dimensional nuclei. At a certain point the resolution limit of the AFM is reached (tip dependent) and the step appears smooth.*

Referring back to figure 5.2.10, a good example of this process may be seen. Before striking the debris on the surface, the resolution limit of the tip is such that the steps appear smooth. After impacting the debris, the tip becomes 'sharper' and therefore resolution is increased. This results in the appearance of the steps changing from being smooth, to appearing pitted. Note that the darker areas of this particular image are lower than the lighter areas - the steps have many small pits. A clearer example of the surface pitting is seen on a poor air jet protected sample as shown below in figure 5.2.12

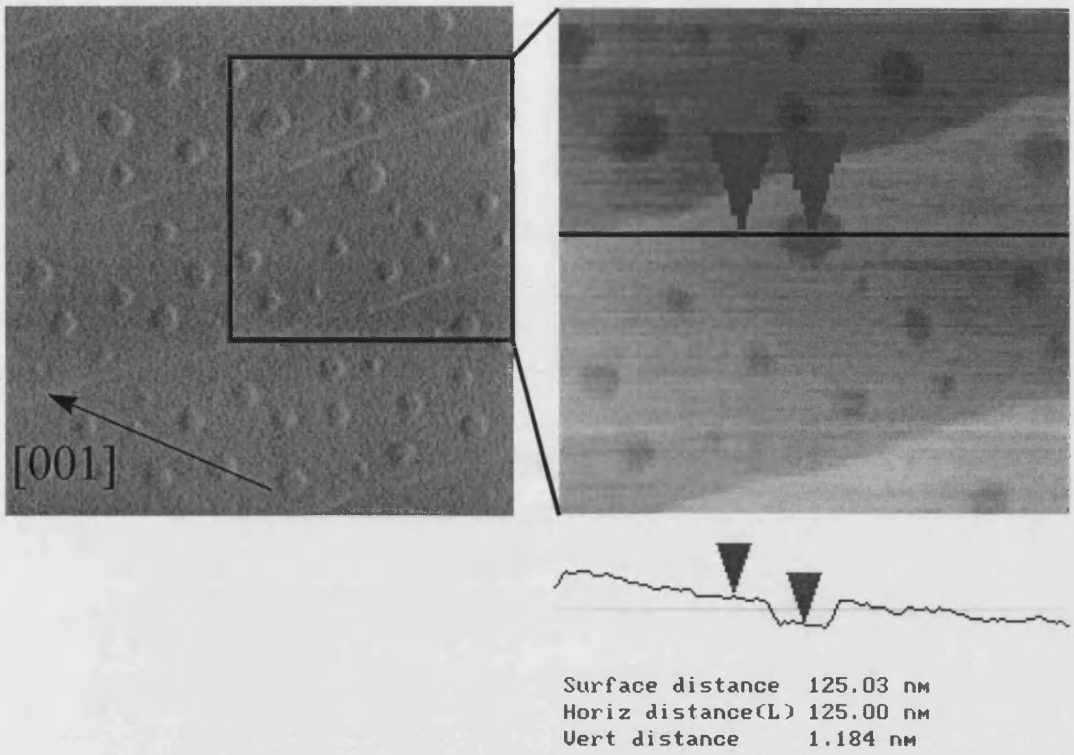

Fig. 5.2.12 *The image on the left is a variable force image of a train of steps on a KAP surface protected with an air jet (1.625 μm area scan). On the right a constant force image reveals the height of the pits to be approx. 1.8 nm*

The constant force image on the right shows the pits in the surface to be of unit cell depth. Note also the difference in contrasts between the variable and constant force modes. In the variable force image the pits may be mistaken as protrusions.

This image highlights the chief concern with the suggestion of a nucleation mechanism causing the 'pitting'. From a purely visual point of view it is difficult to reconcile the idea of a large scale nucleation process with the observed pits seen on the terraces. In order to illustrate how such a process might occur, figure 5.2.13 shows a surface protected under unusual conditions. It should be noted that by its nature the protection method using a jet of air is variable in the rate of removal of solution. Although every effort was made to reproduce the removal process as

accurately as possible between experiments, inevitably there are variations from crystal to crystal, a problem exacerbated by the high resolution of the AFM. In figure 5.2.13 a combination of an unusually 'sharp' tip together with a variation in the removal conditions *across the same crystal* give an illustration of the formation of pits (seen on the far left of the image), from what originally start out as distinct two-dimensional nuclei (seen on the far right of the image)

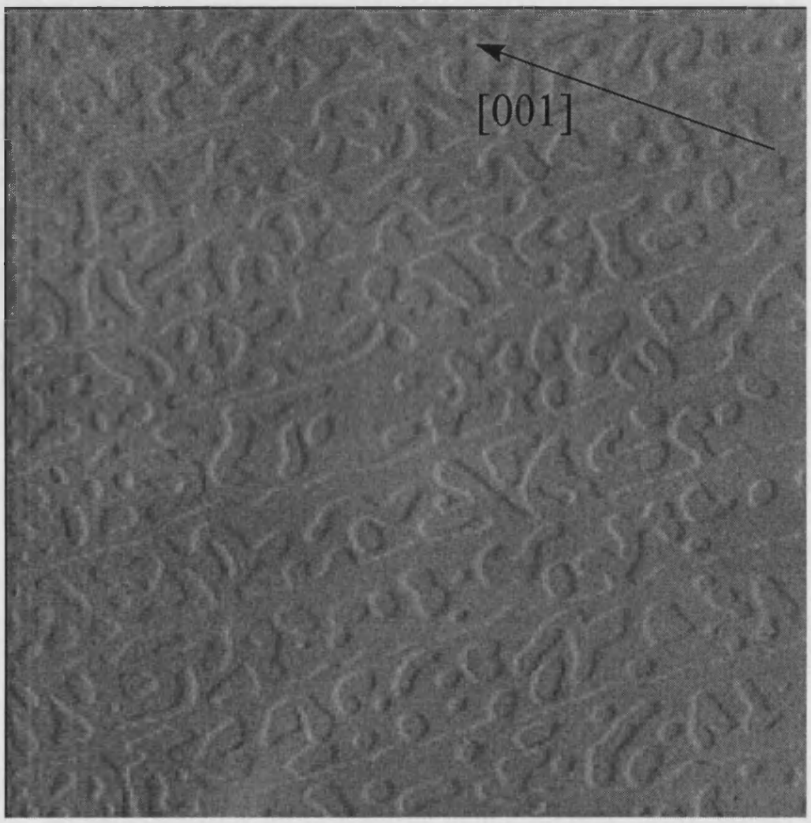

Fig. 5.2.13 *4μm AFM scan of a surface on which the solution removal rate has not been constant - the rate increases from the left to the right of the image - possibly due to a local barrier to the air flow over the crystal. On the right of the image, individual nuclei can be resolved. On the left these have merged, leaving a surface with the typical 'pitted' appearance.*

A constant force scan of a region near the left of image 14, once again confirms that the depth of the remaining pits is of unit cell height. This is shown below in figure 5.2.14.

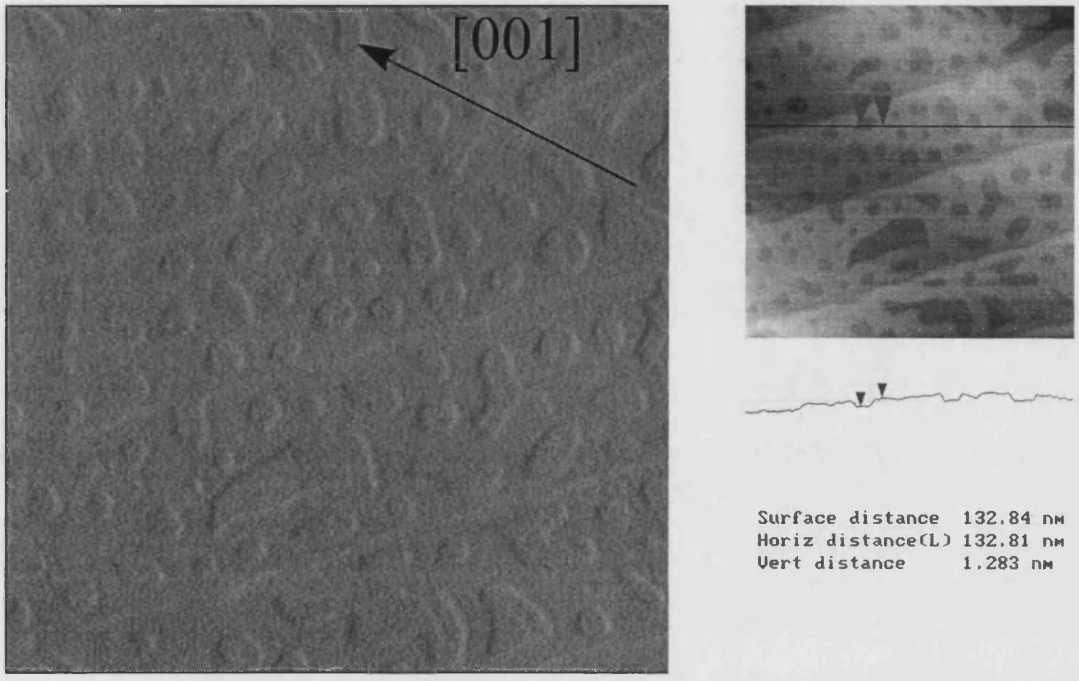

Fig. 5.2.14 *2 μm AFM scan in variable force (left image) and constant force (right image) mode. As before the pits are confirmed to be of unit cell height.*

Because of the importance of this mechanism i.e. the formation of pits from a two-dimensional nucleation and growth mechanism, a further illustration is given below in figure 5.2.15. This is of exactly the same surface as seen in figure 5.2.13, however, the tip quality is inferior. Nonetheless, this image depicts the transition process from nuclei to pits even more clearly. A further point of considerable importance is that the step spacings remain constant across the image, and are therefore not influenced by the variation in protection.

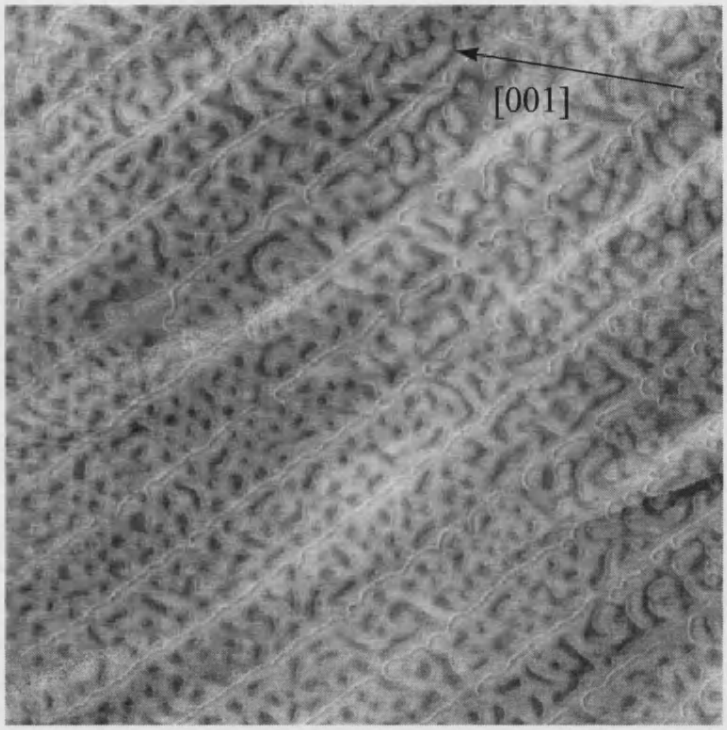

Fig. 5.2.15 *5 μm AFM image of the same surface seen in figure, but using a different tip. Note the two-dimensional nuclei in the top right of the image, compared with the two-dimensional pits, seen at the bottom left.*

It will be recalled that a second damage 'type' was observed on the (010) face of KAP. In this case the damage was limited to samples protected using n-hexane. For this damage type it may also be shown that a deposition mechanism, as described above, corresponds well with the experimental evidence. With reference to figure 5.2.8 the main features of the hexagonal pits may be summarised as follows:

- the pit is bounded by steps which have the damaged appearance typical of those surfaces protected using the slower n-hexane method.
- the terraces within the pit have a completely smooth and undamaged appearance.

- within the pit is a large 'mound' of deposited KAP.

All these features are explained by the deposition mechanism. During removal of the solution, the nucleation and growth sequence already described leaves the majority of the surface containing rough terraced steps as seen on other similarly protected surfaces. If the protection method is not completely successful, it is possible that locally, minute droplets of solution remain and adopt a minimum energy shape on the surface corresponding to the crystallographic directions. Finally these tiny droplets also evaporate, but much more slowly than the regions which have been directly effected by the blast. This means that a two dimensional nucleation and growth mechanism does not occur in as widespread a manner. In fact all the growth occurs at the conical mound lying within the hexagon, resulting in steps which are completely smooth within the hexagon. Taking into consideration the volume of the mounds and the supersaturation at which the crystals were grown it can be calculated that the amount of KAP solution required per mound of deposited KAP varies between about $1x10^{-19}$ and $1x10^{-20}$.

The precise mechanism for the formation of the conical mounds is unclear, however, there are two basic possibilities - one based on two dimensional growth and the other on spiral growth.

In the case of two dimensional nucleation and growth it is possible that due to the lower supersaturation within the droplet compared with the regions effected directly by the blast, a single nucleus (the first to form) provides the growth centre for all the material contained within the droplet. As water evaporates, the droplet becomes smaller and smaller and the solution becomes more supersaturated, thereby

promoting the formation of nuclei on nuclei, until finally all the water evaporates and a conical mound remains.

The main objection to a spiral mechanism is that it is not clear why a spiral should form within all droplets. On the one hand it is possible that due to the high supersaturation and therefore rapid growth of the steps within the droplet the likelihood of dislocation nucleation and corresponding spiral mechanism is increased. On the other hand it may be that dislocations already present on the crystal surface provide the most likely site for droplets of solution to become attached. In this case all droplets would by definition have the possibility for a spiral growth mechanism.

5.2.3 Conclusion

In summary, it may be concluded that on all of the surfaces seen in this study, an inter-step two-dimensional nucleation and growth process occurs during surface protection. In all cases the step spacing does not seem to be disturbed at the micro (as opposed to nano) level. This also follows from theoretical considerations. Normally as the supersaturation increases the step spacing between turns of the spiral decreases. However in the case considered here, the change in supersaturation is rapid enough to cause a change in the growth mechanism thus leaving the relative step spacing undisturbed during removal.

For the purpose of producing the most accurate replica of the surface it is desirable that the nucleation rate be as high as possible. This was shown to be most effectively achieved using a jet of compressed air, and is therefore the preferred protection method for ex-situ AFM studies of the (010) face of KAP.

5.3 GROWTH MECHANISMS OBSERVED ON THE (010) FACE OF KAP

5.3.1 SPIRAL GROWTH MECHANISM OBSERVED ON (010) FACE OF KAP

Having established the likely mechanisms of surface degradation incurred during removal of the crystal from solution, and having confirmed the lack of macroscopic effects on the shape of the hillock due to this process, it is possible to examine the growth features in more detail. In the vast majority of cases spiral growth features, such as those predicted by BCF, are present on the (010) face of KAP. A typical example of a spiral observed using AFM is shown in figure 5.3.1. In figure 5.3.2 a schematic representation of the spiral is also shown, with the relevant axes labelled.

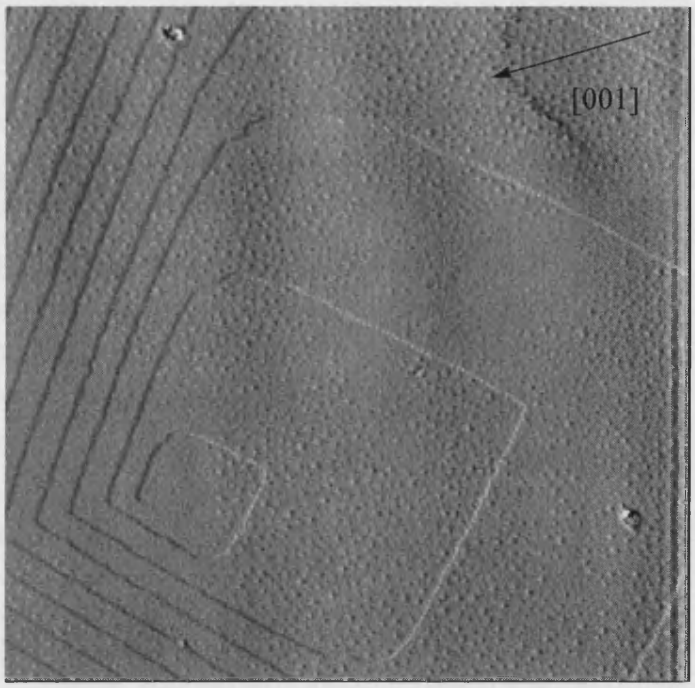

Fig. 5.3.1 *12μm scan of a growth spiral observed on the (010) face of KAP. Two basic features of the spiral stand out, namely the anisotropy and polygonisation.*

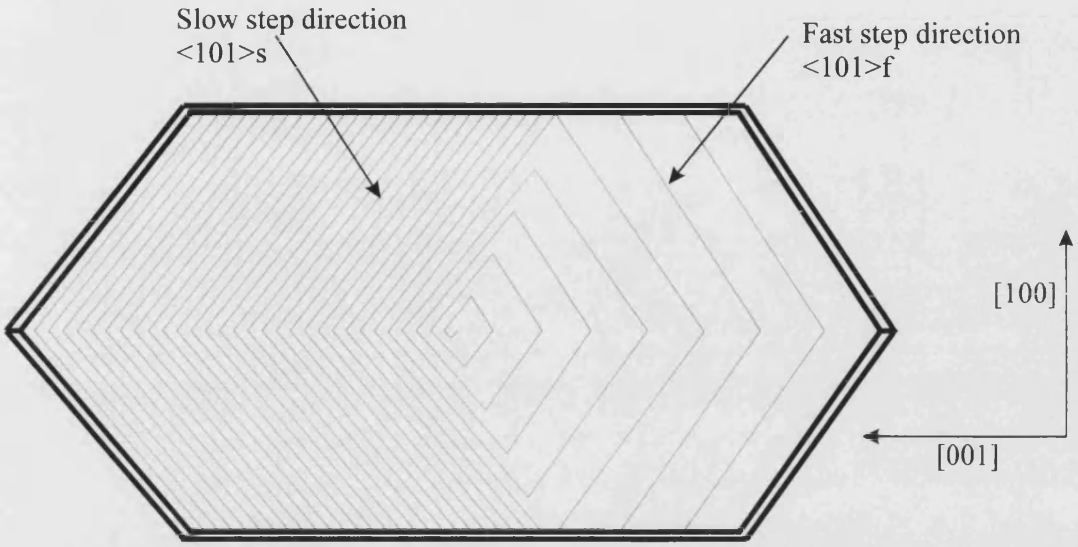

Fig. 5.3.2 *Schematic diagram of the growth spiral highlighting the difference in velocity of steps observed on the (010) face of solution grown KAP crystals.*

The spiral is polygonised with the <101> step orientations dominating. Since these steps move at different velocities the spiral is also anisotropic. In figure 5.3.1 there is not a sharp change in angle between the <101>f and <101>s steps (not shown in the schematic diagram). Instead there are rounded steps oriented in approximately the <001> direction. In some cases these steps were oriented more strongly in the <001> direction (see for example figure 5.2.5 in section 5.2) whilst in other cases they were completely round.

All of the features listed above, which relate to the growth spiral shape, are discussed in a later section (section 5.4).

5.3.2 *Measurement of Step Heights*

In all cases where a spiral mechanism was present on the (010) face of KAP it was possible to measure the step heights. These were found to be invariably of unit cell height, as exemplified on the surface below in figure 5.3.3.

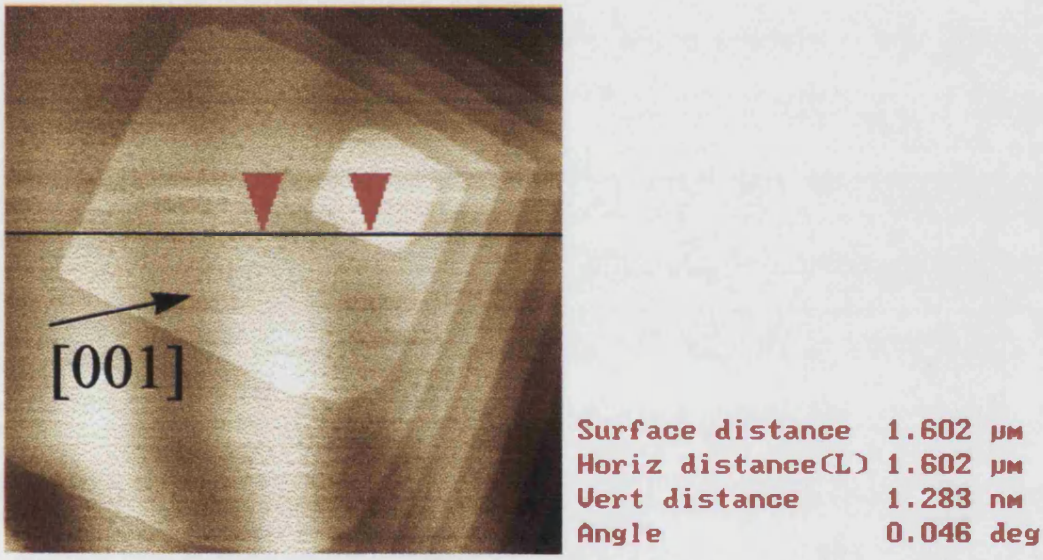

Fig. 5.3.3 *Constant force image of the same crystal surface seen in figure 5.3.1. This allows the determination of step heights as shown in the line scan at the top of the image. The measurements relate to the two markers seen on the images. From the fact the vertical distance is 1.3 nm it is reasonable to assume that these are all unit cell high steps (1.386 nm). This was found to be true on all such spirals measured on the (010) face of KAP.*

In contrast, therefore, to optical methods it is possible to see directly both the spiral and unit cell step heights (with optical methods spirals may only be visualised

directly if they consist of macrosteps. Used in conjunction with other techniques, such as multiple beam interferometry, it is also possible to acquire step height information). From the fact that the steps are of unit cell height it also follows that the theoretical work of BCF may be applied to the growth spirals. It should be noted that this is not the case for spirals consisting of macrosteps, for which the theory is not valid in its original form.

5.3.2.1 Analysis of the Growth Spiral Centre

A further general feature of interest is the centre of the spiral, corresponding to the dislocation core. From the X-Ray topography analysis it appears that the most likely source of spirals is from dislocations with the [110] type Burgers vector. This is the only dislocation type observed in the (010) sector which has a component of the Burgers vector normal to the surface, and is therefore the only dislocation likely to be involved in a spiral growth mechanism. The normal component is in fact [010], corresponding to a unit cell step. From table 5.1.1 (section 5.1) it can be seen that the length of the [110] vector is relatively large - namely 15.3 Å. This length means that the strain energy associated with the dislocation (which varies as $|\mathbf{b}|^2$) is also large. According to Frank's[33] mechanism it is therefore possible that a hollow core may form around the dislocation. In the case of KDP it has previously been shown using AFM that this mechanism occurs for large values of $|\mathbf{b}|$[96].

On the KAP we have studied using AFM a large number of dislocations also revealed a hole at the dislocation core. An example is shown in figure 5.3.4, where the first few turns in the spiral are imaged.

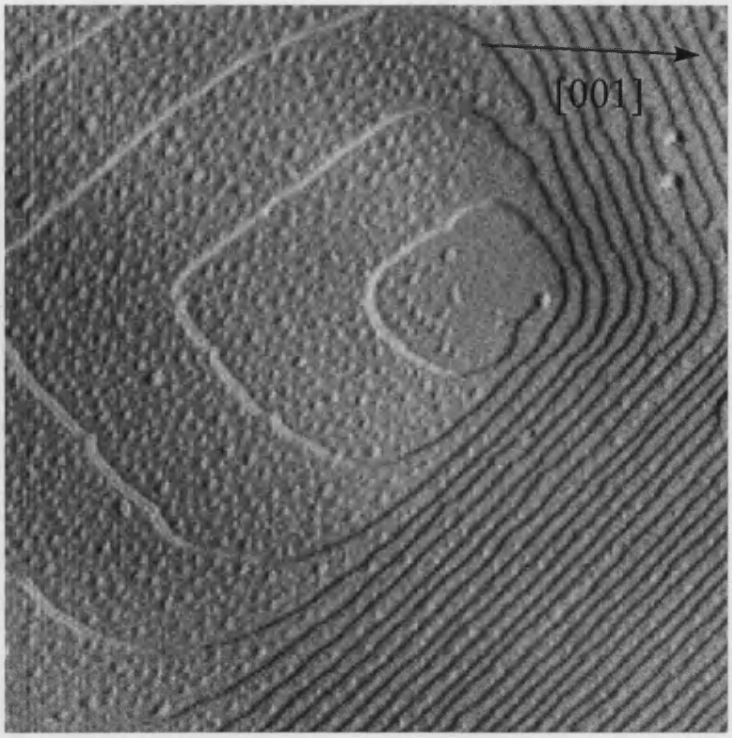

Fig. 5.3.4. *3.5 μm scan of a growth spiral in variable force mode. At the spiral centre a darker region may be seen. In figure 5.3.5 below this is shown to be a dip.*

Figure 5.3.4 shows a variable force image of the central region of a growth spiral. The discontinuity visible at the centre of the spiral is analysed below in a line scan of a constant force image.

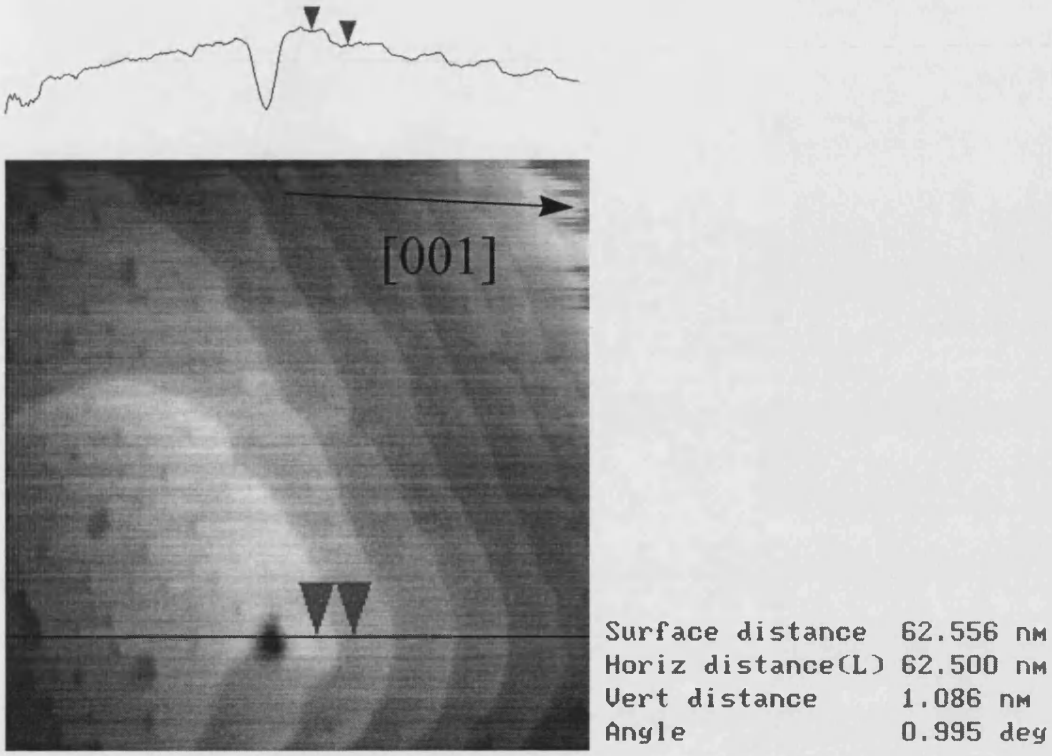

Fig. 5.3.5 *1μm scan of the central region of a KAP growth spiral. The height measurement verifies that the steps are of unit cell dimensions. Also visible on the line scan (above the image) is the large dip at the spiral core.*

Figure 5.3.5 shows a 'dip' at the centre of the dislocation, corresponding to the sinking of the tip into the hole, effectively leaving an image of the tip itself. If the hole were due to the mechanism suggested by Frank, then one would expect to see them at the centre of all growth spirals, particularly since the X-Ray topography work suggests that the large majority of dislocations associated with growth spirals are likely to have the [110] Burgers vector. In actual fact, however, they were only observed at the centre of about thirty percent of all the growth spirals observed. On the basis of this information alone, however, it is not possible to discount the possibility of the dislocations having hollow cores during growth. The problem with

interpretation of ex-situ results in the region near the spiral centre is heightened by the fact that the centre of the spiral is an energetically peculiar site. The dislocation core has a significantly higher energy than the surrounding steps, thus making it considerably less stable in the presence of any adsorbed water. Hence dissolution will commence rapidly at the centre of the spiral and result in a very local 'unwinding' of the growth spiral, transforming it into an etch spiral or pit. Conversely, if no water is adsorbed, then it is possible that during the removal process the rapid increase in saturation leads to deposition of material in the hollow core. Therefore there are two possibilities. Either the cores are not hollow during the growth process and (some random percentage) undergo dissolution near the core after removal *or* the spirals are hollow during growth and (some random percentage) undergo deposition of material in the core during the removal process. In order to resolve this problem it would appear that an in-situ approach is necessary.

In the cases where a hole was not observed at the dislocation core it was possible to investigate the characteristics of the step at the point of origination. A growth mechanism associated with a screw dislocation would be expected to produce an increase in step height - from zero to the height of a unit cell. Figure 5.3.7 confirms that this occurs.

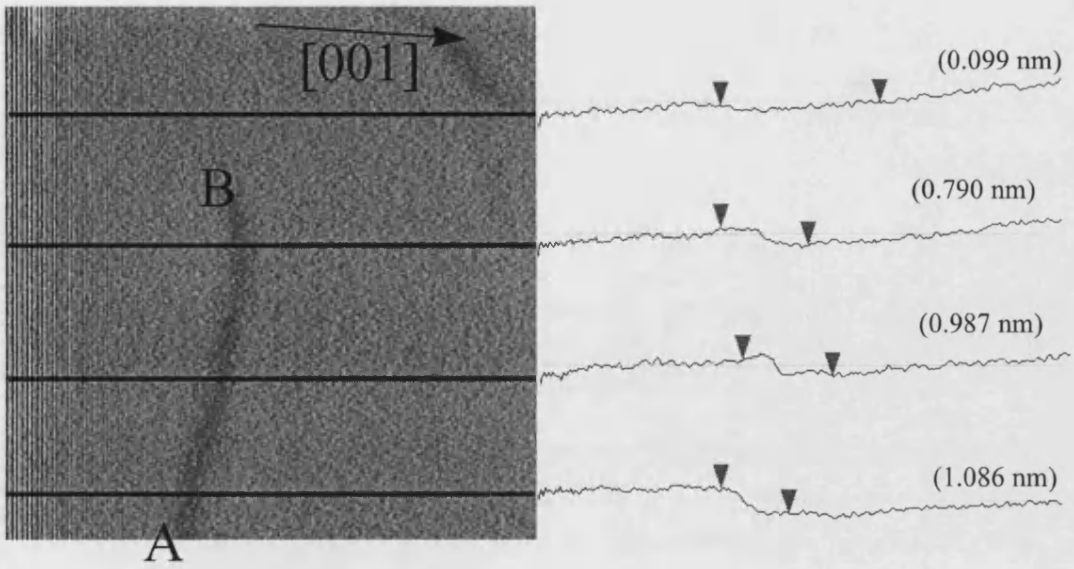

Fig. 5.3.6 *Illustration of the centre of the growth spiral shown in figure 5.3.1. The emergence of a screw dislocation (marked AB) on the surface is verified by the line scans at different points on the surface. The figures in brackets give the vertical height differences between the two markers. Recall that the resolution of the AFM was estimated to be 0.25 nm.*

5.3.3 2D NUCLEATION

During the study of KAP micro crystals nucleated on a glass slide at high (approx 30%) supersaturations, a small proportion of crystals were encountered which differed significantly from the majority in terms of their crystal habit. These crystals were observed to be much thinner platelets, indicating a reduction in the relative growth rate of the (010) face. This fact is illustrated in figure 5.3.7 below. A DICM micrograph of a 'typical' crystal (seen in figure (b)) is shown next to a crystal possessing the thin platelet habit (shown in figure (a)). For simplicity, these two habits will be denoted as 'platelet' and 'thin platelet'. In order to examine the growth mechanism of the thin platelet crystals in greater detail AFM was used.

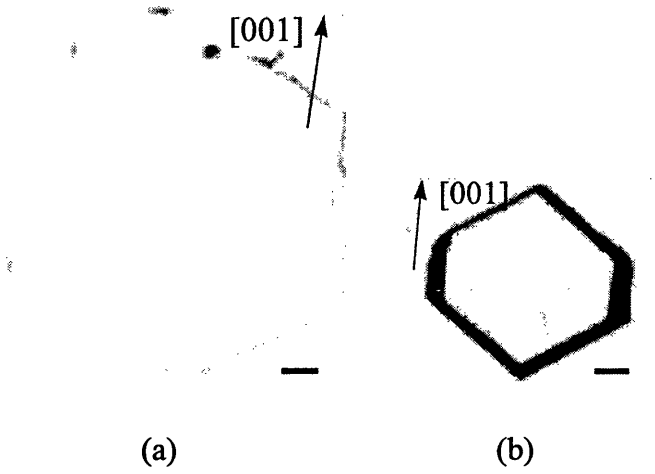

Fig. 5.3.7 *DICM micrograph comparing two micro crystals nucleated on a glass slide under the same conditions (the scale mark is 50 μm). A large difference in height between the crystals shown in figures (a) and (b) is evident from the relative thickness of the black outline surrounding the crystal.*

5.3.3.1 AFM OF THIN PLATELET CRYSTAL SURFACES

On some of the thin platelet crystals observed using AFM the surface appeared very flat, with no outstanding features, on others a spiral mechanism was present, but with an unusual location of the spiral - this is discussed later. Figure 5.3.8, however, shows one of the observed instances where neither of the above was the case. This image is of an area lying in the central region of the (010) face.

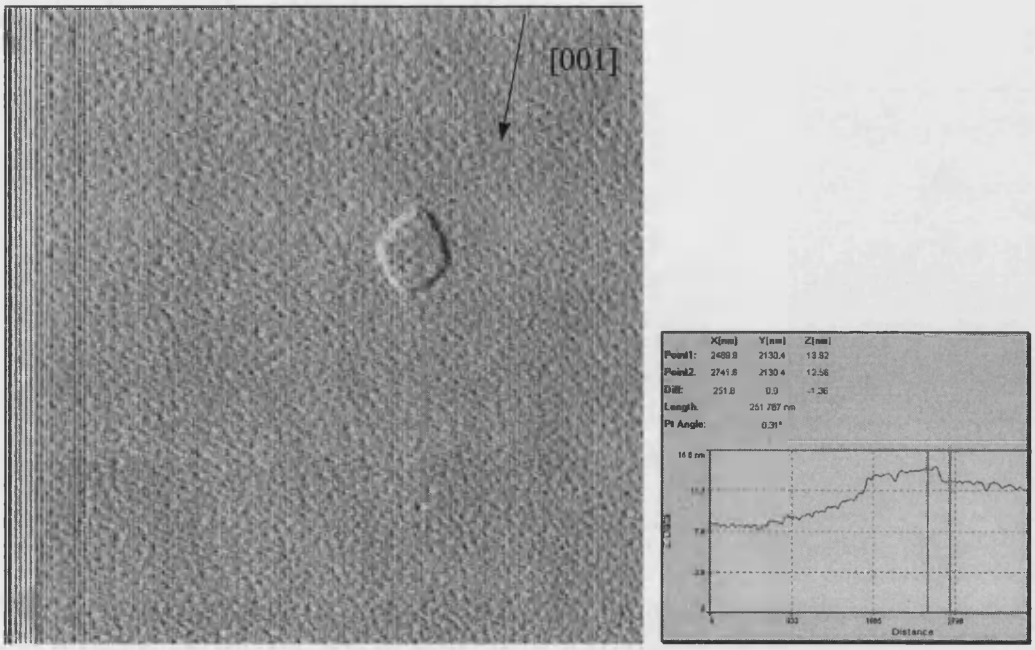

(a) (b)

Fig. 5.3.8 *6.2 μm scan of a thin platelet KAP crystal. The surface is flat apart from the single feature seen in the centre of the image. In (b) the height of this feature is shown to be approx. 10 Å*

The feature seen in figure 5.3.8 has several noteworthy features. Firstly the shape is identical to the central region of growth spirals seen on other crystals with the platelet habit. Secondly, a comparison of the orientation of the feature with the orientation of the edges of the (010) face itself revealed the same relation as for the centre of growth spirals (for an illustration of the orientation of the growth spirals with respect to the edges of the (010) face, see for example figure 5.3.2 above). Constant force microscopy suggested that the feature was of unit cell height, as shown in figure 5.3.8(b). For this image a tube scanner was used, and the constant force mode shows a good example of a common problem associated with this type of scanner, namely cross-coupling. This has the effect of distorting the image such that a curvature is

introduced. Nonetheless, from the vertical distance calibration it is clear that the height is around 1.3 nm, which implies unit cell height. The final point which should be emphasised is that there are no signs of any trains of steps in this image. As a comparison it is useful to look at figure 5.3.13 below, which shows a spiral mechanism on a crystal grown at the same supersaturation. Figure 5.3.13(b) serves to illustrate that steps would always be expected to be seen anywhere on crystal surface with a spiral mechanism controlling the growth.

The combination of all of the above points indicates the possibility that, in fact, a spiral mechanism is not responsible for growth on this surface. A more likely mechanism for this crystal would be a two dimensional nucleation and growth model, where the feature seen on the surface is a single nucleus. This hypothesis is substantiated by further evidence shown in figure 5.3.9. This image shows the edge of the crystal previously seen in figure 5.3.8.

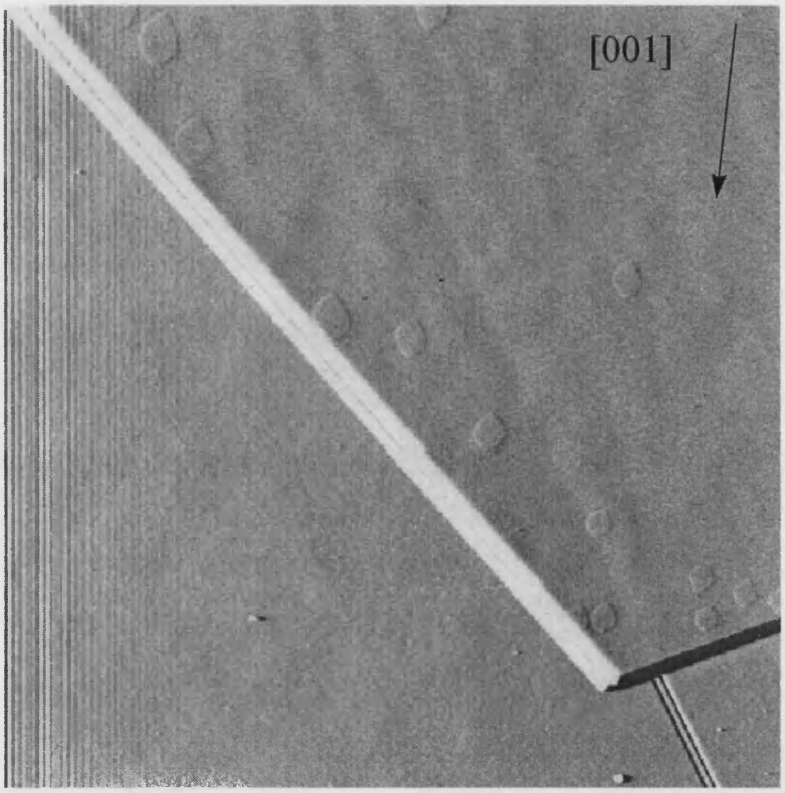

Fig. 5.3.9 *20 μm scan of the edge of the crystal seen in figure 5.3.9. Many polygonised features are visible on the surface of the crystal - in particular in the corner.*

In the above image the tip has scanned over the edge of the crystal. The corner of the (010) face is therefore visible at the bottom right of the image. On the surface of the crystal many more of the two dimensional features are seen. The interesting observation from this image is the fact that the density of the features is much higher than was observed in the centre of the crystal. This fact is shown more clearly in figure 5.3.10, where the average number of these features, in a moving 5 μm window, is plotted for edge-side-edge and edge-centre.

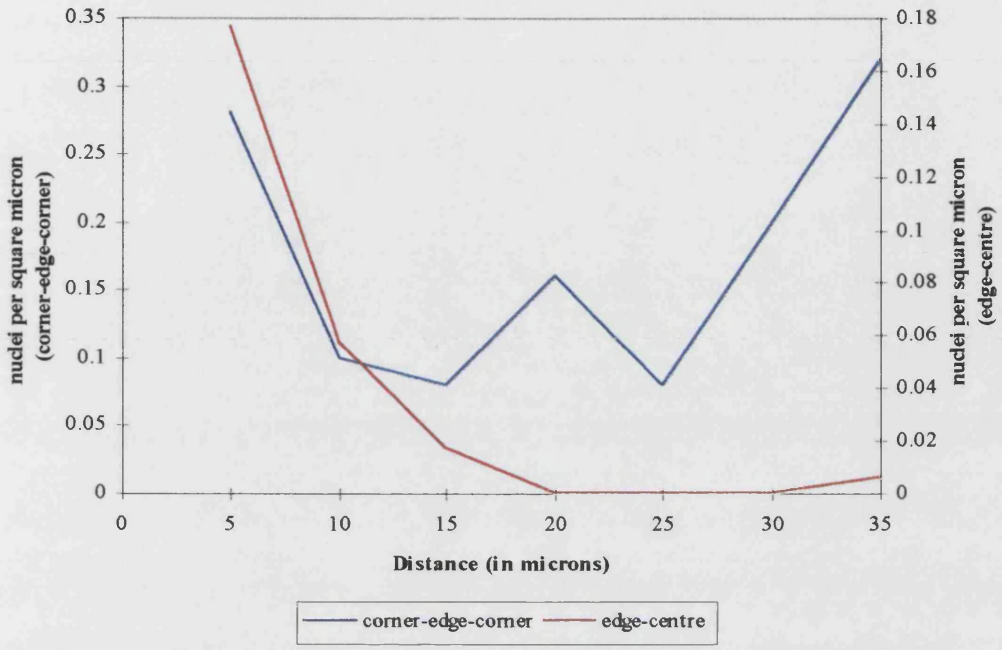

Fig. 5.3.10 *Distribution of two dimensional nuclei across the surface of the crystal shown in figure 5.3.9.*

From this it can be seen that the density of the features is highest at the corners, followed by the edges and finally a very low density is present in the central region. From volume diffusion considerations it follows that the surface concentration above a growing crystal is not constant, this is known as the Berg phenomenon. The concentration will be a minimum at the centre of the crystal, and increase to a maximum value at the edges, where the flux of new material from the bulk is highest[100,101]. Following a similar argument it will be appreciated that the concentration at the corners would be expected to be higher along the edge. Since the nucleation rate of two dimensional nuclei is so sensitive to the supersaturation, it is therefore consistent to expect a nuclei density more or less in line with the concentration gradient over the surface. Figure 5.3.10. provides strong experimental support for this.

If it is accepted that all the two dimensional features seen are nuclei, then from the fact that a large number of nuclei are present on the surface it may also be inferred that the growth is not dominated purely by the nucleation step. This is not in agreement with the observation that the size of all the nuclei observed on the surface lie within a narrow size range. In a nucleation and growth model it would be expected that since the probability per unit time of nucleation occurring at a given supersaturation is equal, a distribution in nuclei size would occur, given that the growth rate is not infinitely fast with respect to the nucleation rate.

An explanation of this point needs to take two things into consideration. Firstly the observation that nearly all thin platelet crystals had flat, featureless (010) faces when observed using AFM. Secondly the protection method used to allow ex-situ experiments. This was justified for the protection of surfaces with a growth spiral, but not necessarily for other growth mechanisms.

Flat surfaces would be most likely to occur if the nucleation and growth mechanism were dominated by the nucleation step. In practice this would mean that the surface would be flat for the majority of the time. As soon as nucleation occurred, rapid growth would again produce a flat surface, until the process repeated itself. In most cases, therefore an ex-situ study would show a flat surface.

The existence of a large number of nuclei confined to a relatively narrow size range suggests, in combination with the above, two things. Firstly all the nuclei nucleated at more or less the same time, and secondly the solution was removed shortly afterwards - otherwise once again a flat surface would be observed. A possible answer to this is a sudden change in supersaturation during or immediately prior to the protection process. For example movement of the crystal with respect to the

solution, might decrease the size of the boundary layer; movement of the droplet/ slide through the air to the high pressure nozzle etc. It will be seen later that this may also effect growth spirals, particularly near the spiral centre, where the spiral will begin to 'wind up' first in the event of a higher supersaturation.

Whatever the exact reason for the appearance of the two dimensional nuclei on the particular crystal in figure 5.3.10, it does not detract from the underlying conclusion: two dimensional nucleation and growth occurs on a fair proportion of KAP micro crystals. This is surprising since with reference to the theory described in section 2.1 it is apparent that a growth mechanism based exclusively on two dimensional nucleation and growth is only likely to occur on a crystal face which is completely free of screw dislocations. Given the high dislocation densities observed in most materials it is therefore very unlikely to encounter two dimensional nucleation and growth as the only growth mechanism on a particular crystal face. This basic concept has been reiterated recently by Frank in his foreword to the Handbook of Crystal Growth[103].

Two dimensional nuclei are therefore expected to be limited to occurring between the steps produced by a spiral mechanism. This phenomena has been observed on KDP[104], and is also the mechanism which was suggested above to be responsible for the damage to KAP terraces during removal from solution.

A possible explanation may be a combination of the fact that KAP has an inherently low dislocation density and the very small size of the crystals studied using the AFM. Shortly after the nucleation phase it is possible that some sectors are defect free, and therefore grow by a two-dimensional nucleation and growth mechanism. If dislocations are present in other growth sectors, however, then this mechanism is

likely to be only temporary as is discussed next. It is worth noting that a different growth mechanism on different faces might be a mechanism for the frequently observed growth rate dispersion of micro crystals.

5.3.3.2 CHANGE FROM A TWO DIMENSIONAL TO A SPIRAL MECHANISM

Given the fact that both a spiral and a two-dimensional growth mechanism have been observed on the (010) face of KAP, the possibility exists of a change between the two mechanisms. Since a spiral mechanism is self perpetuating, it is clear that the only feasible change to a two dimensional mechanism can be inter-step nucleation and growth at very high supersaturations. This was observed during removal of the crystals from solution and was covered in section 5.2. A change from a two dimensional mechanism to a spiral mechanism may be envisaged to occur in two ways. Firstly, the nucleation of a dislocation may occur during the process of many nuclei growing and impinging on one another. At some point during this stochastic process an inclusion might be formed between two growing nuclei, thus giving rise to the possibility of dislocation nucleation. In the case of a screw or mixed dislocation a growth spiral would be likely to form. Secondly, it is possible that dislocations present in sectors other than the (010) sector bend into the (010) sector, and hence form the starting point of a growth spiral. In the case of this mechanism occurring there is also an obvious consequence for the location of the new growth spiral. It must initially lie on the edge of the (010) face.

As was stated in the introduction above, some of the crystals exhibiting a thin platelet habit had a growth spiral mechanism. An example is shown below in figure 5.3.11.

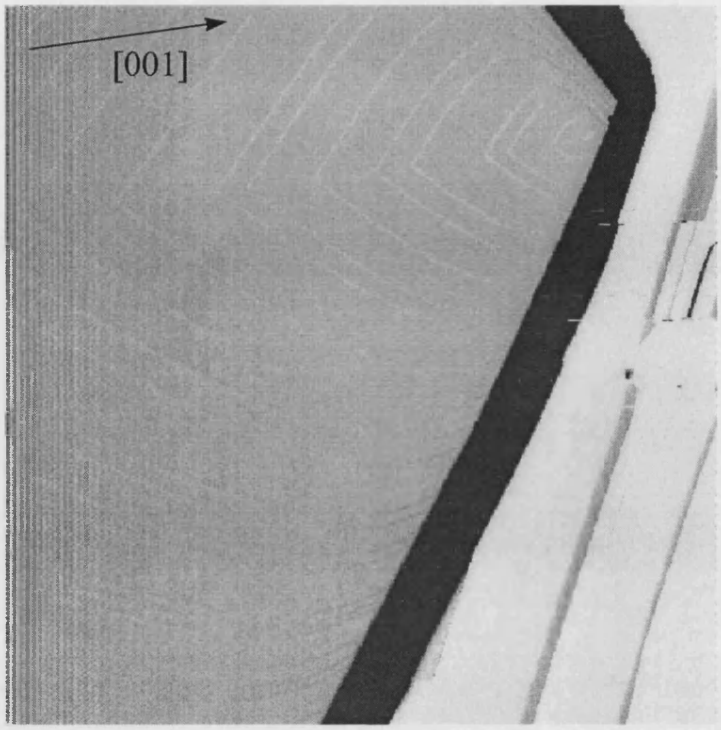

Fig. 5.3.11 *40 μm scan of a thin platelet crystal with a spiral growth mechanism emanating from the edge of the crystal. Note the large and inconsistent step spacing..*

Of course it should be remembered that the allocation of the term 'thin platelet' to a particular crystal is base purely on visual appearance, and is therefore not definitive of a particular growth mechanism. The crystal shown in figure 5.3.9. was extremely thin as measured by constant force microscopy - approx. 200 nm. Other crystals, such as that seen in figure 5.3.11 are considerably thicker - some 1500 nm. Nonetheless both crystals share the characteristic of being considerably thinner (orders of magnitude) than the majority of crystals. The growth spiral seen on the surface of the crystal shown in figure 5.3.11 is unusual in several respects. Firstly the step spacing is large when compared with other platelet crystals. Secondly the spacings exhibit a high variance and finally the centre of the growth spiral lies precisely on the crystal

edge. Note that due to this 'difficult' location of the spiral, the image quality of the spiral is not particularly good. This is due to the fact that the crystal height is orders of magnitude larger than the steps on the surface, making it difficult to contrast only the steps. Furthermore the tip tends to become damaged as it strikes the edge of the crystal during the reverse part of the scan. Below in figure 5.3.13 a section of a topograph is reproduced to illustrate the initial location of dislocations bending between sectors.

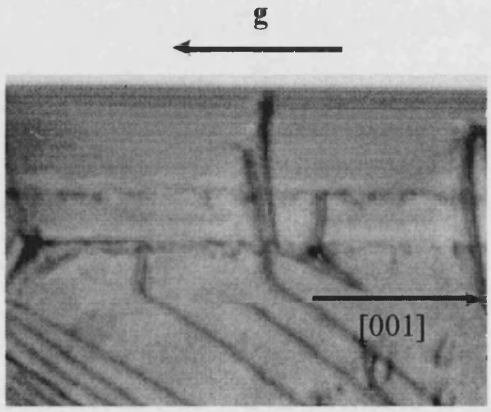

Fig. 5.3.12 *$01\bar{2}$ reflection of dislocations bending into the (010) sector (field of view is approx. 1 mm).*

Some of the bending dislocations are seen to terminate on the 'strain' outline (see section 5.1) of the (010) face. Although this process has occurred randomly in the case of this large crystal, for the case of thin micro crystals the likelihood of a dislocation bending between sectors becomes larger as the ratio of the crystal height to width decreases. For example in figure 5.3.10 above with a height of 200 nm and a surface length of approx. 70 μm a dislocation which had nucleated in the middle of the underside of the crystal would have to have an angle of less than 0.33° with the

bottom (010) face in order not intercept with the top (010) face. The implication, therefore is that any dislocations present in the lower sectors will eventually be forced to change sector if there exists a large discrepancy in the relative growth rates of these sectors and the (010) sector. Of the dislocations which change sector not all will contribute to a change in growth mechanism. As was discussed previously, the sectors containing the highest defect densities are the end type sectors. In these sectors the [001] and [101] type Burgers vectors were most commonly observed. Neither of these dislocations, however, contains a vector component lying perpendicular to the (010) face, and hence no step will be produced on this surface. Although the role of edge dislocations in crystal growth has been discussed at some length by various authors[105-108], here a conservative view is taken and no influence is assumed, particularly since the growth is still observed to occur via a spiral mechanism. In the Lat sectors, no characterisation of the dislocations was possible, and hence it is possible that these, have a Burgers vector which produces a step on the (010) surface. Another possibility is that other dislocation types occur very infrequently within the end sectors, and were therefore not observed in the X-ray topography work. For a growth spiral it is after all only necessary for one such dislocation to be present.

Once a spiral source is established on the surface the growth rate of the face will increase and the interstep distance will become the same as on other crystals grown at the same supersaturation. In figure 5.3.13 a spiral is shown which is near, but no longer on, the crystal edge. The step spacing is equal across the entire spiral (see in particular fig. 5.3.13(b)).

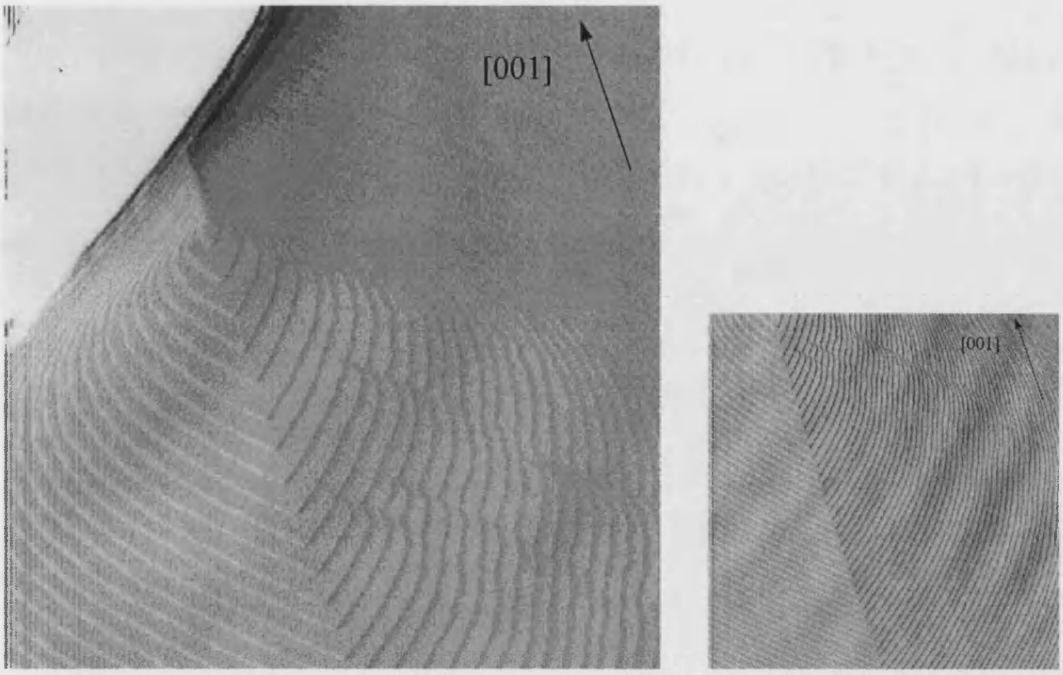

(a) (b)

Fig. 5.3.13 *(a) 11 μm scan of a crystal with a growth spiral near the crystal edge. (b) 20 μm scan of the same crystal showing the step uniformity away from the spiral centre. Compare this with figure 5.3.11 which was grown at the same supersaturation (35%).*

5.4 An Investigation of Growth Spiral Attributes

5.4.1 Growth Spiral Interactions

Up to this point the spirals investigated were dominated by a single dislocation, leading to a growth spiral free of disturbances. A typical example of this was shown in figure 5.3.1 above. However it should be noted that this was not generally the case. Although the X-ray topography work shows that KAP has a very low dislocation density in general, the exact number will vary from crystal to crystal. This may lead to a wide variety of surface topologies. From a fundamental point of view it will be recalled that BCF predict four different types of growth spiral interaction arising from two binary variables. These are:

1. The distance between the spiral sources (i.e. emergence point of the screw dislocation) is greater or less than $10r_c$.
2. The spiral sense is positive or negative.

Because KAP has the characteristic of exhibiting 'V' dislocations, with both arms of the 'V' lying in the (010) sector, the possibility exists that for some time subsequent to nucleation of the dislocation pair, the ends of the 'V' lie within a distance of $10r_c$ of one another. The angle between the 'V's may be estimated from the angles measured on the X-Ray topographs. This may be done most simply from the $00\bar{4}$ reflection since the 'V's lie in this plane. From simple geometry the angle may then be shown to be approximately 17°. Since we know from *(2.13)* that:

$$y_0 = 19r_c$$

then we may estimate the value of r_c from the distance y_0 on the AFM images. Due to the anisotropy of the KAP spiral it is necessary to make an assumption concerning the relative contributions to r_c from the fast and slow step directions. Here an equal contribution from each direction is assumed. Later in section 5.4.2 the exact relation between supersaturation and step spacing will be discussed. Here, however, we consider only two extreme cases: very low supersaturation (1.2%) and very high supersaturation (30%). For these cases the two arms of the [011] 'V' dislocations remain within the critical $10r_c$ distance for a height of:

$h_{30\%} = 0.32\mu m$ &

$h_{1.2\%} = 3.5\mu m$

From this it follows that crystals grown at low supersaturations may experience a significant fluctuation in growth rate due to the co-operation of these dislocations. At higher supersaturations, however, the effect only occurs for a height of a few hundred unit cells and is therefore likely to be far less significant.

Below, the four basic spiral interaction types are discussed with reference to the AFM results.

5.4.1.1 Spiral Distance < $10R_C$

For spiral sources lying within a distance of $10r_c$ of each other, one of the major characteristics is the change in activity of the source. Spirals of opposite sign will have a cancelling effect on one another, therefore leading to substantially reduced or even zero activity. Spirals of like sign will have an increased activity, with the increase being related to the number of co-operating spirals. For these cases

therefore, an in-situ kinetic study is most suitable, since such parameters may then more easily be determined. Because the AFM analysis is limited to studying the morphology of the spiral, determining whether two dislocations of opposite sign have a cancelling effect on each other and therefore reduce the activity of a spiral is not possible. However changes in the morphology of the spiral, which are predicted by BCF to occur for spirals of like sign, are observable. For a more detailed description of these the reader is referred to figures 2.6-2.9 in section 2.1. Essentially, however, a disruption of the step pattern is predicted.

Throughout the study of KAP crystals it was consistently observed that the step spacings with respect to distance from the spiral centre remained nearly constant for a given growth spiral (with the exception of the spirals seen on thin platelet crystals, as discussed in section 5.3). In all crystals the standard deviation was 10% or less of the mean step spacing. In only two cases, studied below, was this not the case. From this it was inferred that two or more sources of the same sign might be within the critical $10r_c$ distance on these crystals. As mentioned above, in order to calculate r_c for KAP at the centre of the spiral it is useful to make the assumption that a critical nucleus will consist of equal components in the [100]f and [100]s directions.

The first instance of the two exceptions is shown in figure 5.4.1. Here a growth spiral is seen which has many disturbances. In order to illustrate the number of dislocations involved, the steps corresponding to several dislocations near the centre of the hillock have been colour coded in figure (b). Since this crystal was grown at a supersaturation of 30%, the value of r_c is approximately 0.05 μm. Accurate measurement of the distance between the red and the green dislocation shows it to be 0.07 μm, and therefore of the correct order of magnitude for interaction to take place.

Although the inter step spacing of the hillock appears to be relatively regular within figure 5.4.1, this is not the case for a distance some way from the centre. This is shown in figure 5.4.2. For this hillock the standard deviation of the step spacing was 25% of the average step distance. Nonetheless, when the large number of dislocations present is considered, it is notable that the spiral shows no major disruptions other than the periodic variation in step spacing.

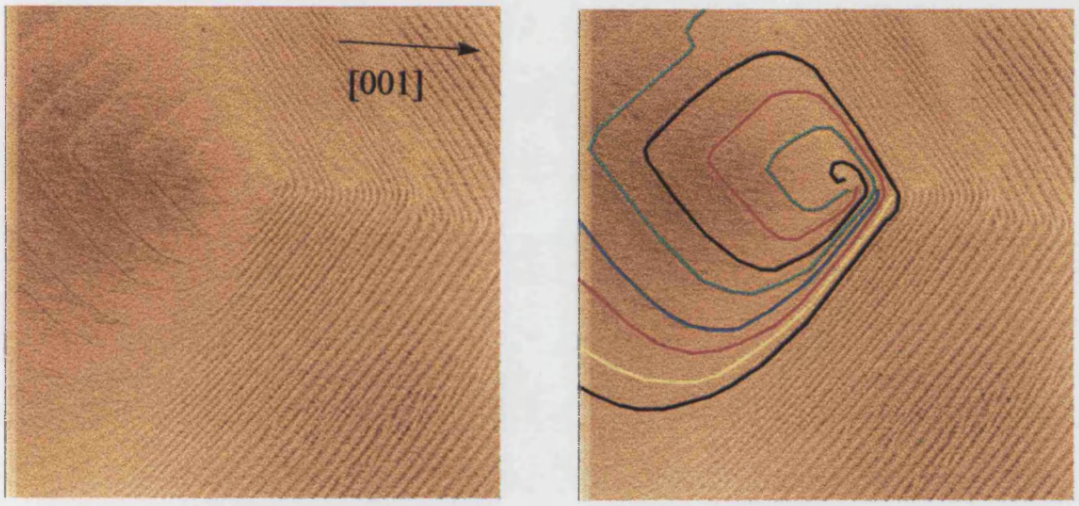

Fig. 5.4.1. *Figure (a) shows a 6 μm scan of a spiral with many dislocations in close proximity at the centre of the spiral. A periodic disturbance in the step spacing is observed away from the spiral centre (see figure 5.4.2). Possibly this arises from the interaction of only the two most closely spaced dislocations - the green and red lines in figure (b) show the steps from these two sources.*

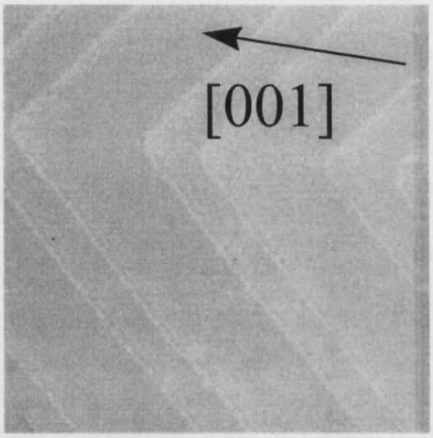

Fig. 5.4.2. *2.5 μm scan of a region of the large step side of the spiral shown in figure 5.4.1, but some 15 turns away from the centre. A periodic variation in the step spacing is visible.*

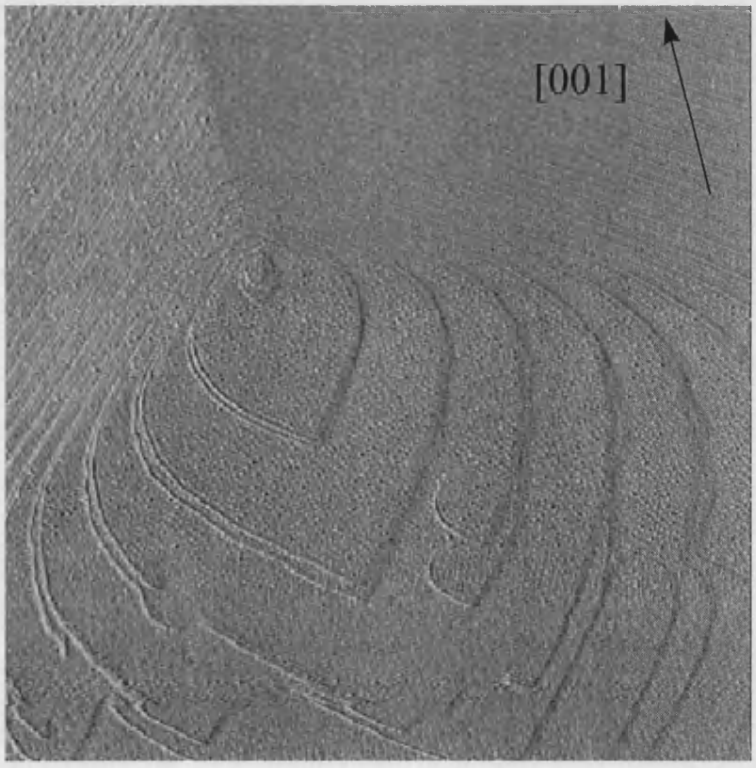

Fig. 5.4.3 *6.5 μm scan of a growth spiral. Many dislocations are present around the growth spiral centre, however, the chief characteristic of interest is the presence of double steps.*

In figure 5.4.3 above the second example of disturbances to step spacings is given. In this case the periodic variation is even more striking.

In order to study the centre of the growth spiral more closely, figure 5.4.4 shows a smaller area scan of the same spiral.

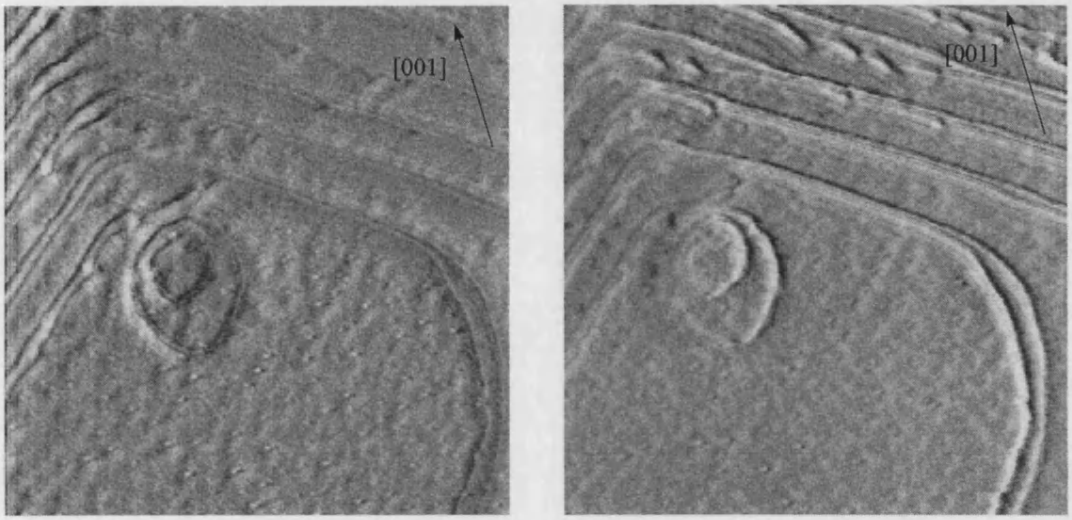

(a) (b)

Fig. 5.4.4 *1.6 μm scan of the spiral centre seen in figure 5.4.3. Both the forward (a) and reverse (b) scan images are included in order to help resolve the very closely spaced steps. In the forward scan the steps on the right of the image are more visible, and vice versa for the reverse scan. A double step is seen to form after the first turns of the spiral.*

Although two distinct dislocations cannot be resolved near the spiral centre, two closely spaced steps may be seen on the first long straight section immediately subsequent to the first two turns. Also notable is the tightly wound centre region of the spiral. Presumably it consists of two dislocations lying too closely spaced to be resolved by the AFM. This would also imply that the dislocations were within the

required distance of $10r_c$ of one another for co-operation to occur. Because of the much closer spacing of these two dislocations compared with the previous example, the step pattern is disrupted from the centre of the spiral onwards and has a higher variation in the step spacing.

In conclusion it may be said that the (010) face of KAP tends to show growth spirals with a minimal amount of disturbance in the step spacings. This implies that the spiral is usually dominated by the activity of only one dislocation source at the centre. In only a few cases were multiple dislocation spirals observed.

5.4.1.2 Spiral Distance > $10R_c$

For dislocations with a relatively large distance apart an activity is predicted which is more or less similar to a single source. The large majority of growth spirals seen on KAP were of this type, although a substantial variation in the number of dislocations per hillock was observed. Several examples are given in the figures below, varying from an almost disturbance-free hillock to over 30 spirals.

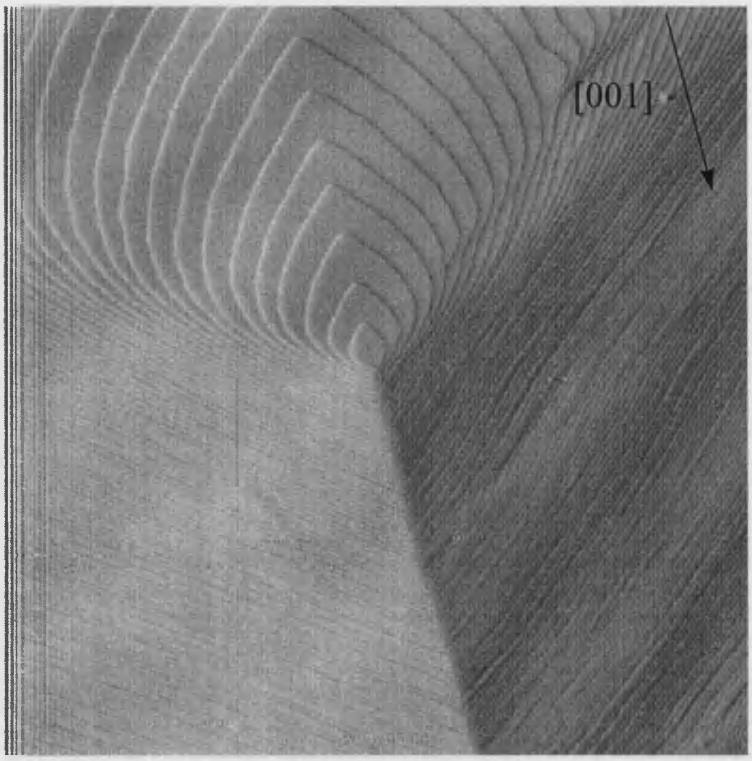

(a)

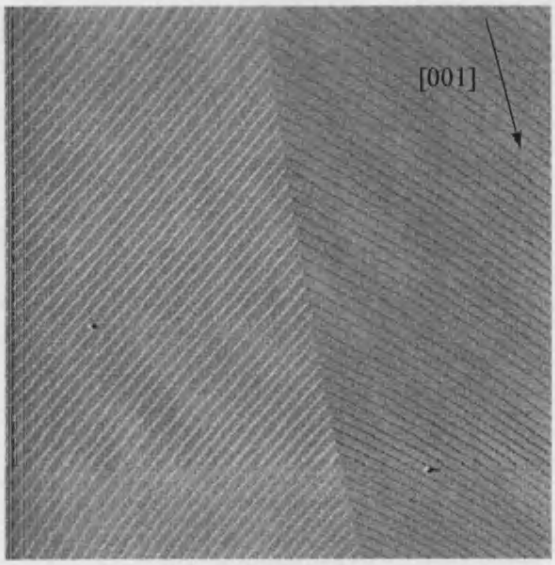

(b)

Fig. 5.4.5 *(a) 9.8 μm area scan of a growth spiral on KAP. Two small disturbances are present on the hillock (see top right of the figure). (b) 20 μm scan of the same crystal, on the large step side, and approximately 10 μm from the spiral centre. This serves to illustrate the uniformity of the step spacing versus distance form the spiral centre.*

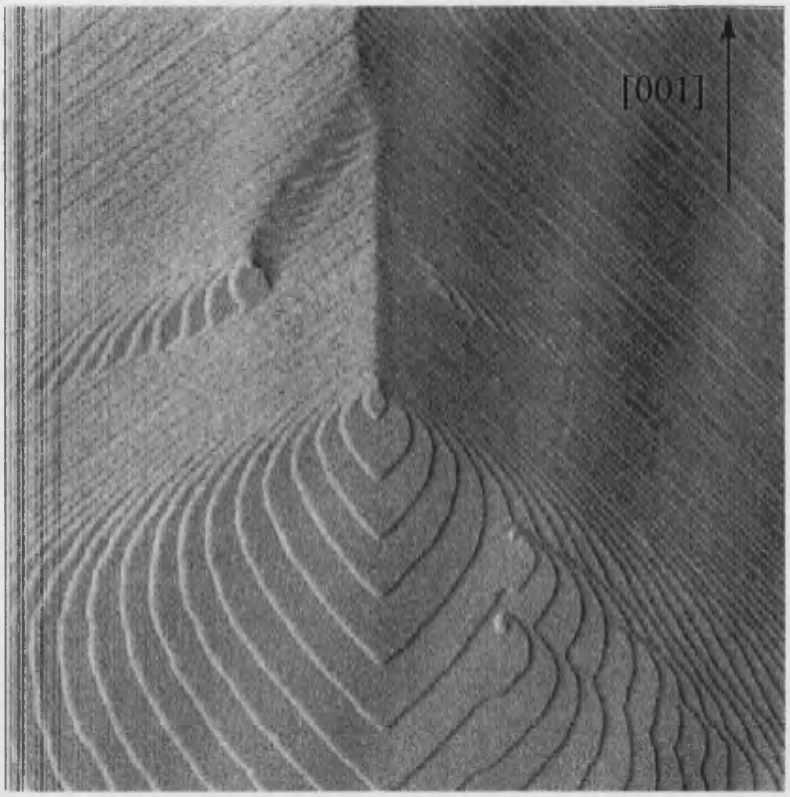

(a)

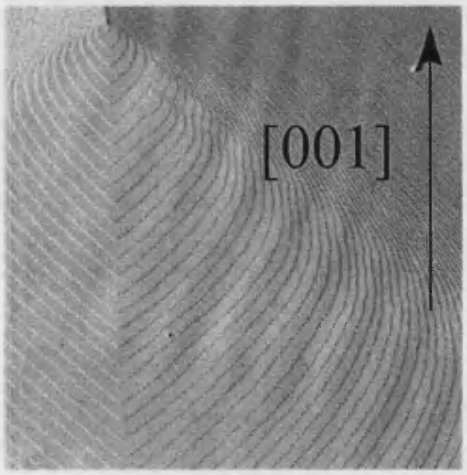

(b)

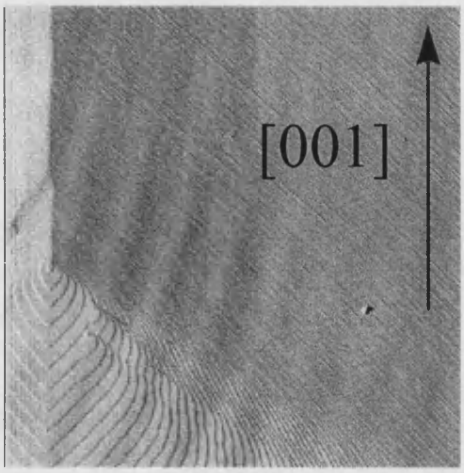

(c)

Fig. 5.4.6 *(a) 10 μm scan of a spiral with four obvious disturbances; two lying above the centre and two below. Close inspection of the bottom right of the image reveals two more steps which terminate and hence are most likely dislocations. Once again 20 μm scans of the region around the hillock (figures b&c) shows that the step spacing remains constant, notwithstanding the disturbances near the centre.*

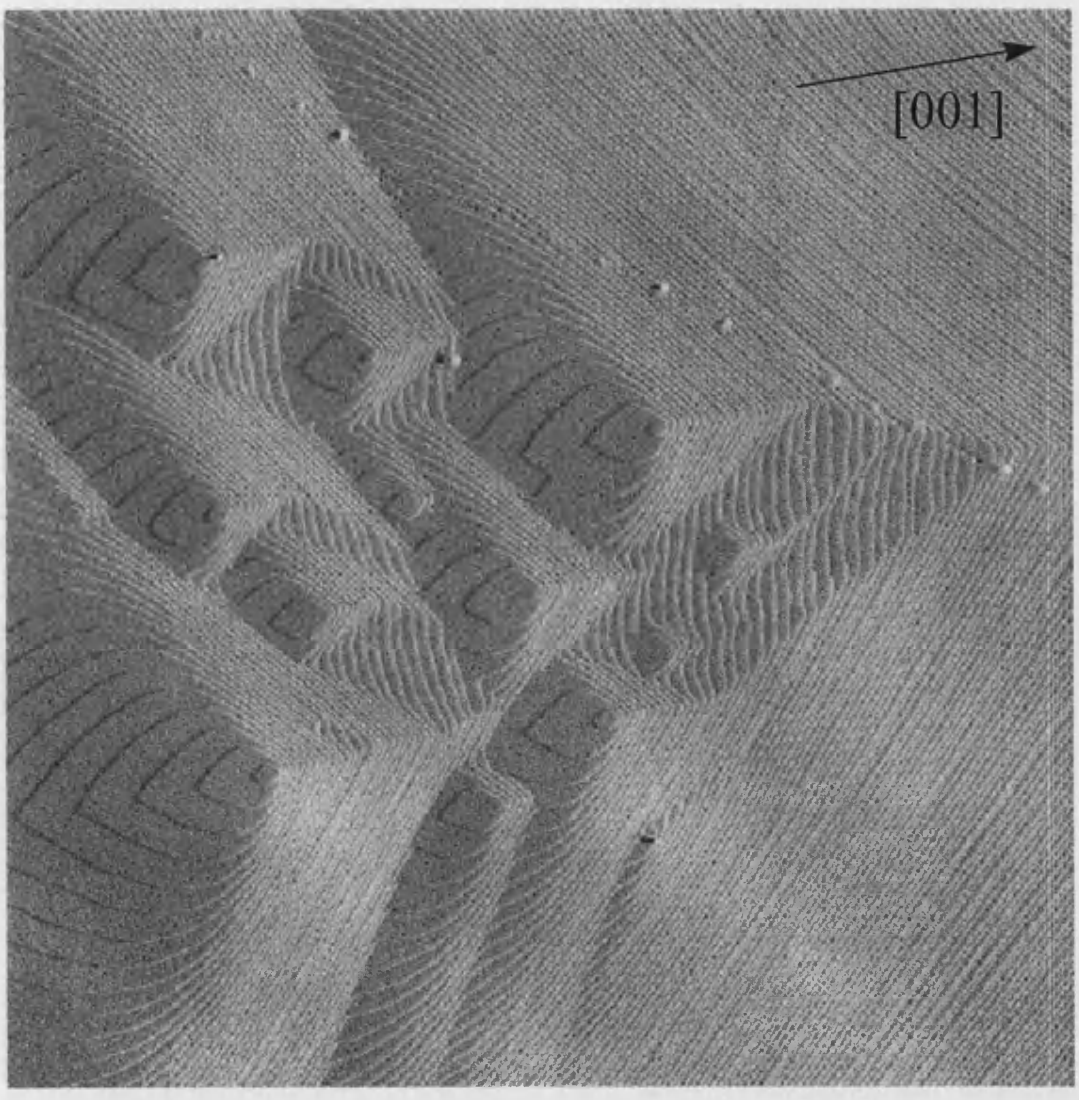

Fig. 5.4.7 *10 μm scan of a KAP crystal surface containing a large number of dislocations. Note that this centrally located dislocation cluster were the only dislocations observed on the whole crystal (approx. 1000 μm²).*

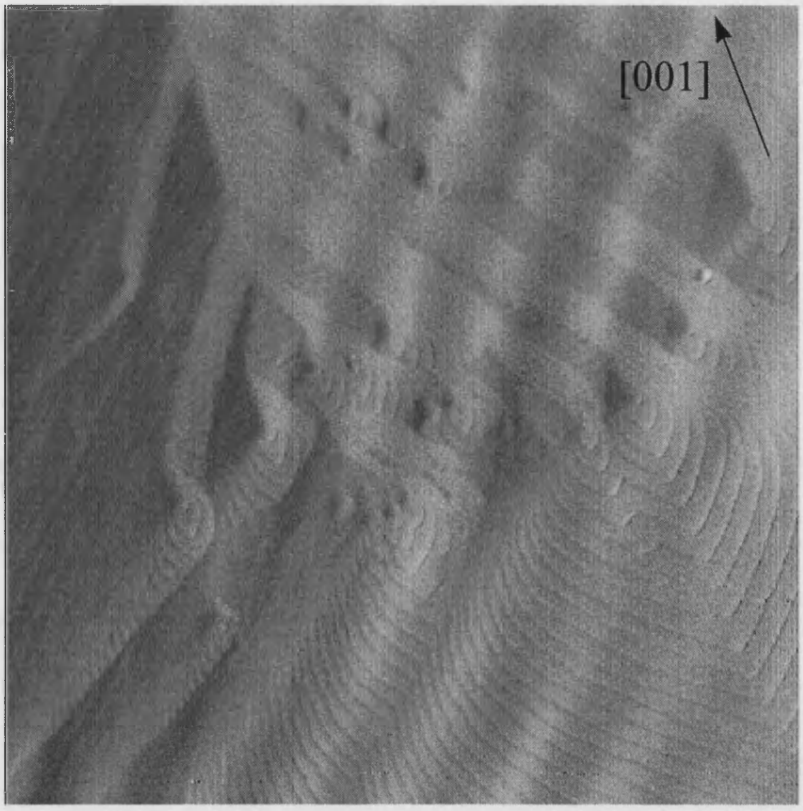

Fig. 5.4.8 *20 μm scan of a large number of different spirals on a KAP surface. Once again the dislocations are clustered around the main growth site. It is very difficult to determine which of these dislocations is controlling the growth.*

The first general point to note about the multiple dislocations observed on the (010) face of KAP, is the type of influence exerted by the different dislocations on the growth spiral. In some cases such as figure 5.4.8, a large group of dislocations are concentrated at the spiral centre. In other cases such as figure 5.4.6 dislocations seem to only have a 'passive' role, and appear as disturbances on the main spiral. In order to facilitate the discussion of these two types it is useful to define a demarcation. To this end it is useful to distinguish between 'major' dislocation spirals and 'minor' dislocation spirals. Major dislocation spirals are defined as those which have at least one complete turn of a spiral around the core. Those which do not, and hence simply

appear as a disturbance on the side of a hillock of a major dislocation spiral are termed minor.

Perhaps the first point to cover is a justification that minor dislocation spirals are in fact dislocations. This follows from the geometrical requirement that a step ending on the middle of a face must be associated with a defect such as a screw dislocation.

From figure 5.4.7 it is obviously possible to have many major dislocation spirals (in this case over 13) at very close proximity. However, in figure 5.4.5 all spirals apart from the main one are minor. An explanation of this behaviour based on dislocation type i.e Burgers vector might normally be reasonable, however for KAP, from the X-ray topography work it seems that there is only one source of steps on the (010) face - the <110> type dislocation.

A potential second source of step producing dislocations was discussed in section 5.4.3., namely dislocations bending from lower sectors into the (010) sector. However, such dislocations will always lie near the edge, and hence it appears unlikely that a combination of these dislocation types could give rise to the effects seen in the images. One reasonable explanation would be that the Burgers vector of both minor and major spirals is the same. The factors determining which spirals become dominant being due to the inter-relationship of parameters such as time delay between nucleation, inter-source distance, number of sources and strength of sources. In order to study these effects it is useful to observe crystals as early in the growth process as possible. A very small crystal is illustrated in figure 5.4.9 below.

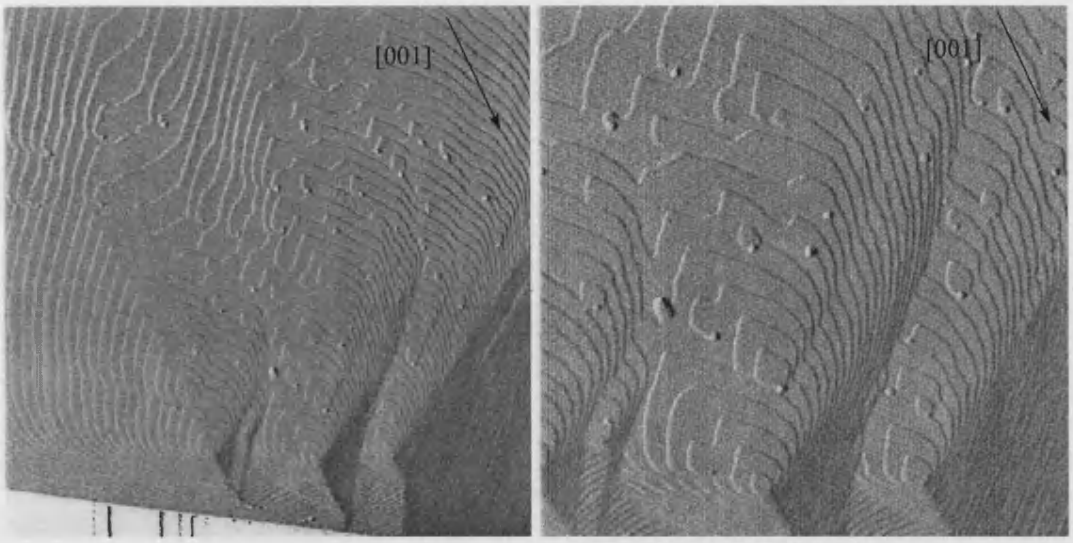

Fig. 5.4.9 *(a) 20 μm AFM image showing approx. 70% of the surface of a micro crystal. At the bottom left of the image it may be seen that the tip has scanned over the edge of the crystal. On the surface a large number of dislocations may be seen, both major and minor. (b) 10 μm scan highlighting the discrepancy in activity of the dislocations lying near the crystal edge, and those in the centre.*

In figure (a) approximately 70% of the entire crystal may be seen, making this one of the smallest crystals observed with the AFM in this study. At the bottom of the image the edge of the crystal is visible. In this image all the major sources lie near the edge of the crystal, whilst the minor sources lie towards the centre. If all the dislocations were of identical Burgers vectors, and the relative dominance of sources were purely due to a 'timing' argument then this situation would be expected to be reversed. It is very likely that most, if not all, of the dislocations in the centre of the crystal nucleated prior to those at the edge. Therefore these should show a far more significant development than observed.

One explanation for the discrepancy in source strength as a function of distance from the edge might be due to the supersaturation gradient which exists across the crystal surface. This was already seen to effect the number of nuclei present on a crystal surface exhibiting a two dimensional nucleation and growth mechanism (section 5.3). The problem with this hypothesis, however, is that it fails to explain why there is such a strong correlation between the distance of the source from the edge and its activity. Whilst it seems reasonable to assume that sources lying significantly further to the centre of the crystal should be less active than those on the edge, it is hard to explain why even amongst the three dominant hillocks those slightly closer to the edge should be more dominant. This fact may be seen more readily with reference to figure 5.4.10 where the normal distance of a given hillock from the crystal edge is shown.

This observation, together with the previous discussions of the origin of dislocations lying at the extremities of the crystal indicate that the group of major sources in figure 5.4.9 are possibly due to dislocations which have bent from lower sectors into the (010) sector. If this is the case they may have Burgers vectors other than the [110], and hence show different (in this case higher) activities.

The influence of relative 'bending' time explains the relation between source dominance and distance from the crystal edge. Those sources lying furthest from the edge are relatively the oldest. This therefore implies that with reference to figure 5.4.10, the younger sources dominate the older ones (given the assumption that these sources have the same Burgers vector). It is not possible to infer from this figure, however, whether the possibility exists for major sources to be reduced to minor ones during the development of the face.

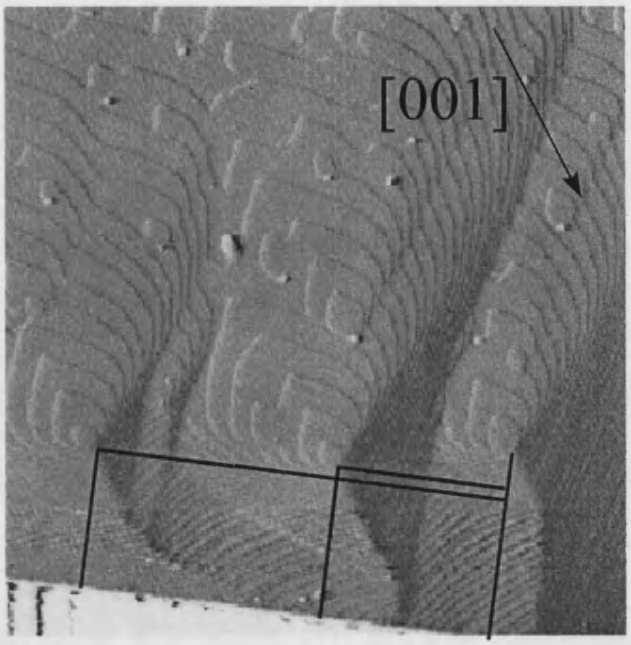

Fig. 5.4.10 *The normal distance of a spiral source from the crystal edge is directly related to its growth step dominance. Those spirals nearest the edge 'grow over' spirals from earlier sources.*

For the case where no bending of dislocations occurs, the clustering of the dislocation sources towards the centre of the crystal (see for example figure 5.4.6) suggests one of two possibilities. The first of these is the nucleation of groups of dislocations on inclusions, thus generally leading to dislocation clusters. With reference to the X-ray topography work, however, it was seen that dislocations in the (010) sector did not generally nucleate at inclusions. In fact, there were no inclusions observed in this sector at all, subject to the resolution constraints. The second, more likely reason, is that at the nucleation stage of the micro crystal a number of defects are generated more or less simultaneously and control the growth. The nucleation of dislocations subsequent to this initial 'core' group would occur both infrequently (given the low

defect density seen in the X-ray topographs) and randomly, therefore not having a significant impact on the spiral shape.

In the multiple spiral images seen so far the supersaturations were all relatively high (approx. 30%). Because of this it is difficult to see whether interactions between dislocations of opposite sign occur, such as shown in figure 2.6 (see section 2.1). For dislocations of opposite sign and $d > 10r_c$, closed loops are predicted to be emitted from the interaction of the two sources. This was seen on KAP at low supersaturation ($\sigma = 1.2\%$), and is shown in figure 5.4.11 below.

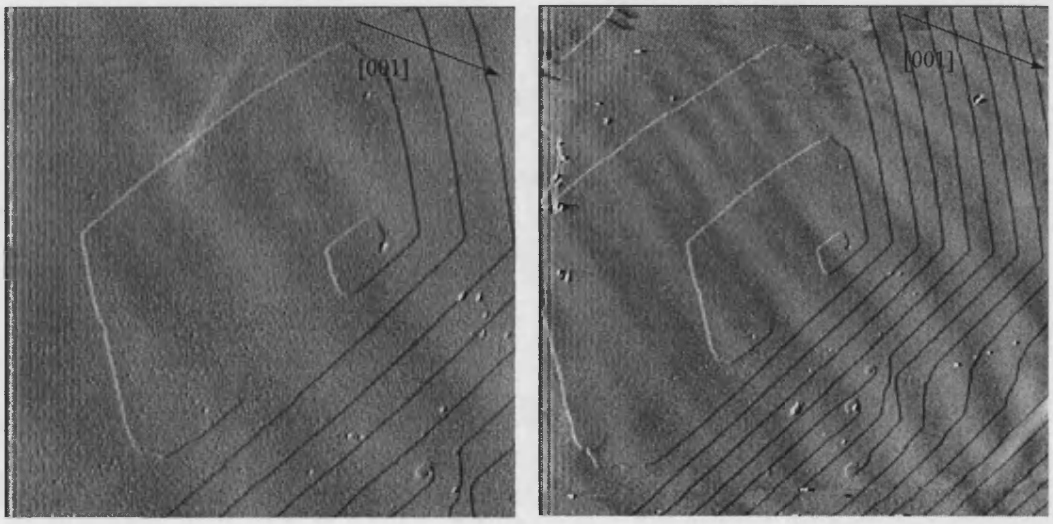

(a) (b)

Fig. 5.4.11 *(a) (13.5 μm scan) Two dislocations of opposite sign produce a step which lies between them. (b) (25 μm scan) Closed loops of steps are produced.*

The low supersaturation makes it easy to see that these two dislocations are producing concentric loops. It is difficult to know how common this mechanism is, since at moderately high supersaturations it becomes impossible to trace the steps between two sources which lie several microns apart.

5.4.2 Dependence of Step Spacing on Supersaturation

BCF have shown that for the case of an archimedian spiral the interstep spacing away from the spiral centre is given by:

$$y_0 = 4\pi r_c \qquad (5.4.1)$$

This was later corrected to:

$$y_0 = 19 r_c \qquad (5.4.2)$$

by Cabrera & Levine[28] and confirmed by others[14]. There have been various treatments of this problem for the case of polygonised spirals[30,109-112]. More recently Budevski et al[32] have shown that step propogation velocity is a function of the step length, for straight steps, thus leading to discrepancies with previous theories in the region very close to the spiral centre. However, they also show that typically within a few turns of the spiral the relationship in (5.4.2) holds (for a four sided polygon y_0/r_c=19.20). Combining (5.4.2) with (2.10) from section 2.1.1 we therefore have:

$$y_0 = \frac{19 V_m \alpha}{kT \ln {}^{C_B}/_{C_E}} \qquad (5.4.3)$$

Note that in equation 5.4.3, $\ln(C_B/C_E)$, the supersaturation ratio, is used rather than approximate form. This is due to the error which would otherwise be incurred when working with high supersaturations.

From equation 5.4.3 an inverse relationship between step spacing and supersaturation ratio is expected. Figures 5.4.12 and 5.4.13 below shows this relationship for KAP crystals grown over the range of supersaturations 1.2-30%.

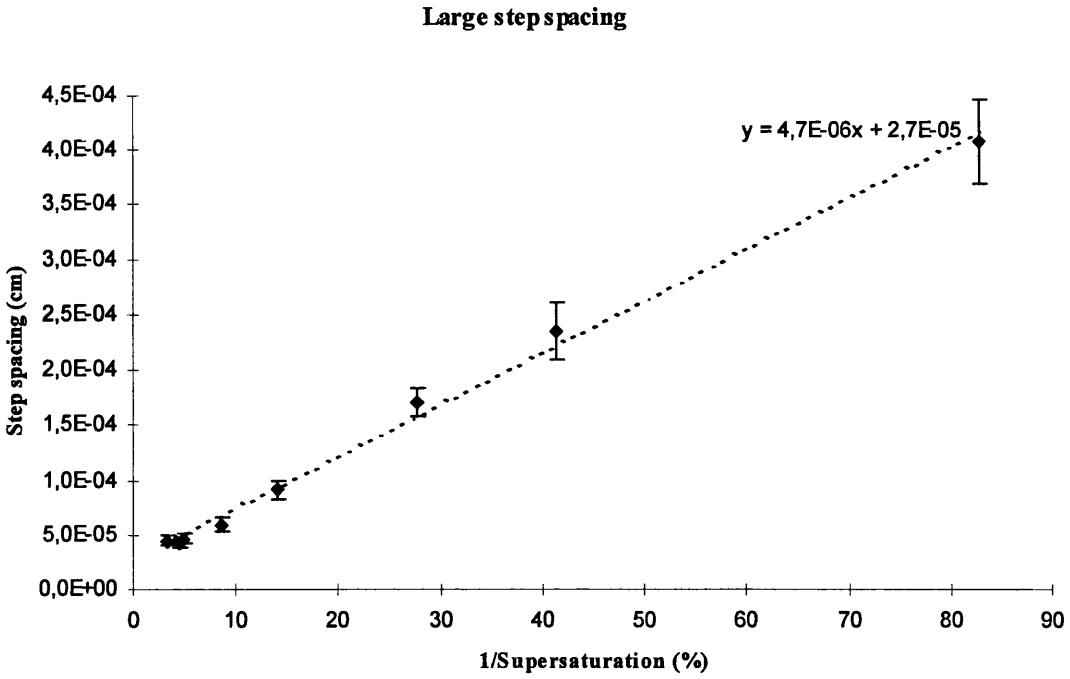

Fig. 5.4.12 *A plot of the inverse relationship as given in equation 5.4.3, for the [101]f steps. Note the good linear fit. The error bars are one standard deviation.*

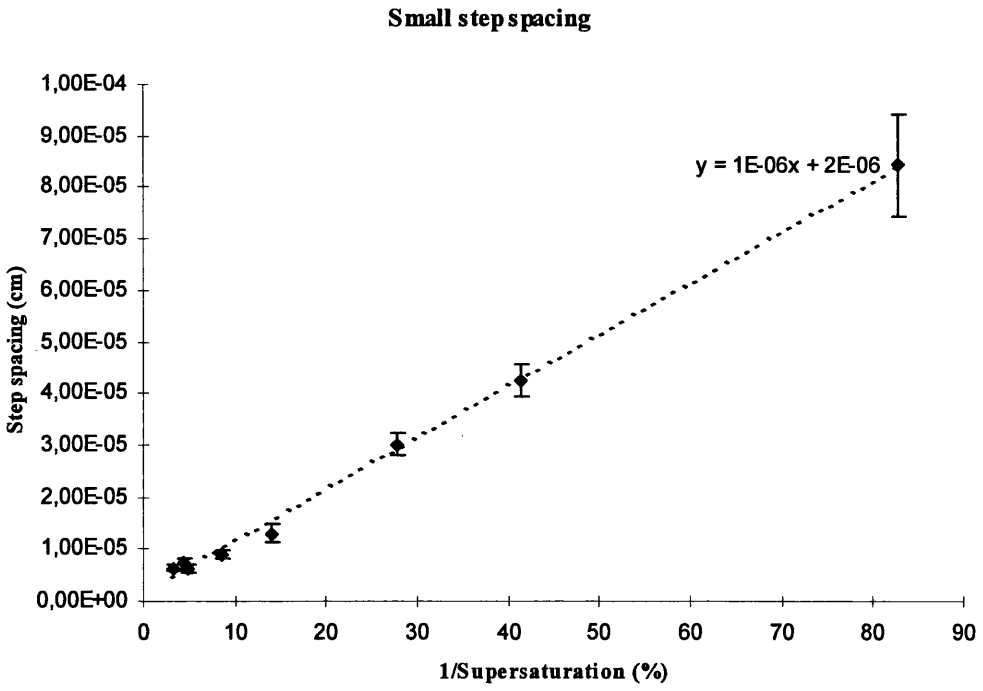

Fig. 5.4.13 *A plot of the inverse relationship as given in equation 5.4.5, for the [101]s steps. Note the good linear fit. The error bars are one standard deviation.*

From the values of the gradients the step free energies may readily be shown to be equal to:

$\alpha_{[101]f} \approx 40 erg/cm^2$ &

$\alpha_{[101]s} \approx 8 erg/cm^2$

This is in good agreement with previous PBC studies[63] which predict $\frac{\alpha_{[101]f}}{\alpha_{[101]s}} = 4$, and also of the correct order of magnitude when compared with other estimates of step edge free energy[14].

From these observations it may therefore be concluded that the variation with supersaturation of both the large and the small step spacing are in good agreement with a theoretical argument based on energetic considerations. It would therefore

appear unlikely that the anisotropy of the spiral is caused by kinetic arguments as has been suggested previously[54].

5.4.2.1 Stress Effects on Step Spacing

Close inspection of figures 5.4.12 and 5.4.13 shows that at the higher supersaturation ranges, instead of tending to zero, the inverse plots deviate from a linear regression towards a constant value. Figure 5.4.14 illustrates this more clearly by omitting the very low supersaturation data.

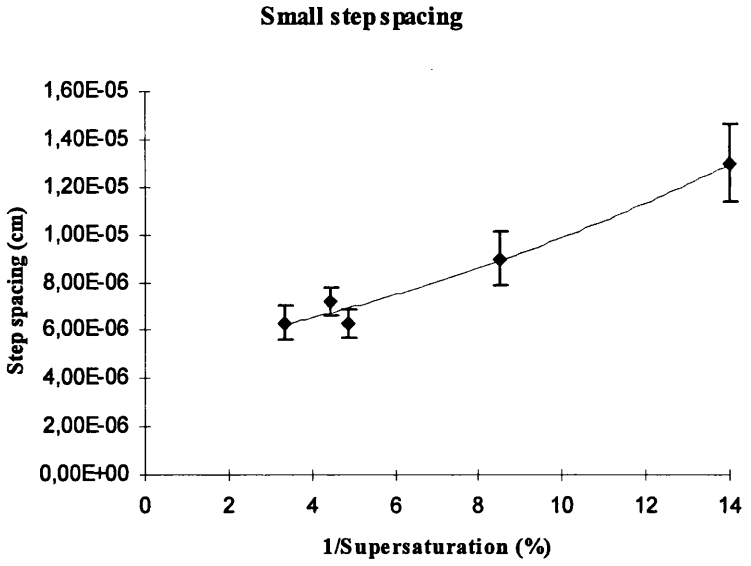

Fig. 5.4.14 *Detail of the high supersaturation region previously seen in figure 5.4.13. The deviation from linearity over this range is more clearly visible. The error bars are one standard deviation.*

This effect may be explained by the fact that at high supersaturations y_o is over estimated by the Cabrera-Levine approximation. The cause of the inaccuracy is the

assumption that surface supersaturation is equivalent to the bulk saturation. This is not the case due to diffusion of growth units into kink sites. Cabrera and Coleman[113] have shown that provided $y_o >> X_s$ the inaccuracy is small and equation 5.4.4 is accurate. However for $y_o < X_s$ the rate of decrease of y_o with increasing σ_r is lower than predicted by Cabrera and Levine. The result of this is that at high values of σ_r a limiting value of y_o is reached and the slope of the hillock becomes independent of σ_r. It is for this reason that faceted crystals always have relatively flat faces.

At the very central region of the spiral there are further factors which influence the step spacing. Firstly, as we have mentioned already, when the spiral is polygonised, the propagation velocity of a step is affected by its length. This dependence is only strong when the length of the step is very short, and hence typically only influences the first turn(s) of the spiral. Secondly, due to the stress field associated with the dislocation core at the centre of a dislocation induced growth spiral, a small change in local supersaturation will occur. This in turn affects the local step spacing - i.e. the first turns of the spiral. Unfortunately, as shown in section 5.4, it is the central area of the spiral which is the least well protected during removal from solution. Further evidence of this fact is provided here in figure 5.4.15. The growth temperature of the crystal in this image was 14° C above room temperature. Due to this temperature differential between the growth and ambient conditions it is very important that removal of the crystal from solution occurs quickly. The crystal in figure 5.4.15 has not been protected correctly as is visible at the centre of the hillock, where the spiral is more tightly wound. Note that it is only this very sensitive region which is affected: further away from the centre the step spacing is the same as on other crystals grown under these conditions. Due to this extreme local sensitivity it seems

unwise to draw any conclusions regarding the differences in y_o which have been observed near the spiral centre. For this region it seems likely that an situ approach would be necessary.

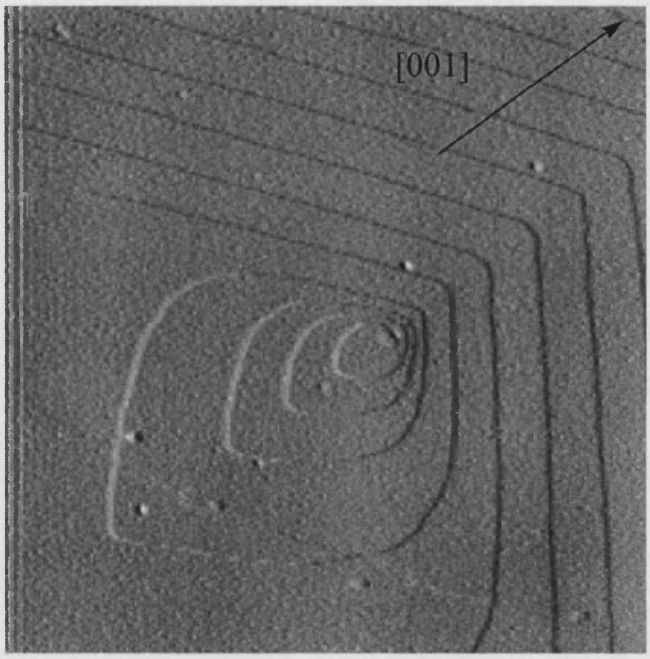

Fig. 5.4.15 *8μm scan of a crystal grown at a temperature of 34 °C and an undercooling of 1 °C. Due to an insufficiently fast removal of the solution, the spiral has wound more tightly at the centre corresponding to the ambient undercooling of approx. 10 ° C. This illustrates the sensitivity of the spiral centre to growth conditions.*

5.4.2.2 MACRO-STEPS

Early work on the motion of steps by Frank[33] and Cabrera & Vermilyea[38] studied the effect of kinematic waves on the surface topology of growing crystals. Although these waves cannot lead to true multiple step heights (macro-steps) they are able to produce variations in the density of steps per unit length. On a macroscopic level it is

therefore possible that these variations appear as steps, and are visible using relatively low resolution techniques such as DICM. Fluctuations in growth parameters at the source of the steps i.e. the point of emergence of the dislocation, may also produce such an effect. On nearly all of the KAP crystals observed, the step spacing has been uniform over the entire crystal face and the step heights have corresponded to one unit cell. This may be a result of the fact that the bulk of the study was concerned with very small (micro) crystals. The occurrence of macro-steps has been suggested to be influenced by the distance travelled by the steps. On a larger crystal this will clearly be further than on a small crystal. This is consistent with the observations on the (010) face of KAP. On large crystals macro-steps (approx. 1cm) were consistently seen; moreover these steps most frequently formed some distance from the spiral centre. On small crystals, variations in step spacing were only rarely seen, and these could always be explained by either the presence of multiple sources, or dislocations bending into the (010) sector. In either of these cases it is possible that the initial disruption in step spacing becomes further enhanced by impurity effects, thus leading to the potential formation of macro-steps. A good example of this is shown in the sequence of figures below. This crystal was unusual in that it had the 'thin platelet' habit with a spiral centre situated at the extremity of the (010) face (therefore indicating a change from a two-dimensional mechanism to a spiral mechanism) and was also relatively large: approximately 0.5 mm. In the first figure (5.4.16) a train of steps are visible. These appear similar to many of the previous images of steps at first sight.

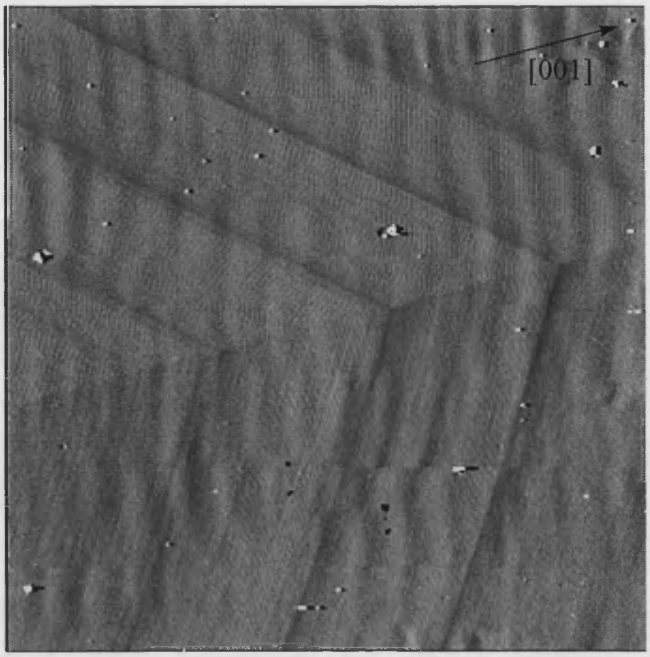

Fig. 5.4.16 *45.5μm image of a crystal grown at high (30%) supersaturation. The train of steps on the [101]s side of the spiral appears relatively normal, until the spacing is compared with other crystals grown at this supersaturation.*

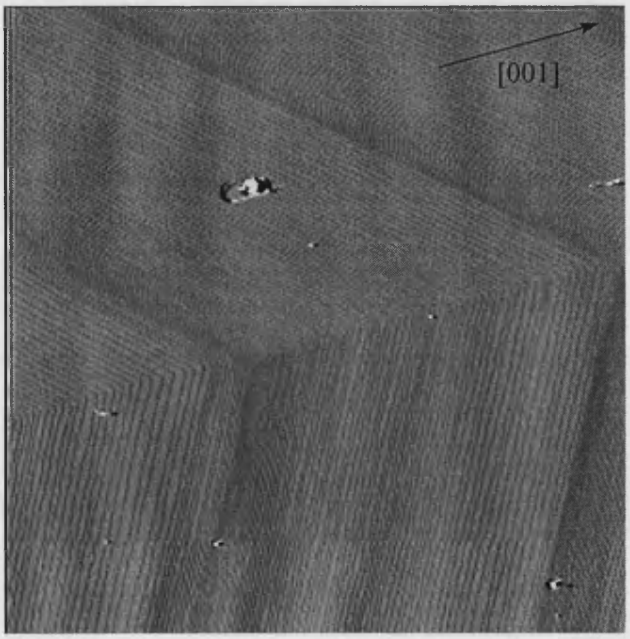

Fig. 5.4.17 *19.7μm image of the same crystal grown as in figure 5.4.16. At this magnification it is clear the steps in the previous figure are, in fact macro-steps*

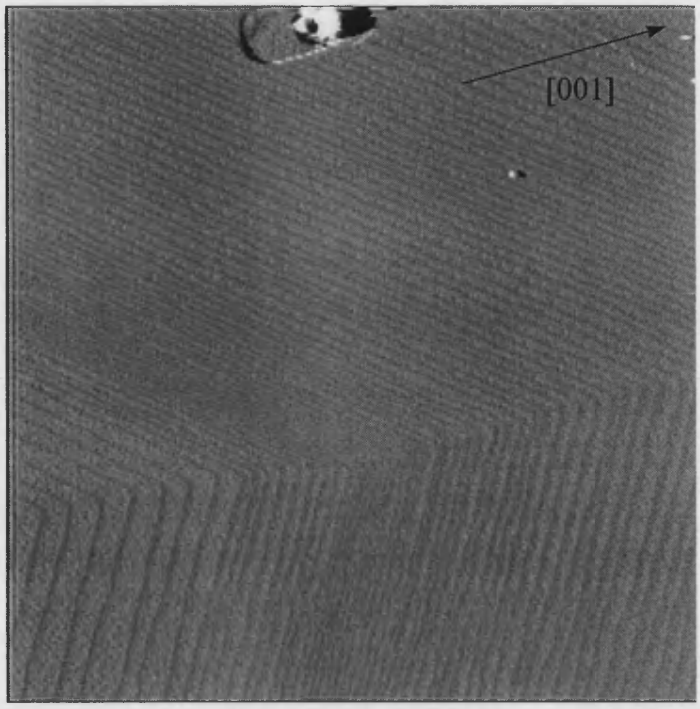

Fig. 5.4.18 *7.6μm image of the same crystal grown as in figure 5.4.16. As the magnification is further increased, the bunching of the steps is seen more clearly. Presumably the bunching is caused by an impurity mechanism which occurs on the already disrupted steps that result from the introduction of a spiral source onto the face.*

5.4.3 IMPURITY EFFECTS

Impurities play a dualistic role in the growth of crystals. On the one hand, impurities are often purposely added to the growth medium in order to modify the crystal habit, or alter the physical properties. On the other hand many crystals are required to be as pure as possible, and in these cases the trace or unintentional impurities are undesirable. The qualitative effect of intentionally added impurities on the shape of the growth spirals on the (010) face of KAP have been previously studied in some depth[61]. This study is therefore restricted to the latter category of impurities - those

not purposely added. The presence of such impurities in commercial KAP has been inferred from the observance of a so called 'dead zone' during growth from solution[63]. This zone is a range of supersaturations in which no growth takes place, although a thermodynamic driving force to do so exists. Assuming that the model described in the theory section holds, then it may be shown that the velocity of a step pinned at two points along its length by impurities will be reduced according to the relation[38]:

$$V = V_0(1-2r_c N_i^{\frac{1}{2}})^{\frac{1}{2}} \qquad (5.4.4)$$

where: V_0 = Velocity of an unhindered step

N_i= Average impurity density

Therefore, as the supersaturation is reduced the size of the critical nucleus (r_c) increases and hence, for a given impurity density a supersaturation limit will exist below which no growth will occur. The range of supersaturations below this limit constitute the 'dead zone'.

In an ex-situ study it is not possible to measure the kinetics of growth and hence the existence of a 'dead zone' may not be determined directly. However, impurities are also likely to have a significant influence on the spiral morphology and this aspect may be studied in some detail.

Utilising the high resolution capabilities of the AFM the influence of trace impurities on step morphology at very low (1.2%) supersaturations have been directly studied. To achieve growth at such low supersaturations, KAP which had been recrystallised very slowly - to optimise purity - was used. An example of such a crystal is shown in figure 5.4.19

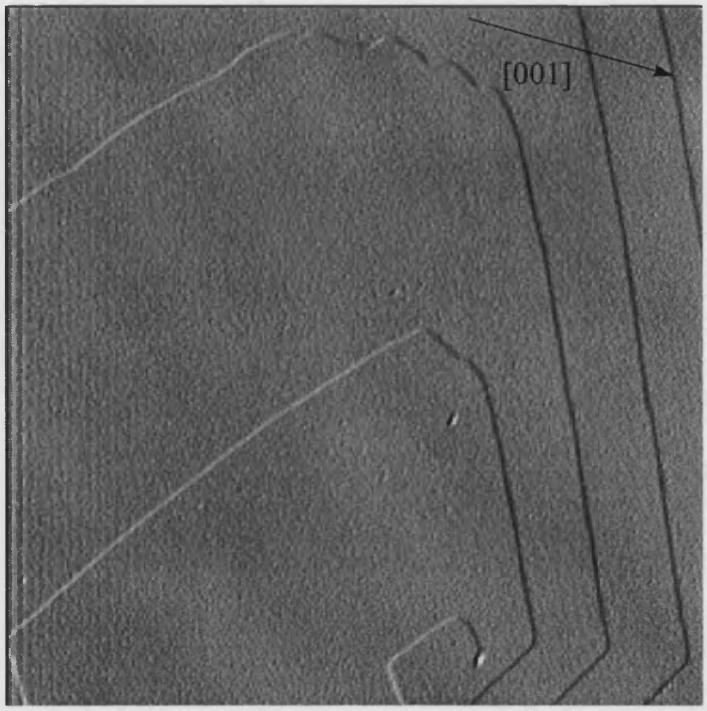

Fig. 5.4.19 *11.5 μm AFM image of a crystal grown at a supersaturation of 1.2%. The (001) steps show an increasing roughness as a function of distance from the spiral centre.*

In figure 5.4.19 the spiral centre is polygonised and the steps are undisturbed. After three turns of the spiral, already a significant degree of disturbance is visible on the [001] steps. As the distance from the spiral centre increases this trend continues. In figure 5.4.20 the [001] steps are shown some 10 turns from the spiral centre. In some cases the steps become so rough that even an average direction is difficult to discern.

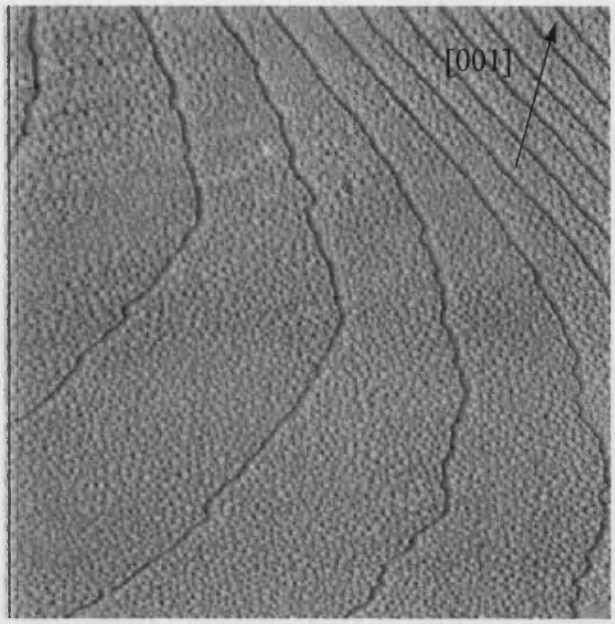

Fig. 5.4.20 *10 μm AFM image of a crystal grown at a supersaturation of 1.2%. The roughening of the [001] steps as a function of distance from the spiral centre is shown.*

Careful inspection of the [101]f steps in figure 5.4.19 reveal that these also show some deviation from linearity after the third turn. As is the case for the [001] steps, the relative disturbance of the [101]f steps increases with distance from the spiral centre. The [101]s steps, however remain straight in all cases. The situation is illustrated more clearly in figure 5.4.21.

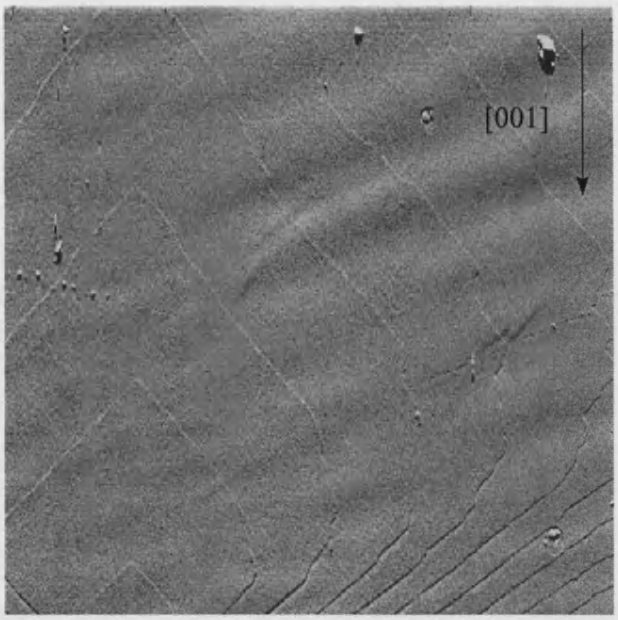

Fig. 5.4.21. *20 μm AFM image of a crystal grown at σ=1.2%. On this image the relative influence of impurity pinning on the different step orientations is shown*

5.4.3.1 Mechanisms of Impurity Effects

From a general point of view two mechanisms may be envisaged in which impurities can influence the crystal growth process. On the one hand the impurities may be considered to adsorb on the surface and remain immobile, thus forming a two dimensional array which advancing steps must negotiate. On the other hand the impurities may diffuse some distance on the surface, before either returning to the solution or adsorbing at a suitable site on a ledge. In both cases the effect is to disrupt the flow of steps, as is observed in figures 5.4.19-21.

In the case of KAP the roughness of a particular step is dependent on the distance of the step from the spiral centre. This is consistent with a mechanism in which the pinning strength of the impurities is relatively high. The further a given step has

travelled, the more impurities it will have encountered, and hence the rougher its appearance will be.

Because of the strong difference in impurity interaction which is seen between the [101]f and [101]s steps, it would therefore also be expected that the ratio of the spacing between these step orientations would show a supersaturation dependence. As the supersaturation is increased, the effect of the impurities would be expected to diminish, and hence the step spacing ratio [101]f/[101]s should increase. This is shown in figure 5.4.22 below.

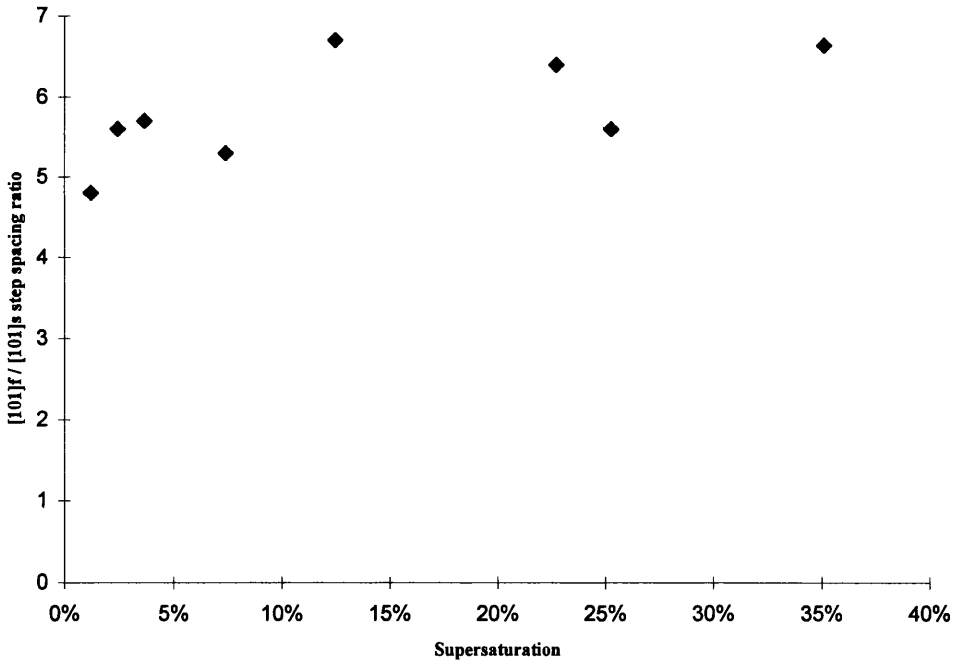

Fig. 5.4.22 *Variation of σ vs step ratio [101]f / [101]s. The ratio increases slowly with increasing σ, which is consistent with the larger impurity interaction observed in the [101]f direction at low values of σ.*

Although figure 5.4.22 shows a general trend toward increasing [101]f/[101]s step spacing ratio with respect to supersaturation, the change is small. This therefore implies that despite the much more disturbed appearance of the [101]f steps when compared with the [101]s steps, there is only a small differential in the relative velocities of the two as a function of supersaturation. This indicates that whilst the impurities clearly have a pinning action on the steps, provided the distance between the impurities is larger than the critical radius r_c, there is very little reduction in the step velocity.

From figure 5.4.21 it is clear that the steps may be ranked in terms of susceptibility to impurity induced disturbances as follows: [001]>[101]f>[101]s. This ranking is in good agreement with other studies where impurities were added intentionally[61]. In one ex-situ study using AFM on crystals grown at very low supersaturations, it was found that as the amount of the impurity Cr^{3+} was increased the polygonised spiral became completely round, with the different orientation steps becoming sequentially round, in the same order as the ranking given above[114].

A comparison with the results of the XRT study are also useful. Referring to figure 5.4.1 as a typical example of the X-ray topographs seen, it may be concluded that the lowest defect density occurs in the Lat sectors. In contrast the [001] steps show the highest degree of impurity induced disturbance. However, as we will discuss below, the [001] steps may be considered to be something of a special case, making direct comparisons with the two [101] orientations more complex. When comparing the two [101] directions there is a reasonable agreement between the AFM images and the X-ray topographs. In the End(f) sectors a large number of inclusions were observed, whereas none were observed in the End(s) sectors. This corresponds with

the higher impurity influence seen on the [101]f step direction when compared with the [101]s step direction.

In order to explain these observations the first point to consider, is that of the three step orientations, the [001] steps are substantially different. In the [001] direction the chain energy of the PBC's is low, and hence the kink density is likely to be high. Therefore, if a relatively large diffusion distance on the surface is assumed (see section 5.4.3) then a large number of sites are available for impurities to enter and pin the step (this of course also implicitly assumes a kink absorption impurity mechanism, rather than a terrace adsorbed mechanism). A relatively disturbed step morphology is therefore expected. In the case of the [101]f and [101]s steps no difference in relative kink density is expected, therefore ruling out the above mechanism for the differences seen in these orientations.

In this case two other factors may be responsible. For the [101] steps we have discussed the argument put forward by Jetten[54] regarding a possible explanation for the anisotropy of the growth spiral, i.e. the different rates of absorption of the growth units into the spiral in the [001] and $[00\bar{1}]$ directions may possibly be attributed to the different bonds which are formed. If integration of the K^+ ion is assumed to be the rate determining step for growth then it was shown that the difference in attachment energies of K^+ on the [101] steps in the [001] and $[00\bar{1}]$ directions is equal to 10.8 kcal/mol. Absorption of growth units would therefore be favoured in the low energy direction. Since it is known that some of the impurities present in KAP are metallic contaminants such as Pb and Fe ions, a similar argument to the incorporation of the K^+ ions may be followed. Therefore it is possible that other

metallic ions will also be incorporated more readily in the step directions with the lowest attachment energy, leading to a higher concentration of the impurities on the faster growing (i.e. lower energy) steps. This would result in the higher level of disturbance observed on the step morphology. The main criticism of this mechanism is the fact that in the case of the spiral anisotropy an energetic argument, as proposed in the previous section, seems to fit in better with the experimental observations. Nonetheless the possibility does exist that this mechanism could hold in the case of impurities.

A final possibility is one based on geometric arguments. Due to the large difference in step spacing between the [101]f, [001] and [101]s sides of the spiral, a difference in the amount of impurity adsorbed per step is likely to occur. From all of the AFM images seen previously it will readily be appreciated that the length of step present per unit area on the (010) face is far higher (approx. 5 times) on the [101]s side of the spiral than the [101]f side. This therefore implies that regardless of whether the impurities are considered to have any surface mobility, a higher amount of disturbance would be expected on the steps with the relatively larger terraces.

5.4.4 GROWTH SPIRAL SHAPE

Since the pioneering work of Burton, Cabrera & Frank, the occurrence of both polygonised and circular growth spirals has been well documented, and has been covered theoretically by many authors. The effect of various parameters such as temperature, impurities, kink density, step edge free energies, distance of steps from source etc, have been addressed in a number of studies - see for example the review

by Sunagawa & Bennema[29]. On KAP it was observed that over a limited range of temperature (20°C - 35°C) the effect of temperature on spiral morphology was negligible. Significant changes in spiral morphology over this temperature range, however, were observed as a function of supersaturation. These changes are discussed below.

5.4.4.1 Polygonisation Dependence on Supersaturation

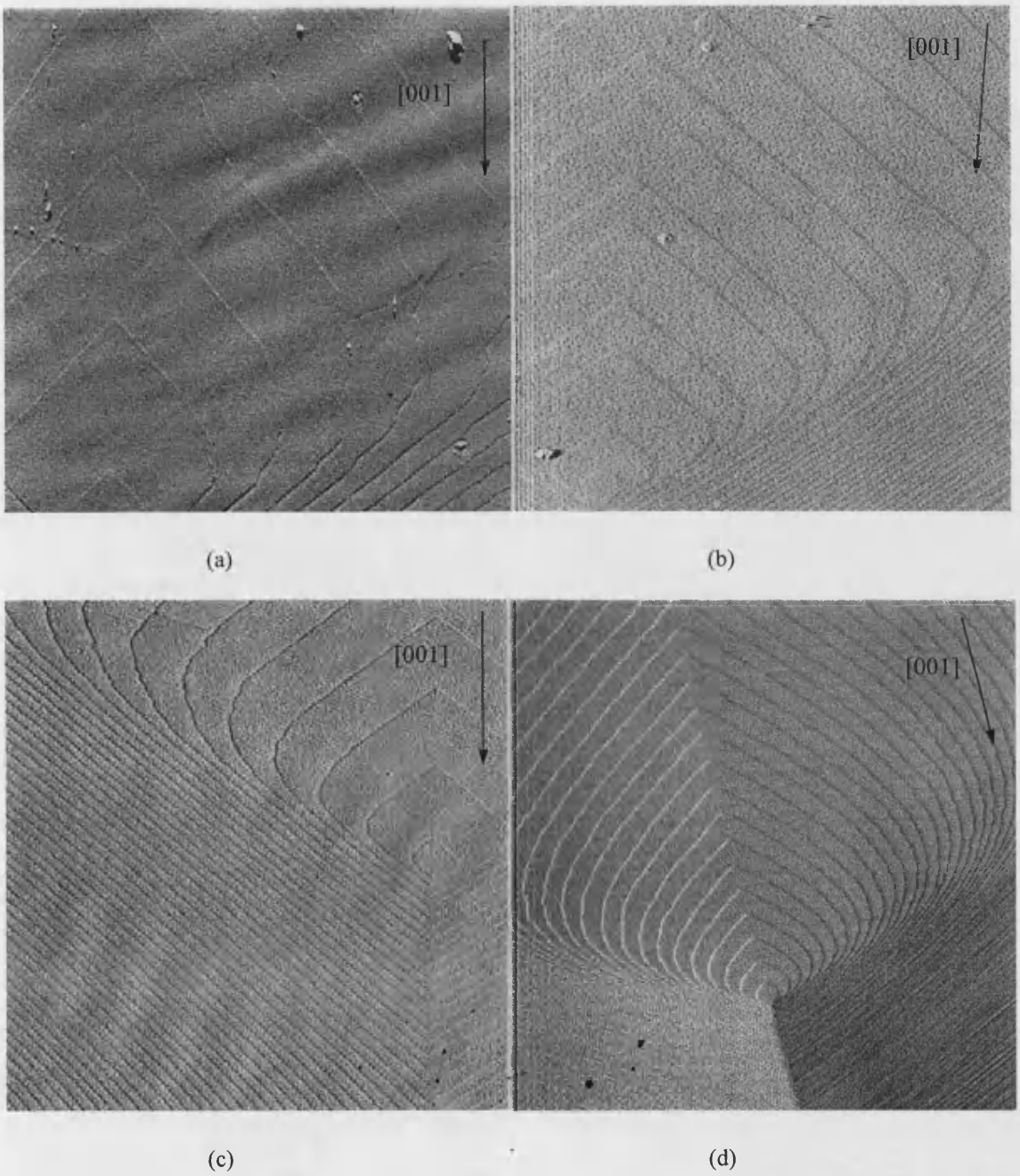

Fig. 5.4.23 *Series of AFM images of spirals present on the (010) face of KAP crystals grown over a range of supersaturations - (a) 20μm, σ=1.2% (b) 10μm, σ=7.2% (c) 20μm, σ=11.8% (d) 10μm, σ=30.1%. A change in the shape of the spiral is evident.*

At very low supersaturations (figure (a)) the spiral shape is dominated by the influence of impurities. As the supersaturation is increased, the pinning influence of the impurities is overcome (figure (b)) and the spiral takes on a completely polygonised form, with all step directions [001], [101]f and [101]s becoming straight. As the supersaturation is further increased the (001) steps begin to become less polygonised, and finally at even higher supersaturations (figure (d)) the [101]f steps also begin to undergo this transition.

Because it has been shown that trace impurities are commonly present in KAP, notwithstanding attempts to ensure the highest level of purity, the first question to address is whether these may be the cause of the spiral becoming progressively rounder as a function of supersaturation. Broadly speaking the observations do seem to fit within a kink adsorbed impurity mechanism. At low supersaturations impurities are expected to have their strongest influence. If they block a large number of kink sites and thereby increase the effective inter-kink distance then it is possible that $X_0 > X_s$. This will cause a polygonisation of the spiral. As the supersaturation is increased, the impurities are more easily displaced and the relationship between X_0 and X_s may be reversed: $X_s > X_0$. In this case the spiral will become rounder. Thus the spiral would be expected to become rounder with increasing supersaturation, as seen in figure 5.4.23 (a-d). A strong argument against this mechanism is, however, provided in previous work by Hottenhuis[61] using intentionally added impurities. In these studies it was always seen that the addition of impurities *caused* rounding of the spiral. The clearest example is in a study using ethylene diamine tetraacetic acid (EDTA)[61]. EDTA is well known for its strong complexing properties, in particular with trivalent cations. Initially a KAP crystal was grown in a nominally pure solution.

The spiral was seen to be polygonised (using DICM). On the addition of impurities (both Fe^{3+} and Ce^{3+}) the spiral became round. At this point a surplus of EDTA was added to the solution. Within 10 seconds the spiral reverted to a polygonised form. The evidence is therefore that the spiral becomes polygonised on the removal of impurities. Therefore at high supersaturations where the influence of impurities is low, the spiral would be expected to be polygonised. With reference to figure 5.4.23 it will be clear that this is not the case.

The next mechanism which needs to be considered is one related to bulk diffusion aspects. In the case of the KAP crystals studied with AFM it should be noted that due to practical limitations at was not possible to ensure that the growth conditions were identical for all supersaturations. At low supersaturations a long period of growth is required due to the low step velocity, and stirring of the solution is possible to eliminate a diffusion boundary layer. At the higher end of the supersaturation range, growth is extremely rapid and stirring is not possible due to the problem of secondary nucleation[63]. This means that it is possible that bulk diffusion effects may be more dominant at higher supersaturations than at lower supersaturations. Even in a situation where all other conditions were equal it might still be expected that at very high supersaturations and hence high step velocities, transport of growth units to kink sites may become the limiting factor. Several recent studies exist, which consider the influence of diffusion on the shape of the spiral[19,115,116]. Enckevoort[115] has summarised the findings of several of these as follows 'If growth is completely governed by volume or surface transport, the growth spirals/ hillocks must be circular, elliptic or dendritic, if integration at the kink positions of the steps plays a role these features are often more or less polygonised.' Thus it seems possible that a

rounding of the spirals may occur at higher supersaturations due to an increase in the influence of diffusion effects relative to the influence of integration at the kink sites. The main argument against this idea is that the same factors should contribute to produce a rounding of all the steps present. On KAP, however, a large discrepancy in the degree of rounding of different step orientations is seen. On this basis a diffusion related mechanism appears unlikely.

Given that the above two general mechanisms (impurities and bulk diffusion effects) do not explain the experimental observations satisfactorily, it is necessary to study the basic parameters which control the spiral shape in more detail.

From theoretical considerations it will be recalled that the polygonisation of growth spirals in general is dependent in the relative size of two variables namely, the inter-kink spacing X_0 and the mean surface diffusion distance X_s. BCF assumed that in contrast to vapour growth, crystal growth from solution does not involve surface diffusion. This assumption has been questioned by a number of workers[22,23,24]. In the case of KAP it can be shown that surface diffusion, does occur to a significant degree. This follows from a comparison of crystals grown at the same supersaturation, but with different growth mechanisms. It was shown (section 5.3) that at high supersaturations two dimensional nucleation and growth occurs. However, on all of the crystals observed on which a spiral mechanism was present, no inter-step nuclei was ever observed. This can only be the case if the growth units arriving on the surface of the crystal are able to diffuse sufficiently far to arrive at suitable growth sites on the ledge. This therefore means that the average distance travelled on the surface of a crystal must at least be equal to half the distance of the large step spacing at high (30 %) supersaturations. This is equal to a distance of about

500 nm. It should be emphasised that this represents a minimum distance. The actual value of X_s may of course be substantially higher.

Returning to the problem of the observed rounding of the spirals as a function of supersaturation, it may be seen that any explanation has to cover two points. Firstly the fact that spirals become rounder as the supersaturation increases and secondly that the different step orientations are affected to a different degree.

The first point may be understood in terms of the variables X_s and X_0. For the spirals to go from a polygonised shape to a more round shape the following inequality must be satisfied:

$$X_s > X_0 \qquad (5.4.5)$$

Therefore either an increase in the surface diffusion distance (X_s), or a reduction in the inter kink distance (X_0) is required. Considering X_s first, it is not likely that an increase in supersaturation would lead to a longer surface diffusion distance. In fact, due to the relatively higher number of adsorbed growth units per unit time present on the surface at higher supersaturations, and the associated increase in the number of intermolecular collisions it is more conceivable that the mean free path actually decreases[117].

The influence of increasing the supersaturation on the crystal morphology in general has been understood in terms of kinetic roughening (see section 2.1.3)[118,119,120]. More recently this has been studied using Monte Carlo simulations[117,121,122], from which conclusions regarding the *step* as opposed to face morphology may be also be drawn. In general it is noted that increasing the supersaturation leads to a 'roughening' of the steps. This therefore corresponds to an increase in the number of kinks, or a decrease in the average inter-kink spacing X_0. For a constant (or slightly decreasing) X_s the

condition in the inequality (5.4.2) is therefore satisfied. In general it is therefore possible that as the supersaturation is increased, a decrease in the inter-kink spacing relative to the surface diffusion distance may lead to a rounding of the spirals.

The second part of the discussion relates to the relative difference in the degree of rounding of the different step orientations. These are affected by an increase in supersaturation in the following order:

[001]>[101]f>[101]s

As discussed above, the chain energy of the PBC in the [001] direction is relatively low and is therefore fundamentally different in structure to the two <101> directions. It is likely to have a high kink density. For this reason it should be the first step direction to be effected by the roughening process, as is observed experimentally. The difference between the two <101> directions is more subtle. For reasons discussed in more detail later, the step spacings are different by about a factor of five in the slow and fast directions. Because of this there exists a larger surface step area per unit length of ledge on the [101]f steps. This means that, on average a larger number of growth units will be available per kink site. The result of the larger step area, therefore, is to increase the effective ratio of X_s/X_0, which in turn increases the likelihood of the onset of a round spiral.

6. CONCLUSION

6.1 SUMMARY

Atomic force microscopy offers a unique tool with which to study the crystal growth interface. This fact was demonstrated by studying the (010) face of the model compound KAP. In order to study the crystal growth interface over a large range of supersaturations, it is currently still necessary to use an ex-situ approach. This is due to the large differential between step velocity on the crystal surface and scanning speed of the AFM piezo. In the first instance it was therefore necessary to develop a suitable protection method for the removal of crystals from solution. Protection methods which had been used previously[54,61] to study KAP surfaces using optical methods were found to be unsuitable - damage was visible on the surface when viewed by the higher resolution AFM. In order to address this problem a novel removal method was developed involving withdrawal of the interface through a high pressure (50 Pa) jet of compressed air. The success of this method indicates that the critical variable when protecting KAP crystal surfaces during removal from solution is the removal rate of the solution. It is likely that this situation also applies to a number of other crystal growth systems and therefore the protection method may well have broader applicability. It may, however, be advisable to use an inert gas rather than air in the more general case.

In order to be able to make the structural link between defect structure and observed growth features, which follows from the ideas published by BCF[11], a comprehensive

dislocation characterisation of KAP was performed using X-Ray topography. The main findings of this study may be summarised as follows:

- Crystals of solution grown KAP which are grown and handled with care show a very low number of defects.
- The dislocation with the smallest Burger's vector - the [001] - is observed most frequently, and is present in all sectors.
- The most common Burger's vector of dislocations observed within the (010) sector was <110>. This dislocation was also the only one observed within the (010) sector able to produce a step on the surface. In the case of a spiral growth mechanism, it is therefore this dislocation which is likely to be responsible.

A comprehensive ex-situ study of the (010) face of KAP was performed using AFM. Over the supersaturation range studied (approximately 0.5% - 30%) two growth mechanisms were observed. A spiral growth mechanism was observed over the entire supersaturation range, and was present on the large majority of crystals studied. The growth spirals observed were all of unit cell height (1.3 nm), exhibited anisotropy and were polygonised in form. In some instances the spiral centre appeared to be hollow, however a conclusive explanation for this observation was not possible.

On a minority of the crystals studied, a two dimensional nucleation and growth mechanism was observed at high supersaturations (from approx. 15%). Surfaces exhibiting this growth mechanism were usually found to be flat and featureless in the ex-situ studies. In one case a large number of two dimensional nuclei were observed. These nuclei were not equally dispersed over the surface, but showed a higher density at the edges relative to the crystal centre. An even higher density was found at the

corners of the crystal surface. This observation is in agreement with studies[101] showing the existence of a concentration gradient across a growing crystal surface in solution.

The occurrence of the two dimensional nucleation and growth mechanism implies that the (010) sector of these crystals was free from dislocations with a component of the Burgers vector normal to this face. On such crystals it was shown to be likely that if dislocations were present in any other sectors, then these would most likely bend into the (010) sector at some point during growth, thereby giving rise to a change of mechanism - from two dimensional nucleation and growth to the more common spiral mechanism.

All of these observations are in good agreement with the X-ray topography results. The only dislocation observed in the (010) sector with a component of the Burger's vector normal to the face was the <110>. This dislocation will give rise to a unit cell height step on the surface. The low defect density observed in general indicates that the possibility of a defect free sector (particularly on very small crystals) is relatively high. Finally the bending of dislocations from lower sectors into the (010) sector was observed frequently.

During the large survey made of KAP crystals using AFM, many different growth spirals were observed. In most cases it was found that a small number, ranging from one to thirty, of spirals were present at the centre of the dominant growth hillock(s) on the surface. On these dominant hillocks disturbances, in the form of steps terminating on the surface, were frequently observed. Presumably these were due to dislocations which had nucleated during growth on inclusions as observed on the X-ray topographs.

In a few cases co-operating spirals were observed. For this to occur it is necessary for two dislocations to be within a distance of $10r_c$ of one another. Due to the low dislocation density in KAP this is therefore likely to occur only occasionally. The effect of co-operating spirals on the step spacing is to cause a double train of steps to wind up into a spiral. Some distance from the spiral centre this manifests itself as periodic variation in the step spacing.

On larger crystals, macrosteps were often visible using DICM or even the naked eye. On micro-crystals, however, they were seldom observed.

Because the <101> step velocities in the $[00\bar{1}]$ direction and [001] direction are not equivalent on the (010) face of KAP an anisotropic spiral results. The variation in the step spacing of both the fast and slow steps with respect to supersaturation was measured. In both cases an inverse relationship with the supersaturation was observed. This is in agreement with the theoretical predictions of BCF.

A strong relation between the shape of the spiral and the supersaturation was observed. At very low supersaturations the spiral was dominated by impurity effects giving rise to disturbances in the step trains. The degree of disturbance was noted to be a function of both the step orientation and the distance 'travelled' by the step. The degree of disturbance was highest for steps in the [001] direction, followed by the <101>s direction and <101>f direction. Because of the fact that there is no PBC predicted in the [001] direction these steps may be expected to contain a higher number of kinks and therefore possibly be more susceptible to impurity blocking. A conclusive explanation for the difference observed between the <101>s and <101>f directions is not immediately obvious.

As the supersaturation is increased the blocking effect of the impurities is seen to diminish, thus leaving a polygonised spiral with straight, well defined orientations. As the supersaturation is further increased the spiral becomes less polygonised. As in the case of impurities, a difference in the relative roundness of the steps is observed as a function of step orientation. Again the [001] direction are the roundest, followed by the [101]f and [101]s directions. An explanation for this behaviour may be derived from the basic variables which control the shape of the spiral - X_o and X_s. At low supersaturations the spiral is polygonised and hence $X_o > X_s$. Monte Carlo simulations have shown that as the supersaturation is increased the steps may undergo a process of progressive roughening. This amounts to an increase in the line density of kinks on a step i.e. X_o decreases. Since X_s is unlikely to change significantly, then at very high supersaturations it is possible that $X_s > X_o$. In this case a round spiral is predicted. The difference in degree of rounding between the different step orientations may be explained using the same concept as for the impurity effects. The [001] direction has no predicted PBC's and therefore possibly a higher kink density (i.e. low X_o). Therefore an increase in supersaturation would influence this step orientation first.

6.2 FURTHER WORK

Because of the fact that all of the work here was performed ex-situ, a number of interesting questions remain relating to the material KAP which lend themselves to an in-situ study. In particular the region close to the centre of the spiral would be interesting to study. From this it would be possible to analyse whether the spiral core

is hollow. Furthermore it would be interesting to see how the steps develop near the spiral centre as it 'turns'. It would also be useful to verify that the step spacing does indeed remain unchanged during removal from solution as hypothesised here.

Due to the low defect density seen in KAP it should be possible to slice sections from crystals which are dislocation free. This could be verified by topographing both before and after slicing. These slices could then be used as seed crystals for in-situ AFM at low supersaturations. In this manner it should be possible to directly see either a two dimensional nucleation and growth mechanism operating, or the nucleation of dislocations.

Because of the fact that the crystals observed in this study are very thin, it should in theory be possible to dissolve them back until they are thin enough to allow the use of TEM to directly view dislocations. In some cases, such as the crystal shown in section 5.3 exhibiting two dimensional nuclei, the crystal was only 200 nm thick. This would probably be sufficiently thin for direct imaging of defects using TEM without further treatment. Using a combination of TEM, AFM and interferometry on a microscope, a very detailed analysis of the crystal growth variables would be possible. Of course this group of analytical tools could be used to study crystal growth of micro-crystals on a wide range of solution grown materials in addition to KAP.

For ex-situ studies, the protection mechanism developed for KAP has the potential of being applicable across a wide range of crystals, since there is no danger of solubility. This could prove particularly useful for materials for which a non-soluble protection liquid is not readily available.

7. REFERENCES

1.) J.G. Burke, *Origins of the Science of Crystals*, University of California Press, Berkley, Los Angeles (1969)

2.) J. Bohm, *Crystal Res. Tech.*, **16** (1981) 275

3.) J.W. Gibbs, *Collected Works*, Longmans, Green & Co., New York (1928)

4.) W.E. Garner, *Disc. Faraday Soc. No. 5*, (1949)

5.) J.B. Rome de Lisle, *Cristallographie*, 2nd Edn. (1783)

6.) I.N. Stranski, *Z. Phys. Chem.*, **136** (1928) 359

7.) W. Kossel, *Nachr. Gess. Wiss. Gittingen,* **2** (1927) 135

8.) R. Becker & W. Döring, *Ann. Phys. Lpz.*, **24** (1935) 719

9.) M. Volmer, *Kinetik der Phasenbildung*, Steinkopff, Dresden und Leipzig (1939)

10.) F.C. Frank, *Phil. Mag.*, **41** (1950) 200

11.) W.K. Burton, N. Cabrera & F.C. Frank, *Phil. Trans. Roy. Soc. London*, **A234** (1951) 299

12.) S.W.H. de Haan, V.J.A. Meeussen, B.P. Veltman, P. Bennema, C. van Leeuwen, G.H. Gilmer, *J. Crystal Growth,* **24/25** (1974) 491

13.) A. Kelly & G.W. Groves, *Crystallography and Crystal Defects*, Longman, London (1970)

14.) W. Kossel, *Ann. Physik,* **21**, (1934) 455

15.) M. Ohara & R.C. Reid. *Modelling Crystal Growth Rates from Solution*, Prentice-Hall Inc., New Jersey (1973)

16.) F.C. Frank, *Disc. Faraday Soc. No. 5*, (1949) 48

17.) W.K. Burton, N. Cabrera & F.C. Frank, *Nature*, **163**, (1949) 398

18.) D.P. Woodruff, *The Solid-Liquid Interface*, Cambridge University Press (1973)

19.) H. Müller-Krumbhaar, T.W. Burkhardt & D.M. Kroll, *J. Crystal Growth,* **38** (1977) 13

20.) J. Frenkel, *J. Phys. U.S.S.R.,* **9** (1945) 392

21.) W.K. Burton & N. Cabrera, *Disc. Faraday Soc. No. 5*, (1949) 33

22.) G.H. Gilmer, R. Ghez, N. Cabrera, *J. Crystal Growth,* **8** (1971) 79

23.) P. Bennema, *J. Crystal Growth,* **5** (1969) 29

24.) P. Hartman, *Acta Cryst.,* **9** (1956) 721

25.) P. Hartman & W.G. Perdok, *Acta Cryst.,* **8** (1955) 49

26.) P. Hartman & W.G. Perdok, *Acta Cryst.,* **8** (1955) 521

27.) P. Hartman & W.G. Perdok, *Acta Cryst.,* **8** (1955) 525

28.) N. Cabrera & M.M. Levine, *Phil. Mag.* **1** (1956) 450

29.) I. Sunagawa & P. Bennema, *Preparation and Properties of Solid State Materials Vol. 7 (Ed. R.W. Wilcox), Dekker,* New York (1982) 1

30.) R. Kaischev, *Growth Cryst.* **3** (1962) 29

31.) R. Boistelle & A. Doussoullin, *J. Crystal Growth,* **36** (1976) 336

32.) E. Budevski, G. Staikov & V. Bostanov, *J. Crystal Growth,* **29** (1975) 316

33.) F.C. Frank, *Acta Crystallogr.*, **4** (1951) 497

34.) A.R. Verma, *Crystal Growth and Dislocations*, Butterworths, London (1953)

35.) B. van der Hoek, J.P. van der Eerden, P. Bennema, *J. Crystal Growth,* **56** (1982) 621

36.) H.J. Leamy & G.H. Gilmer, *J. Crystal Growth,* **24/25** (1974) 499

37.) K.A. Jackson, *Liquid Metals and Solidification,* ASM, Cleveland, Ohio (1958) 174

38.) N. Cabrera & D.A. Vermilyea, *Growth and Perfection of Crystals,* John Wiley & Sons, New York (1958) 411

39.) F.C. Frank, *Growth and Perfection of Crystals (Eds. Doremus, Robert & Turnbull),* John Wiley (1958)

40.) M.J. Lighthill & G.B. Whitham, *Proc. Roy. Soc. London,* (1955) 281

41.) M.J. Lighthill & G.B. Whitham, *Proc. Roy. Soc. London,* (1955) 317

42.) S. Amelinckx, W. Bontinck & W. Dekeyser, *Phil. Mag.,* **2** (1957) 1264

43.) G. Binning, H. Rohrer, Ch. Gerber, E. Weibel, *Phys. Rev. Lett.* **49** (1982) 57

44.) G. Binning, C. Quate, Ch. Gerber, Phys. Rev. Lett. 56 (1986) 930

45.) Digital Instruments website: WWW.DI.COM

46.) J. Miltat, *Characterisation of Crystal Growth Defects by X-Ray Methods (Eds. B.K. Tanner & D.K. Bowen),* Plenum Press, London & New York (1980) 401

47.) A.R. Lang, *Diffraction and Imaging Techniques in Materials Science, Vol II: Imaging and Diffraction Techniques (Eds S. Amelinckx, R. Gevers & J. van Landuyt) North Holland Publishing Co.,* Amsterdam, New York & London (1978) 623

48.) A.R. Lang, *Charaterisation of Crystal Growth Defects by X-Ray Methods (Eds. B.K. Tanner & D.K. Bowen),* Plenum Press (19XX)

49.) G. Boehm & K. Ulmer, *Z. Angew. Phys.* **29** (1970) 287

50.) G. Boehm & K. Ulmer, *J. Crystal Growth* **10** (1971) 175

51.) J. Eggs & K. Ulmer, *Z. Angew. Phys.* **20** (1963) 118

52.) I.S. Rez, *Cesk. Cas. Fis* **18** (1963) 31

53.) Y. Okaya, *Acta Crystallogr.* **19** (1965) 879

54.) L.A.M.J. Jetten, *Thesis*, University of Nijmegen (1983)

55.) M.H.J. Hottenhuis, J.G.E. Gardeniers, L.A.M.J. Jetten, P. Bennema, *J. Crystal Growth* **92** (1988) 171

56.) J. Mýl & Jos Kvapil, *Collection Czech Chem. Commun.* **25** (1960) 194

57.) J. Mýl & Z. Šolc, *Collection Czech Chem. Commun* **25** (1960) 2414

58.) Z. Šolc, J. Kvapil, J. Vlcek, Krist. *Tech.* **8** (1973) 59

59.) W.S. Hendrixson, *J. Amer. Chem. Soc.* **42** (1920) 724

60.) S.B. Smith, *J. Amer. Chem. Soc.* **53** (1931) 3711

61.) M. Hottenhuis, *Thesis,* University of Nijmegen (1988)

62.) L.A.M.J. Jetten & J.G.E. Gardeniers, *Potassium Hydrogen Phthalate: Growth and Morphology in Relation to Crystallographic Structure (in Thesis: L.A.M.J. Jetten),* University of Nijmegen (1983)

63.) W.J.P. van Enckevort, L.A.M.J. Jetten, *J. Crystal Growth* **60** (1982) 275

64.) W.J.P van Enckevort, *Progr. Crystal Growth Charact.* **9** (1984) 1

65.) L.A.M.J Jetten, B. van der Hoek & W.J.P. van Enckevort, *J. Crystal Growth* **62** (1983) 603

66.) M. Hottenhuis, C.B. Lucasius, *J. Crystal Growth* **94** (1989) 708

67.) K.B. Harvey & G.B. Porter, *Introduction to physical Inorganic Chemistry,* Addison-Wesley, Reading (1963)

68.) M. Hottenhuis, A. Oudenampsen, *J. Crystal Growth* **92** (1988) 513

69.) M. Hottenhuis, C.B. Lucasius, *J. Crystal Growth* **78** (1986) 379

70.) M. Hottenhuis, C.B. Lucasius, *J. Crystal Growth* **91** (1988) 623

71.) L.A.M.J. Jetten, J.G.E. Gardeniers & P. Bennema, *In-Situ Measurements of the Step Kinetics on the (010) face of KAP (in Thesis: L.A.M.J. Jetten),* University of Nijmegen (1983)

72.) L.A.M.J. Jetten, J.W.M. van Kessel & L.C.E.J.M. ten Horn, *In-Situ Observations with Digital Video Equipment (in Thesis: L.A.M.J. Jetten),* University of Nijmegen (1983)

73.) Y.M. Gerasimov, G.I. Distler, V.M. Kanevsky, E.I. Kurtakova, E.I Suvorova, T.M. Okhrimenko & G.S. Belikova, *Crystal Res. & Technol.,* **18** (1983) 1283

74.) A.E.D.M. van der Heijden, M. Elwenspoek, *J. Crystal Growth* **99** (1990) 1087

75.) A.E.D.M. van der Heijden, M. Elwenspoek, J.P. Eerden, *J. Crystal Growth* **98** (1989) 398

76.) M.P.W. Derks, A.E.D.M. van der Heijden, M. Elwenspoek, *J. Crystal Growth* **94** (1989) 527

77.) J. George & S.K. Premachandran, *J. Phys. D: Appl. Phys.*, **14** (1981) 1277

78.) Z. Qing-Lan, *Acta Phys. Sinica* **37** (1988) 1345

79.) Z. Qing-Lan, H. Yi-Sen, *Acta Phys. Sinica* **38** (1989) 1134

80.) Z. Qing-Lan, H. Yi-Sen, *J. Synthetic Crystals* **19** (1990) 249

81.) Z. Qing-Lan, H. Yi-Sen, *J. Appl. Cryst.*, **26**, (1993) 243

82.) Z. Qing-Lan, H. Yi-Sen, J. Cheng, *J. Synthetic Crystals* **18** (1990) 249

83.) P.E. Hillner, A.J. Gratz, S. Manne & P.K. Hansma, *Geology*, **20** (1992) 359

84.) P.E. Hillner, A.J. Gratz, S. Manne & P.K. Hansma, *Ultramicroscopy*, **42** (1992) 1387

85.) A.J. Gratz, P.E. Hillner, *J. Crystal Growth*, **129** (1993) 789

86.) P.E. Hillner, A.J. Gratz, S. Manne & P.K. Hansma, *Faraday Discuss.*, **95** (1993) 191

87.) A.J. Malkin, T.A. Land, Yu.G. Kuznetsov, A. McPherson, J.J. DeYoreo, *Phys. Rev. Lett.* **75** (1995) 2778

88.) A.J. Malkin, Yu.G. Kuznetsov, W. Glantz, A. McPherson, *J. Phys. Chem.* **100** (1996) 11736

89.) S.D. Durbin, W.E. Carlson, *J. Crystal Growth*, **122** (1992) 71

90.) S.D. Durbin, W.E. Carlson & M.T. Saros, *J. Phys. D,* **26** (1993) B128

91.) A. McPherson, A.J. Malkin, Y.G. Kuznetsov, *Structure*, **3**, (1995) 759

92.) T.A. Land, A.J. Malkin, Y. G. Kuznetsov, A. McPherson, J.J. De Yoreo, *Phys. Rev. Lett.,* **75** (1995) 2774

93.) K. Maiwa, M. Plomp, W.J.P. van Enckevoort, P. Bennema, *J. Crystal Growth* **186** (1998) 214

94.) A.J. Gratz, S. Manne, P.K. Hansma, *Science*, **251** (1991) 1343

95.) A.J. Gratz, P.E. Hillner, P.K. Hansma, *Geochim. Cosmochim. Acta*, **57** (1993) 491

96.) J.J. De Yoreo, T.A. Land, L.N. Rashkovich, T.A. Onischenko, J.D. Lee, O.V. Monovskii, N.P. Zaitseva, *J. Crystal Growth* **182** (1997) 442

97.) J.J. De Yoreo, T.A. Land, B Dair, *Phys. Rev. Lett.,* **73** (1994) 838

98.) J.J. De Yoreo, T.A. Land & J.D. Lee, *Phys. Rev. Lett.,* **78** (1997) 4462

99.) D. Bosbach & W. Rammensee, *Ultramicroscopy,* **42-44** (1992) 973

100.) H. Klapper, *Characterisation of Crystal Growth Defects by X-Ray Methods (Eds. B.K. Tanner & D.K. Bowen),* Plenum Press, London & New York (1980) 133

101.) K. Onuma, K.Tsukamoto, I. Sunagawa, *J. Crystal Growth* **98** (1989) 377

102.) K. Maiwa, K.Tsukamoto, I. Sunagawa, *J. Crystal Growth* **102** (1990) 43

103.) F.C. Frank, *Handbook of Crystal Growth (Ed. D.T.J. Hurle)*, North Holland Elsevier Science Publishers, Amsterdam (1994) 1

104.) J.J. De Yoreo, Z. Rek, N.P. Zaitseva, T.A. Land & B. Woods, *Presented at ICCG XI,* The Hague (1995)

105.) J.N. Sherwood & T. Shripathi, *Faraday Discuss.* **95** (1993) 173

106.) J.N. Sherwood & T. Shripathi, *J. Crystal Growth.* **88** (1988) 358

107.) J.N. Sherwood & T. Shripathi, *Faraday Discuss.* **95** (1993) 253

108.) E. Bauser & H. Strunk, *J. Crystal Growth,* **69** (1984) 561

109.) P.G. Vekilov & Yu. G. Kuznetsov, *J. Crystal Growth,* **119** (1992) 248

110.) R. Kaischev, E. Budevski, & J. Malinowski, *Z. Phys. Chem.*, **204**, (1955) 348

111.) C. Chapon & A. Bonissent, *J. Crystal Growth*, **18** (1973) 103

112.) N. Cabrera, *Structure and Properties of Solid Surfaces,* Chicago Uinversity Press, Chicago (1953) 295

113.) N. Cabrera & R.V. Coleman, *The Art and Science of Growing Crystals (Ed. J.J. Gilman)*, Wiley, New York (1963) 13

114.) R. Price & P.J. Halfpenny, *Publication in preparation*

115.) W.J.P. van Enckevoort, *Science & Technology of Crystal Growth (Eds. J.P. van der Eerden & O.S.L. Bruinsma),* Kluwer, Netherlands (1995) 355

116.) J.P. van der Eerden, *Thesis,* Univesity of Nijmegen (1979)

117.) R.F. Xiao, J.I.D. Alexander & F. Rosenberger, *Phys. Rev. A*, **43** (1991) 2977

118.) G.H. Gilmer & K.A. Jackson, *Current Topics in Materials Science (Eds E. Kaldis & H.J. Scheel),* North-Holland, Amsterdam (1977) 79

119.) A.A. Chernov, *Ann. Rev. Mater. Sci.,* **3** (1973) 397

120.) C.E. Miller, *J. Crystal Growth,* **42** (1977) 357

121.) R.F. Xiao, J.I.D. Alexander & F. Rosenberger, *Phys. Rev. A*, **38** (1988) 2447

122.) R.F. Xiao, J.I.D. Alexander & F. Rosenberger, *J. Crystal Growth*, **100** (1990) 313

APPENDIX I: LIST OF PUBLICATIONS

P.A. Campbell, G.R. Ester and P.J. Halfpenny, 'In-situ studies of potassium hydrogen phthalate (KAP) crystal dissolution by scanning probe microscopy', *J. Vac. Sci. and Technol.*, **14(2)** (1996) 1373, Presented at STM '96, Snowmass, Colorado

G.R. Ester, R. Price and P.J. Halfpenny, 'An atomic force microscopic investigation of surface degradation of potassium hydrogen phthalate (KAP) crystals caused by removal from solution' *J.Crystal Growth*, **182** (1997) 95

G.R. Ester and P.J. Halfpenny, 'Observation of two dimensional nucleation on the {010} face of potassium hydrogen phthalate (KAP) crystals using ex-situ atomic force microscopy' *J Crystal Growth*, **187** (1998) 111

G.R. Ester and P.J. Halfpenny 'An investigation of growth-induced defects in crystals of potassium hydrogen phthalate (KAP)', *Phil Mag.*, **A 79** (1999) 593

G.R Ester, R. Price and P.J. Halfpenny 'The relationship between crystal growth and defect structure: A study of potassium hydrogen phthalate using x-ray topography and atomic force microscopy' presented at '4th Symposium on X-ray Topography and High Resolution Diffractometry' XTOP 98, Durham (1998). *J. Phys. D: Appl. Phys*. In press

R. Price, G.R. Ester and P.J. Halfpenny 'Supersaturation-dependent polygonisation of growth spirals during crystallisation from solution investigated using atomic force microscopy' - accepted for publication in *Proc Roy Soc A*.